Lappeenrannan teknillinen yliopisto
Lappeenranta University of Technology

Jero Ahola

APPLICABILITY OF POWER-LINE COMMUNICATIONS TO DATA TRANSFER OF ON-LINE CONDITION MONITORING OF ELECTRICAL DRIVES

Thesis for the degree of Doctor of Science (Technology) to be presented with due permission for public examination and criticism in the auditorium 1382 at Lappeenranta University of Technology, Lappeenranta, Finland on the 29th of August, 2003, at noon.

Acta Universitatis
Lappeenrantaensis
157

ISBN 951-764-783-2
ISSN 1456-4491

Lappeenrannan teknillinen yliopisto
Digipaino 2003

Abstract

Lappeenranta University of Technology
Acta Universitatis Lappeenrantaensis 157

Jero Ahola

Applicability of Power-Line Communications to Data Transfer of On-line Condition Monitoring of Electrical Drives

Lappeenranta 2003
ISBN 951-764-783-2, ISSN 1456-4491

The research of power-line communications has been concentrated on home automation, broadband indoor communications and broadband data transfer in a low voltage distribution network between home and transformer station. There has not been carried out much research work that is focused on the high frequency characteristics of industrial low voltage distribution networks. The industrial low voltage distribution network may be utilised as a communication channel to data transfer required by the on-line condition monitoring of electric motors. The advantage of using power-line data transfer is that it does not require the installing of new cables.

In the first part of this work, the characteristics of industrial low voltage distribution network components and the pilot distribution network are measured and modelled with respect to power-line communications frequencies up to 30 MHz. The distributed inductances, capacitances and attenuation of MCMK type low voltage power cables are measured in the frequency band 100 kHz – 30 MHz and an attenuation formula for the cables is formed based on the measurements.

The input impedances of electric motors (15-250 kW) are measured using several signal couplings and measurement based input impedance model for electric motor with a slotted stator is formed. The model is designed for the frequency band 10 kHz – 30 MHz. Next, the effect of DC (direct current) voltage link inverter on power line data transfer is briefly analysed. Finally, a pilot distribution network is formed and signal attenuation in communication channels in the pilot environment is measured. The results are compared with the simulations that are carried out utilising the developed models and measured parameters for cables and motors.

In the second part of this work, a narrowband power-line data transfer system is developed for the data transfer of on-line condition monitoring of electric motors. It is developed using standard integrated circuits. The system is tested in the pilot environment and the applicability of the system for the data transfer required by the on-line condition monitoring of electric motors is analysed.

UDC 004.7 : 658.588.1 : 621.313
Keywords: Power-line communications, condition monitoring, low voltage power cable, electric motor

Acknowledgements

This research work has been carried out during years 2000-2003 in the laboratory of Electric Power Systems in Lappeenranta University of Technology. The work has been done under a technology program Tesla (1998-2002) in the research project "Management of Electrical Systems in Industrial Plants". The research has mainly been financed by the Technology Development Centre Tekes and ABB Oy.

I would like to thank all the people that are participated in the preparation of this thesis. Especially, I wish to thank the supervisor of thesis, professor Jarmo Partanen, for giving me the opportunity to carry out this thesis and for his interest in my research work. I would also like to thank my colleague M.Sc. Tuomo Lindh for a good co-operation and for his valuable ideas that have helped me greatly during the research.

I wish to thank professor Pertti Silventoinen for his comments and helping me in measurements. I also thank D.Sc. Markku Niemelä for helping me several times in practical things concerning electric motors and electrical drives.

I would like to thank the pre-examiners of this doctoral thesis, professor Matti Lehtonen and professor Raimo Sepponen for their valuable comments and corrections.

I am also grateful to Mrs Julia Vauterin and M.Sc. Sara Taskinen for helping me to improve my English language.

I am deeply indebted to my parents Pirkko and Pertti for giving me a good life basis and for a support during this work.

Financial support by Tekniikan edistämissäätiö, Walter Ahlstömin säätiö, Sähköinsinööriliiton säätiö, Imatran Voiman säätiö, Ulla Tuomisen säätiö and Lahja ja Lauri Hotisen rahasto is gratefully acknowledged.

Lappeenranta, July the 7th, 2003

Jero Ahola

Contents

Abstract

Acknowledgement

Contents

Abbrevations and Symbols

1. Introduction 13
1.1 History of Power-Line Communications 13
1.2 European Power-Line Communications Standard 16
1.3 Scope of the Work 17
1.4 Motivation 18
1.4.1 Demand for the On-line Condition Monitoring of an Electric Motor 18
1.4.2 Methods for Sensor Level Data Transfer 23
1.4.3 On-line Condition Monitoring of a Small-Scale Hydropower Generator 24
1.5 Research Methods 26
1.6 Key Results 27

2. High Frequency Characteristics of Industrial Low Voltage Distribution Network Components 29
2.1 Introduction to Chapter 2 29
2.2 Characteristics of Indoor and Public Low Voltage Distribution Networks 31
2.3 High Frequency Characteristics of Low Voltage Power Cables 32
2.3.1 Low Voltage Power Cable as Transmission Line 35
2.3.2 Transmission Line Equations for the Two-Conductor Transmission Line 36
2.3.3 Effect of Transmission Line Discontinuity 38
2.3.4 Determination of Transmission Line Parameters by Input Impedance Measurements 40
2.3.5 Input Impedance Measurements 41
2.3.6 Characteristic Impedance and Propagation Velocity 44
2.3.7 Signal Attenuation 49
2.3.8 Applicability to Power-Line Communications 55
2.4 Input Impedance of an Electric Motor 58
2.4.1 Input Impedance Measurements 60
2.4.2 Measurement Based Input Impedance Model for Power-Line Communications 67
2.4.3 Effect of Electric Motor on Power-Line Communications 72
2.5 Characteristics of DC-Voltage Link Inverter 74
2.5.1 Noise Generated by the DC-Voltage Link Inverter 75
2.5.2 Input Impedance of the DC-Voltage Link Inverter 78
2.5.3 Effect of the DC-Voltage Link Inverter on Power-Line Communications 79
2.6 Input Impedance of the Distribution Transformer 80

3. Characteristics of the Pilot Distribution Network 83
3.1 Introduction to Chapter 3 83
3.2 Modelling the Power-Line Channels 84
3.3 Amplitude and Phase Responses of the Pilot Environment 86
3.3.1 Characteristics of the Pilot Environment in the Frequency Band 3 – 148.5 kHz 91
3.3.2 Characteristics of the Pilot Environment in the Frequency Band 148.5 kHz – 30 MHz……. 92
3.4 Channel Capacity Analysis and Bit Error Probability 92
3.4.1 Noise Measurements and Channel Capacity Estimation 94

4. Data Transfer Tests and Test Equipment 100
4.1 Introduction to Chapter 4 100
4.2 Equipment Build for Data Transfer Tests 100
4.3 Data Transfer Tests 104
4.4 Applicability of the Developed Power-Line Communications System 111
4.5 Use of Power-Line Data Transfer in an Industrial Environment 113
4.6 Suggestions for Future Work 113

5. Summary and Conclusions 115
5.1 Introduction to Chapter 5 115
5.2 Key Results of the Work 115
5.3 Usability of the Results 117
5.4 Conclusions 117

References 119

Appendix I 124

Appendix II 136

Abbrevations and Symbols

Roman letters

c	distributed capacitance
c_0	speed of light in vacuum
d	distance
f	frequency
g	distributed conductance
h	impulse response
i	current, instantaneous
l	distributed inductance
$l_{\mathrm{i,dc}}$	distributed internal inductance at direct current
n	index
r	distributed resistance
s	Laplace operator
x	place
$\mathbf{x}$	discrete time series
t	time
$\tan\delta$	dissipation factor
u	voltage, instantaneous
v_{p}	propagation velocity
B	bandwidth
C	channel capacity
C_{hf}	high frequency capacitance
F_{S}	sampling frequency
$\mathbf{H}$	channel's transfer function
$\mathbf{I}$	current
$\mathbf{I}^{+}$	current propagating to positive direction
$\mathbf{I}^{-}$	current propagating to negative direction
$\mathbf{I}_{\mathrm{min}}$	minimum current
$\mathbf{I}_{\mathrm{max}}$	maximum current
$\mathbf{I}_{\mathrm{n}}$	noise current
I_{N}	nominal current
L	length
L_{hf}	high frequency inductance
L_{lf}	low frequency inductance
L_{m}	magnetisation inductance of electric motor
L_{s}	leakage inductance of stator coils
P_{N}	nominal power
P_{tx}	transmitted power
R_{hf}	high frequency resistance
R_{lf}	low frequency resistance
$\mathbf{X}$	coefficient of discrete Fourier transform

S/N	signal to noise ratio
$\mathbf{T}$	transmission matrix
$\mathbf{U}$	voltage
$\mathbf{U}^{+}$	voltage propagating to positive direction
$\mathbf{U}^{-}$	voltage propagating to negative direction
$\mathbf{U}_{\mathrm{min}}$	minimum voltage
$\mathbf{U}_{\mathrm{max}}$	maximum voltage
$\mathbf{U}_{\mathrm{n}}$	noise voltage
$\mathbf{U}_{\mathrm{rx}}$	voltage at receiver
$\mathbf{U}_{\mathrm{tx}}$	voltage at transmitter
$\mathbf{Z}_{0}$	characteristic impedance
$\mathbf{Z}_{\mathrm{in}}$	input impedance
$\mathbf{Z}_{\mathrm{in,rx}}$	input impedance at receiver
$\mathbf{Z}_{\mathrm{in,tx}}$	input impedance at transmitter
$\mathbf{Z}_{\mathrm{ino}}$	input impedance when end of the cable is open
$\mathbf{Z}_{\mathrm{ins}}$	input impedance when end of the cable is short-circuited
$\mathbf{Z}_{\mathrm{L}}$	load impedance
V_{N}	nominal voltage

Greek letters

α	attenuation coefficient
β	propagation coefficient
δ	skin depth, Dirac delta
ε_{0}	permittivity of vacuum
$\varepsilon_{\mathrm{r,i}}$	relative permittivity of insulation material
φ_{v}	phase of echo
γ	propagation constant
γ_{b}	bit error probability
λ	wavelength
μ_{0}	permeability of vacuum
$\mu_{\mathrm{r,c}}$	relative permeability of conductor material
$\mu_{\mathrm{r,i}}$	relative permeability of insulation material
$\boldsymbol{\rho}_{\mathrm{v}}$	complex attenuation factor
σ_{c}	conductivity of conductor material
σ_{i}	conductivity of insulation material
θ	angle
τ_{g}	group delay
τ_{v}	delay of echo
ω	angular velocity
$\boldsymbol{\Gamma}_{\mathrm{R}}$	reflection coefficient

Acronyms

A/D	analog to digital
ADSL	asynchronous digital subscriber line
AM	amplitude modulation
AMR	automatic meter reading
AS-I	AS interface
ASIC	application-specific integrated circuit
AWGN	additive white gaussian noise
BER	bit error ratio
CD	carrier detection
CTS	carrier frequency transmission
CRC	cyclic redundancy check
CSMA	carrier sense multiple access
DC	direct current
DFT	discrete Fourier transform
DSP	digital signal processor
EMI	electromagnetic interference
EMC	electromagnetic compatibility
FEM	finite element method
FH	frequency hopping
FSK	frequency shift keying
IDFT	inverse discrete Fourier transform
IGBT	insulated gate bipolar transistor
IR	infra red
ISM	industrial, scientific and medical
GENELEC	European Committee for Electrotechnical Standardization
GPRS	general packet radio service
MTL	multiconductor transmission line
OFDM	orthogonal frequency division multiplexing
OOK	on-off keying
PE	protective earth
PEN	protective earth and neutral
PC	personal computer
PLC	power-line communications, power-line carrier
PSK	phase shift keying
PVC	polyvinyl chloride
PWM	pulse width modulation
QAM	quadrature amplitude modulation
RCS	ripple carrier signalling
SWR	standing wave ratio
TEM	transverse electromagnetic
USART	universal synchronous asynchronous receiver transmitter
WLAN	wireless local area network
VDSL	very high speed digital subscriber line

1. Introduction

The power-line communications (PLC) has been applied as a data transfer method in both public electricity distribution networks and indoor distribution networks. The profile of these applications has been different. The devices developed for domestic use are mainly designed for the purpose of controlling electric devices at home. For example, the current and most common functions are: control of lights, fire alarming system and heating controlling. The systems and devices used by distribution companies are mainly meant for automatic meter reading (AMR), tariff changing, energy consumption monitoring and load management applications. During the last years the conception of providing broadband Internet access through a low voltage distribution network has aroused a hot discussion. The characteristics of power-line channels and the applicability of different digital modulation techniques have been widely researched. Due to technical and regulatory problems, the idea of providing Internet services through the distribution network was at least partly buried. Despite of this drawback, the power-line channel is still an appropriate channel for to control devices and transfer data that do not require a wide bandwidth or critical data transfer. An example for this kind of application is data transfer related to the condition monitoring of industrial low voltage electric motors.

1.1 History of Power-Line Communications

The early history of power-line communications is introduced in (Brown, 1999). According to (Brown, 1999), the idea of using power-lines for signalling is old. In 1838, Edward Davy proposed remote electricity supply metering for the purpose of checking the voltage levels of batteries at unmanned sites in the London–Liverpool telegraph system (Fahie, 1883). In 1897, Joseph Routin and C. E. L. Brown patented their power-line signalling electricity meter in Great Britain (Routin, 1897). Chester Thoradson from Chicago patented his system for remote reading of electricity meters in 1905 (Thoradson, 1905). Thoradson's system used an additional wire for signalling, which, however, was not taken into use because the commercial benefits of the system were insufficient.

The carrier frequency transmission (CTS) of voice over high voltage transmission networks began in the 1920's. The extensive network offered a bi-directional communications channel e.g. between transformer stations and power plants. It was important for management and monitoring purposes, because there was no full-coverage of telephone network at the beginning of electrification. Due to the favourable transmission characteristics, low noise levels and relatively high carrier frequencies (15 kHz – 500 kHz), the maximum distance between transmitter and receiver could be even 900 kilometres with a transmit power of 10 W (Dostert, 2001). First, only voice was transmitted and amplitude modulation (AM) was used in transmission, as carrier frequency transmission was brought into use. Later, telemetering and telecontrolling functions were implemented.

Simultaneously with the carrier frequency transmission over high voltage networks, the ripple carrier signalling (RCS) was implemented for medium and low voltage distribution networks. According to (Dostert, 2001), the first practical applications of RCS systems constructed in Germany were the Telenerg project by Siemens in Potsdam in 1930 and Transkommando constructed by AEG in Madgeburg and Stuttgart in 1935. RCS systems were primarily meant for load management functions e.g. switching heating on/off. Contrary to CTS, the data transfer of RCS was unidirectional. The RCS operated at low carrier frequencies about 125-3000 Hz. Due to the low frequency, the injected carrier signal propagated with minor losses in the medium and the low voltage distribution networks and passed through the distribution transformers.

However, at low carrier frequency, the input impedance of the distribution network was also low. Thus, the RCS transmitter required enormous transmit power. Transmit powers between 10 and 100 kW were commonly used. From the very beginning, RCS was used to transmit digital information. The modulation methods amplitude shift keying (ASK) and frequency shift keying (FSK) were mainly used in modulation because of their simplicity of implementation. Due to the low carrier frequency and simple narrowband modulation methods, the data rates of RCS systems were also low.

The next generation devices meant for load management in medium and low voltage distribution networks were based on more effective modulation methods providing higher data transfer rates. The transmit power decreased and some of the systems supported bi-directional data transfer. The decrease in transmit power was reached by increasing the frequency of the carrier signal and using more sophisticated communication electronics. An example of this kind of system is Enermet MELKO™, which was published in 1984 (figure 1.1). It provided a data transfer rate of 50 bits/s and was capable of transferring bi-directional data in medium and low voltage distribution networks between substation and measurement and control units. The frequency band 3025-4825 Hz and PSK (phase shift keying) modulation was used in data transmission (Pitkänen, 1991). The main functions supported by the MELKO™ system are remote meter reading and load management. Due to the low frequency, the carrier signal passes through the low voltage distribution transformers. The MELKO™ systems are still used in Finnish distribution companies. Corresponding systems for distribution network companies are: ABB DLC-M™ and RMS PowerNet™. They use carrier frequencies ranging from 10 kHz to 100 kHz. Thus, the required transmit power is lower than with MELKO™ and distribution transformers have to be bypassed.

Figure 1.1. Coupling unit (left) and substation (right) of Melko™ load management system. The Melko™ systems are commonly used in Finnish distribution companies.

The invention of integrated circuits in 1958-59 by Jack Kilby from Texas Instruments and Robert Noyce from Fairchild Semiconductor and the invention of microprocessor in 1971 by Ted Hoff at Intel launched the development of low-cost integrated circuits for power-line communications. In consequence of the advancements in modulation techniques, in processing capacity and in error control in 1980's, the data transfer capacity of the integrated circuits for power-line communications improved significantly.

The first low-cost power-line data transfer module for domestic use was published by Pico Electronics. The developed product was named "Experiment #10" or abbreviated X-10. The sale of these X-10 modules started in 1979. The X-10 transmitter uses a carrier frequency of 120 kHz and simple OOK (on-off keying) modulation in signalling (Kingery, 1999). In addition, the X-10 protocol defines the sending and the receiving windows in time space. A single bit can be transmitted at every zero crossing of the mains voltage. According to this, the maximum data rate of the X-10 is respectively 120 b/s in the USA and 100 b/s in Europe. Nowadays, there are about ten companies producing X-10 compliant products for the remote controlling of electric appliances in domestic electricity networks. Later, the X-10 was followed by more sophisticated power-line communication systems offering larger data transfer rates as e.g. LonWorks and CEBus.

The idea of using electricity distribution networks and domestic networks for broadband communications arouse in the 1990's along with the development of Internet. The research of power-line channel characteristics, modulation techniques and communication protocols in-

creased dramatically. The research of channel characteristic has enhanced the frequencies up to 30 MHz, because multi-megabyte data rates would require a wide bandwidth. Several integrated circuits and power-line communications systems for broadband communications were presented. The first large-scale field trial was carried out by Nor.Web in Great Britain. It was launched in 1997. The results of the test were negative and led to the withdrawal of the company already in 1999. According to Nor. Web, the Internet access through power-lines would not be economically feasible. However, the reasons for the withdrawal were probably the resistance of radio amateurs, regulations and technical problems, which made the business economically unfeasible. Later, power-line communications field trials in public low voltage distribution networks have been carried out by several distribution companies in Europe.

1.2 European Power-Line Communications Standard

For the European Union, Norway and Switzerland the regulations concerning signalling on low voltage electrical installations are presented in the European standard EN 50 065-1 (EN, 1991) (figure 1.2). The standard differs significantly from the standards applied in the USA or in Japan, where frequencies almost up to 500 kHz can be used for power-line communications. The European standard replaces the several individual standards that existed earlier in each individual European country. It specifies the frequency bands allocated to the different applications, limits for the transmitter output voltage in the operating bands and limits for conducted and radiated disturbances. In addition, the methods for measurement are defined. The standard does not specify modulation methods or functional features. The frequency band A (9 – 95 kHz) is reserved for the use in distribution companies and the frequency bands B, C and D are reserved for domestic use. A special CSMA (carrier sense multiple access) protocol is defined for the frequency band C (125 – 140 kHz). The characteristic of the standard (EN, 1991) is the limiting of the maximum output voltage of the transmitter. It does not primarily define the power spectral density of transmitted signal. The frequency band defined in (EN, 1991) is later in this work designated GENELEC band.

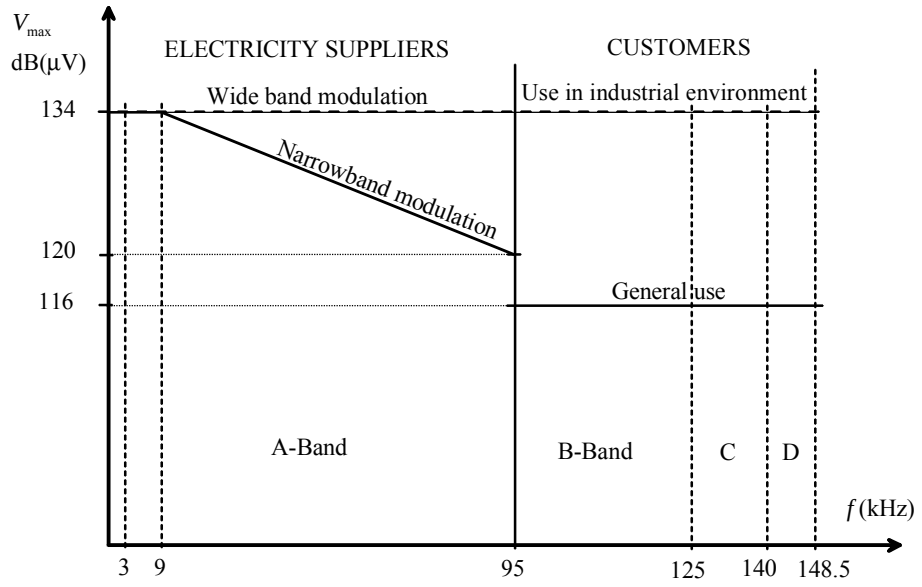

Figure 1.2. European standard concerning signalling on low voltage electrical systems (EN, 1991). The standard defines the maximum output voltages of the transmitter and the frequency bands for signalling. The frequency band A is reserved for the use in distribution companies and frequency bands B, C and D are reserved for domestic use. In this work, frequency band is called GENELEC band.

1.3 Scope of the Work

The scope of this work is to research the applicability of power-line communications for sensor level data transfer required by the on-line condition monitoring system of electrical motors. Sensor level data transfer means the lowest level digital and analog data transfer on the field level of an industrial information system (figure 1.4). Typically, sensor level data transfer is performed between the controlling unit and simple devices, such as measuring devices or actuators. The protocols used in sensor level data transfer are simple when they are compared to standard field bus protocols. One of the most well-known industrial sensor level data transfer protocol is AS-i. In this work, sensor level data transfer means the communication between the intelligent condition monitoring sensors installed in electric motors and the receiver unit that is connected to the industrial field bus. The main objectives of this work are:

1. Measuring, analysing and modelling of characteristics of an individual industrial low voltage network components and pilot environment with respect to power-line communications for frequencies up to 30 MHz
2. Development and tests of a narrowband power-line data transfer system for the on-line condition monitoring of electric motors

The channel used for data transfer is an industrial low voltage distribution network. The topology of the network is dependent on the type and scale of the industrial plant. Thus, the characteristics of the environment are also dependent on the type and scale of the industrial plant. In industrial environments, the distribution network mainly consists of power cables, electric motors, inverters and a distribution transformer. The topology of the distribution network and the devices connected to the network determine the network characteristics. Hence, the characteristic of individual network components will be measured and modelled. Finally, a pilot distribution network will be formed and the characteristics of the whole network will be researched.

The analysis is performed for frequencies up to 30 MHz. Currently, signalling in a low voltage distribution network in Europe is restricted to the frequency band 3-148.5 kHz by standard (EN, 1991). However, there are reasons for selecting the upper frequency limit to 30 MHz. First, it is possible that new frequency bands will be standardised for power-line communications, which is according to (Strong, 2001) unlikely at least in short-term. Secondly, the results of the research can be applied to analyse the propagation of electromagnetic emissions of power electronic devices in the distribution network or to analyse the current and voltage oscillations in the feeder cable of inverter. The third reason is the possibility to apply power-line data transfer between motor and feeding inverter. This requires knowledge of the high frequency characteristics of the motor, motor feeder cable and inverter.

The second scope of the work is to construct and test a power-line communication system for the sensor level data transfer required by the on-line condition monitoring of electric motors. There are some requirements that have to be fulfilled:

- The European standards concerning power-line communications have to be fulfilled
- Affordable price in small manufacturing amounts
- Adequate data transfer rate
- Connectivity to industrial field bus

This work does not focus on modulation techniques, communication protocols or on the forming of new communication channel models or noise models. Additionally, this work does not concentrate on signalling in the feeder cable between inverter and motor. The goal of this work is to give an insight into the high frequency characteristics of components of an industrial low voltage distribution network and to develop a power-line modem that is technically and economically feasible for the data transfer of on-line condition monitoring of electric motors.

1.4 Motivation

1.4.1 Demand for the On-line Condition Monitoring of an Electric Motor

According to (Spare, 2001), moving from the concept of time-based maintenance to the concept of predictive maintenance may reduce significantly the operation and maintenance costs of the utility company. The same applies for industrial companies and industrial processes, where electric motors play a key role.

Electric motors have an important role in industrial processes. A failure of motor operation at a critical location leads to the interruption of the process, which correspondingly leads to economical losses. Electric motors are often considered to be very reliable devices. On the other hand, many researches have indicated that the part of motor failures is significant when interruption times of industrial processes are identified. According to the research carried out in StoraEnso Kaukopää paper integrate, less than 40 % of the total number of process interruptions are caused by electrical systems (Lempiäinen, 1995). The amount of interrupts caused by electric motors from the total faults of electrical systems is small. However, a failure of an electric motor may easily cause a long interruption time (figure 1.3).

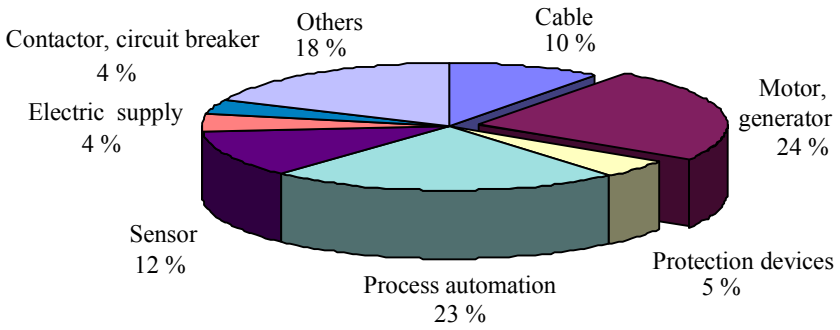

Figure 1.3. Relative total interruption times caused by electric systems in Kaukopää paper integrate (Lempiäinen, 1995). The faults attributed to the electric motors and the process automation form the most significant part.

According to (Albrecht, 1986), the failures of electric motors are caused by: bearings (40%), stator (37%), rotor (10%) and other reasons (12%). The reason of the failure may be for example overheating, humidity or chemicals. In order to monitor the condition of the bearings, temperature of the motor or humidity of the motor on-line, there has to be installed a condition monitoring sensor in the motor. However, the usability of on-line monitoring is questionable if the sensor does not have data transfer capabilities. Hence, the complete on-line condition monitoring system requires sensor level data transfer capabilities. Estimated sensor level data transfer rates required by some condition monitoring functions of a single electric motor are illustrated in table 1.1.

Table 1.1. Estimated minimum data transfer rates for on-line condition monitoring functions of a single electric motor at sensor level.

Measurement	Fault	Required data transfer rate/motor	
		Low sensor level data processing	High sensor level data processing
Vibration	Bearing failure	100 b/s	20 b/s
	Motor asymmetry	100 b/s	20 b/s
	Rotor failure	100 b/s	20 b/s
	Machine failure	100 b/s	20 b/s
	Machine asymmetry	100 b/s	20 b/s
Temperature	Contamination	1-10 b/s	1 b/s
	Fan failure	1-10 b/s	1 b/s
	Overloading	1-10 b/s	1 b/s
Humidity	Water leakage	1-10 b/s	1 b/s

In many respects, the required data transfer rates depends on the amount of processing capacity at the condition monitoring sensor level. The more processing is performed at the sensor level, the less data transfer capacity is required. The measurements that are required to indicate the faults of electric motors are presented in (Lindh, 1999). The required sensor level data transfer rates (table 1.1) are estimated by determining, which kind method is required for the analysis and how often the analysis has to be performed. Generally, data transfer rates required for the on-line condition monitoring functions of electric motors are low, but they can be considered higher than the data transfer rates required for the automatic reading of electricity meters.

In addition to the sensor level data transfer, the complete condition monitoring system requires an interface for the connection to the existing information systems of the industrial plant (figure 1.4). Generally, in industrial plants a field bus interface is required because the condition monitoring system is located at the field level of the plant and field buses are the main bus types at that level. Connectivity to the existing information systems is required, because the monitoring of the electric motors may be included in the automation system of the plant or it may be completely outsourced and remotely performed by the third party. Additionally, some kind of expert system or human based analysis is required to determine e.g. whether the defected bearing should be replaced. It also requires connectivity to the information systems that are at a higher level in the hierarchy of the industrial information system (figure 1.4).

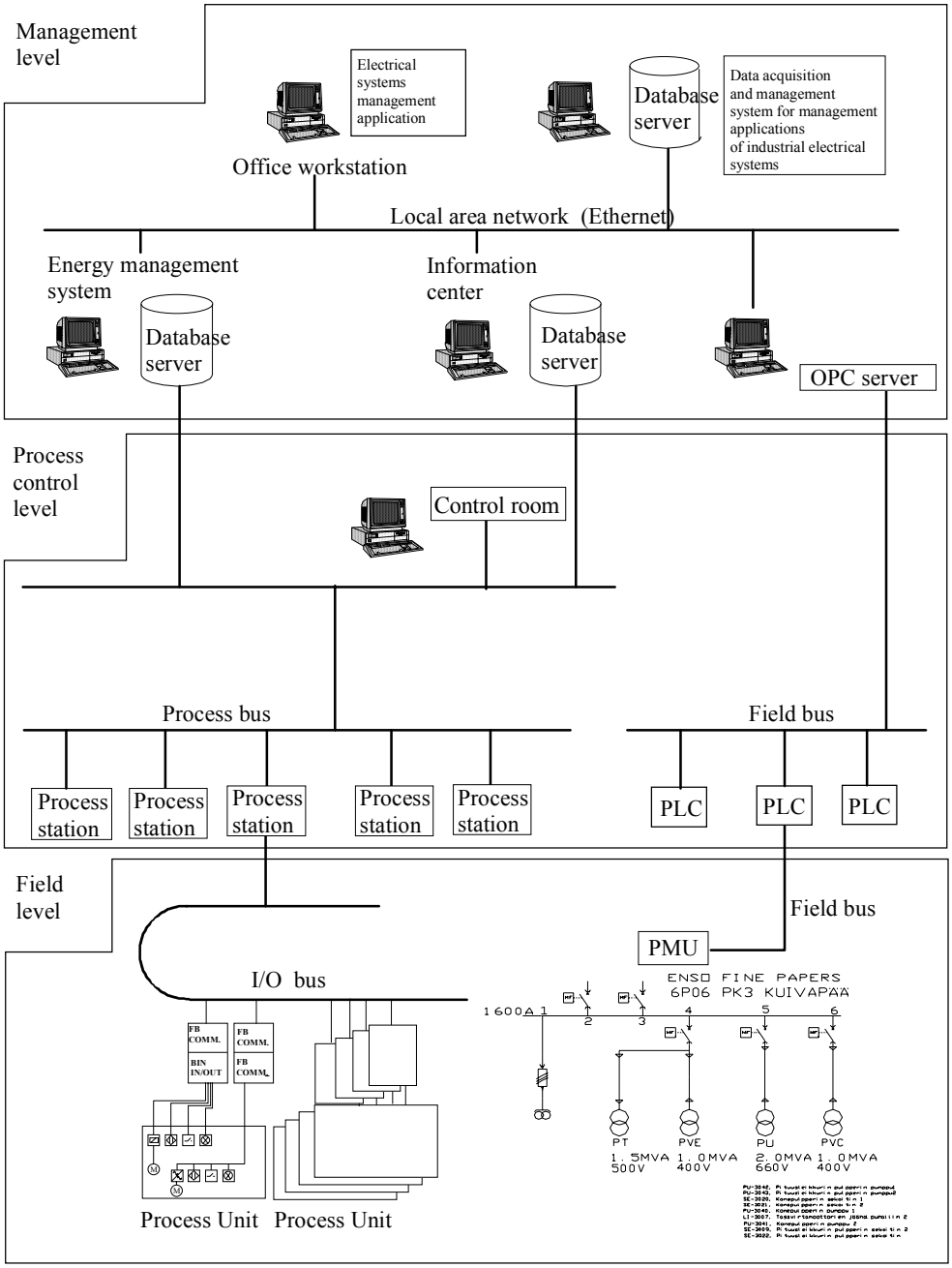

Figure 1.4. Hierarchy of industrial information systems (Ahola, 2000). It consists of three main levels: the field level, process control level and management level. The sensor level can be considered to be a sublevel of the field level. The industrial processes and electricity distribution are located at the field level.

In case of outsourced maintenance and diagnostics, problems may arise if the on-line condition monitoring system is part of the information system of the industrial plant. There exist two issues causing problems. First, the access for diagnostics into the information system of the industrial plant has to be granted to the third party. Secondly, the data produced by the condi-

tion monitoring sensors have to be transferred from the field level to the management level of the industrial plant. Generally, the Internet access to the information system of the industrial plant is through the management level of the plant. The problems are both technical and also security is concerned. This issue is analysed in article (Lindh2, 2001) and a single solution to the field level data access from Internet is presented.

Practically, a probable solution for the remote maintenance and diagnostics is the complete separation of the condition monitoring system from the information system of the industrial plant (figure 1.5.). The sensor level data transfer from the intelligent condition monitoring sensors installed at the field level of the plant is carried out using various methods, such as power-line communications, short range radios and conventional twisted pairs. The sensors send the condition monitoring data to the receiver unit, which has a standard field bus interface. The receiver unit is connected to the device that provides Internet access for the remote diagnostics. The Internet access is provided using e.g. radio communications, like GPRS (general packet radio service), or wired communications, like ADSL (asynchronous digital subscriber line). The measurement data are stored in databases together with the data of the monitored devices. These are used together in the analysis determining whether there exists need for maintenance or repairs.

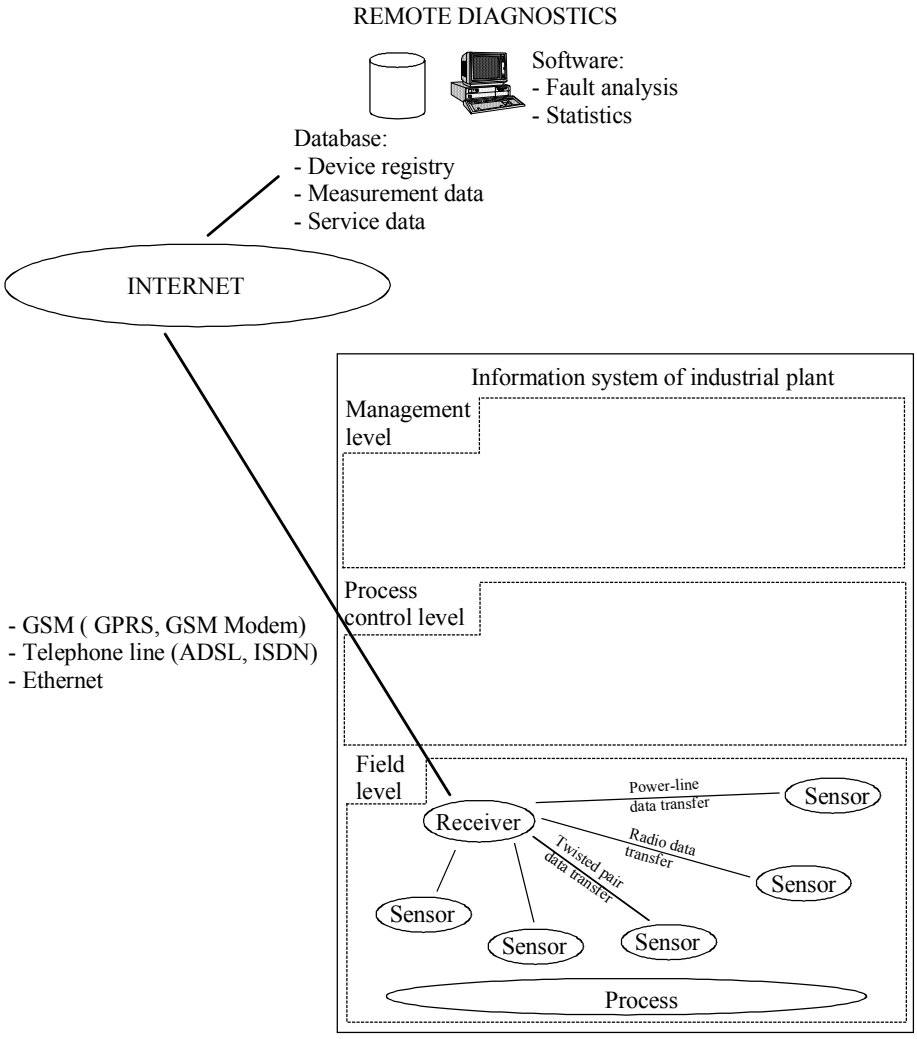

Figure 1.5. Possible solution for outsourced diagnostics of the industrial plant. Condition monitoring sensors are installed on the monitored devices. The sensor level data transfer is performed using various methods, such as power-line and radio communications. The Internet access required by the remote diagnostics is provided e.g. by using wired or wireless telephone network. There is Internet access directly to the field level of the industrial plant.

1.4.2 Methods for Sensor Level Data Transfer

There are multiple ways to perform the sensor level data transfer required by the on-line condition monitoring system of electric motors. The most reliable and the most common way to transfer data is to use wires as e.g. twisted pair, coaxial cable or optical fibre. However, the cable is exposed to a hostile environment and a single sensor will cease to work in case of a cable failure. In addition, the installation of the cable is expensive as retrofitting. Further, according to the maintenance personnel, no extra cables to the motors are wanted in industrial plants.

Short-range radio offers an alternative for sensor level data transfer. It does not require extra cabling. The condition monitoring sensor network can be created using radio communications

e.g. Bluetooth, WLAN (wireless local area network), or other non-standard radio systems operating at ISM (industrial, scientific and medical) frequency bands. It is possible to install multiple condition monitoring sensors and a single receiver that collects the condition monitoring data send by the sensors and links the data to the information systems of the plant. However, the use of radio communications in industrial plants may be problematic:

- The metallic structures prevent the propagation of radio signals
- The concrete walls attenuate radio signals
- Other radio equipment operating at the same frequency band causes disturbances
- Some industrial devices generate radio disturbances
- The required data transfer distance may be too long for short range-radio
- The condition monitoring sensor with radio communications requires also power supply

Compared to radio communications, the power-line communications has the same advantages. The low voltage distribution network forms a communications network that is already installed. Multiple sensors can send data along the power-lines to the same receiver. The power-line data transfer does not require extra cabling. The low voltage power cable is used as a communications channel. In addition, many of the problems typically belonging to radio communications can be avoided. The power-line data transfer is immune to the physical structure of the industrial plant, as e.g. walls or floors. The operating distance of power-line communications is longer than that of the short-range radio communications. The supply power required by the condition monitoring sensor may be directly taken from the terminals of the monitored electric motor. However, there exist several problems that are the same for power-line communications as for radio communications. The functionality of both systems is dependent on the characteristics and noise content of the environment. Hence, power-line communications is not a generally appropriate method for transferring critical data.

In addition to the communications methods discussed above, also IR (infra red) data transfer could be applied as a sensor level data transfer method. It is a low-cost method to implement, components are widely available and it does not require extra wires for data transfer. However, the infra red ray does not pass through floors or walls and the data transfer distance will be only metres if there is no line of sight between receiver and transmitter. Furthermore, in industrial plants, there exist numerous noise sources, e.g. lights and other equipment emitting infra red light disturbing the communications.

1.4.3 On-line Condition Monitoring of a Small-Scale Hydropower Generator

The condition monitoring of an asynchronous generator in a small-scale hydropower plant is a possible application for an on-line condition monitoring system equipped with power-line communications capabilities. The total power output of the small-scale plant is in ranged from 50 kW to 3 MW and the maximum size of a single generator is about 250 kW. The proposed on-line condition monitoring system is illustrated in figure (1.6). It consists of sensors that are installed in the generators. The sensor monitors vibrations, humidity and temperature. The vibration measurement is required for the analysis of the bearing condition, the humidity measurement is to analyse of possible leakage and the temperature measurement is to detect overloading of the generator. The condition monitoring sensor installed in the generator takes supply power from the terminals of the generator. The measurement data are transferred from the sensor to the receiver unit installed at the mains switching board by using power-line data transfer. The receiver unit is connected to the field bus of the power plant. The final analysis of the measurement data is carried out at a PC workstation, which is e.g. directly connected to the field bus of the plant. Figure 1.7 shows a picture of a small-scale hydropower plant and the

mains switching board of the plant. The low voltage generator and turbine are combined into a single package, which is installed under water (figure 1.8).

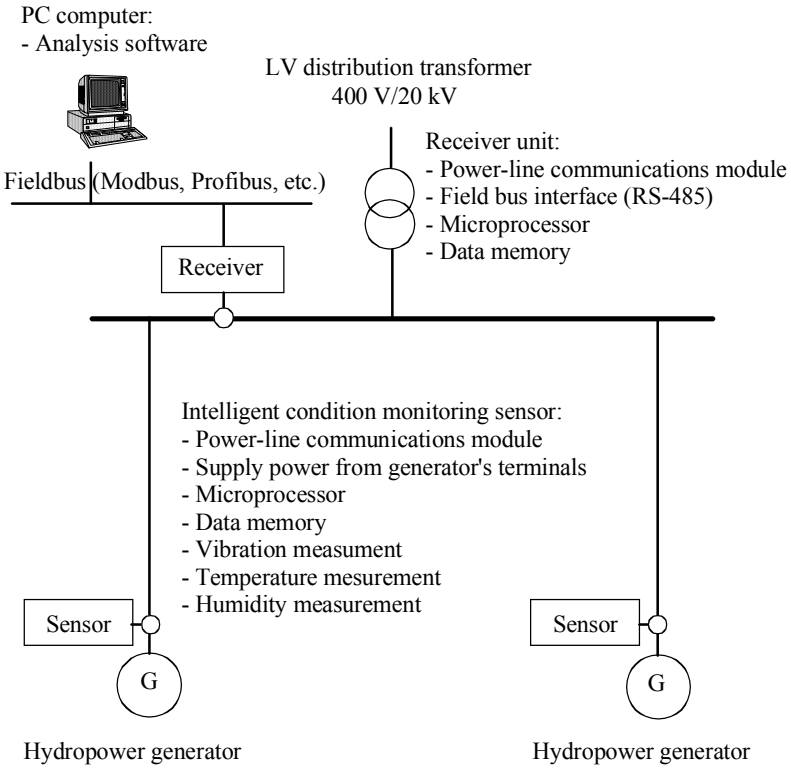

Figure 1.6. Possible topology of the on-line condition monitoring system of generators in a small-scale hydropower plant.

Figure 1.7. A small-scale hydropower plant offers the possibility to apply for the power line communications system under research and development. Picture of a small-scale hydropower plant in a rural area (left). The mains switching board of the plant (right).

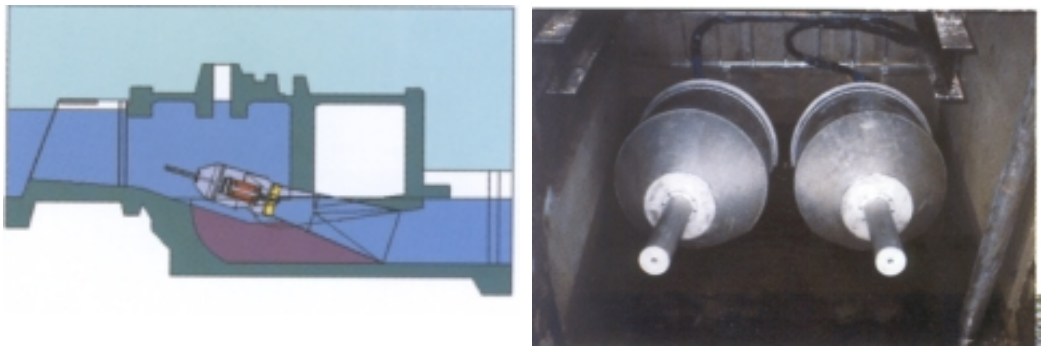

Figure 1.8. Location of the underwater generators (left). There are two low voltage asynchronous generators (right). The intelligent condition monitoring sensors would be installed inside the generators.

1.5 Research Methods

This work is mainly based on the theory of electromagnetism, information theory, computer simulations, extensive laboratory measurements and data transfer tests. Because of the complexity of electromagnetic phenomena in industrial low voltage distribution networks the importance of measurements and laboratory tests is considerable. Furthermore, one of the main objectives of this work is to develop and test a power-line communications system for purpose of data transfer of on-line condition monitoring of electric motors.

In the beginning of the research, the structure of the industrial low voltage distribution network is analysed. Secondly, the main components of the network, which are low voltage power cables, electric motors and inverters, are measured and modelled. Finally, a pilot environment is build from the measured components and its' characteristics are analysed and modelled with respect to power-line communications.

In the second part of the work, a power-line communications system is developed using standard integrated circuits. The applicability of the developed system is determined by performing data transfer tests in the pilot environment. Finally, the results of the tests are analysed.

The devices used for the measurements use low voltages in the measuring (~1 V). Thus, the applicability of the models and the results should be carefully considered if e.g. voltage levels (~100V) are analysed. However, the voltage levels used in the measurements are close to the voltage levels used in power-line communications and close to the voltage levels of high frequency noise produced by active appliances that are connected to low voltage distribution networks. The characteristics of cabling, electric motors, transformer and power-line channels are measured without the mains voltage switched on. According to the experimental work carried out by (Anastasiadou, 2002), this should not significantly affect the results. However, the situation will be different if there are active appliances, as e.g. rectifiers connected to the distribution network.

1.6 Key Results

The main results of this work can be divided into two parts:

1. Theory and measurement based modelling of distribution network components and analysis of the pilot distribution network.
2. Determination and tests of a low cost power-line communications system that is developed using standard integrated circuits.

There are two main scientific contributions in this research. The first contribution is comprised of measurements, analysis and modelling of MCMK low voltage power cables in the frequency band 100 kHz – 30 MHz. The second contribution is a measurement based termination impedance model for a low voltage electric motor with slotted stator for the frequency band 10 kHz – 30 MHz.

The input impedances of MCMK low voltage power cables were measured in the frequency band 100 kHz – 30 MHz using several signal couplings. According to the measurements, the transmission line parameters for the cables were determined and a general attenuation formula for the cables was formed. The characteristic impedances of the MCMK cables are low compared to conventional data transfer cables due to insulation layer that is thin in proportion to the conductor cross-sectional dimensions. Generally, the characteristic impedances of the cable vary within the range of 5 to 50 Ω depending on the signal coupling and the structure of the cable. The signal attenuation in the cable increases as a function of frequency. In the frequency band 100 kHz – 30 MHz, the main loss mechanism of the low voltage power cable is the dielectric loss of the PVC (polyvinyl chloride) insulation material. Generally, the signal attenuation in the researched low voltage power cables in the frequency band 100 kHz – 30 MHz corresponds to the attenuation of generally used low-cost data transfer cables.

The input impedances of six electric motors (15-250 kW) were measured in the frequency band 10 kHz – 30 MHz using several signal couplings. According to the measurements, the input impedances of all motors behave similarly in the frequency band 10 kHz – 30 MHz. When the

input signal is coupled between the phases, there exists a strong parallel resonance in the frequency band 10–100 kHz and a strong serial resonance in the frequency band 1–20 MHz. When the input signal is coupled between the phases and the motor frame, there exists only a strong serial resonance in frequency band 1-20 MHz. At parallel resonance frequency, the input impedance of the motor is in the order of kilo-ohms. At serial resonance frequency, the input impedance of the motor is in the order of ohms, respectively. These resonance frequencies originate from the parasitic components of the slotted stator winding. The rotor and the end plates do not significantly affect the high frequency behaviour of the input impedance. According to the measurements and analysis, a simple input impedance model for electric motors was developed. The model describes the main characteristics of the electric motor in the frequency band 10 kHz – 30 MHz. Regarding power-line communications, the interface of the motor and power cable is practically always mismatched. Although the absolute value of the input impedance of the motor may be close to the characteristic impedance of the cable, the input impedance of the motor is either capacitive or inductive.

An inverter that is connected to a low voltage distribution network can be considered to be an effective noise source as well as a nonlinear and time-variant load impedance. As power-line communications is concerned, these characteristics are harmful. According to the noise current measurements performed for the frequency band 9 kHz – 30 MHz, the disturbances generated by the inverter spread out to the whole measured frequency band. The disturbances mainly arise from the three-phase rectifier unit and the inverter stage. The time-variant input impedance is problematic when the injected carrier signal is coupled between the phase conductors. The forward biased phases of the rectifier unit effectively short-circuited the carrier signal injected into the distribution network. However, the situation may be different if devices equipped with three-phase rectifiers are also equipped with the mains side input filters.

The signal voltage attenuation in communications channels in the pilot environment was measured. The simulation models for the measured channels were formed applying developed high frequency models for cables and motors. The standard transmission matrix theory and two-port models were applied as a modelling tool. At least in the pilot environment, the simulated and measured frequency responses are corresponding for frequencies up to 15 MHz.

Channel capacity estimations were carried out for the pilot environment. The estimates give theoretical channel capacities of 50-250 Mb/s for the frequency band 3 kHz – 30 MHz and more than 1 Mb/s for the frequency band 3-148.5 kHz at a transmit power level of about 10 mW.

In the second part of the work, a power-line communications system for purposes of on-line condition monitoring of electric motors was developed for the GENELEC frequency band. The system was build using standard integrated circuits. Thus, the cost of the communications equipment could be reduced. The system was designed so that there is possibility of connecting it to a standard industrial field bus. The system was tested in the pilot environment. The signal coupling between the phase conductors is problematic when an appliance equipped with a six-pulse rectifier is connected to the distribution network close to the transmitting or receiving power-line modems. According to the requirements and test results, the designed modems are appropriate for data transfer required for the on-line condition monitoring of electric motors.

2. High Frequency Characteristics of Industrial Low Voltage Distribution Network Components

2.1 Introduction to Chapter 2

An industrial low voltage distribution network consists of the low voltage cabling and electrical appliances that are connected to the distribution network. The topology of the distribution network may vary from simple to complicated. In the simplest case, there is only a single motor or generator connected directly to the distribution transformer by a low voltage power cable. In a more complicated case, there may be multiple electric motors or generators under the same distribution transformer. Part of the motors may be controlled by variable speed drives. According to (Lakervi, 1989) and (Bostoen, 2000), the maximum practical length of a low voltage distribution cable is about 500 metres.

A simple industrial low voltage distribution network is illustrated in figure 2.1. It describes the main circuit of a small-scale hydropower plant. The main loads in the network are two generators and two auxiliary motors for the hydraulics of the generators. The total length of the distribution network is about 100 metres. There are no variable speed drives connected to the distribution network. Therefore, the noise level of the network is probably low and the environment is probably favourable for power-line communications. Figure 2.2 illustrates the most significant low voltage motors and other loads for a section of a paper machine. There are two distribution transformers and about 10-20 large loads under a single distribution transformer. In addition, there are numerous auxiliary motors e.g. for ventilation and for lubrication. The total length of the distribution network is longer than in the previous case, because the mains switching board is separated from the process. Further, there are many branches in the distribution network and some of the motors are controlled by variable speed drives, which increases the noise level in the distribution network. The environment is probably problematic for the power-line data transfer.

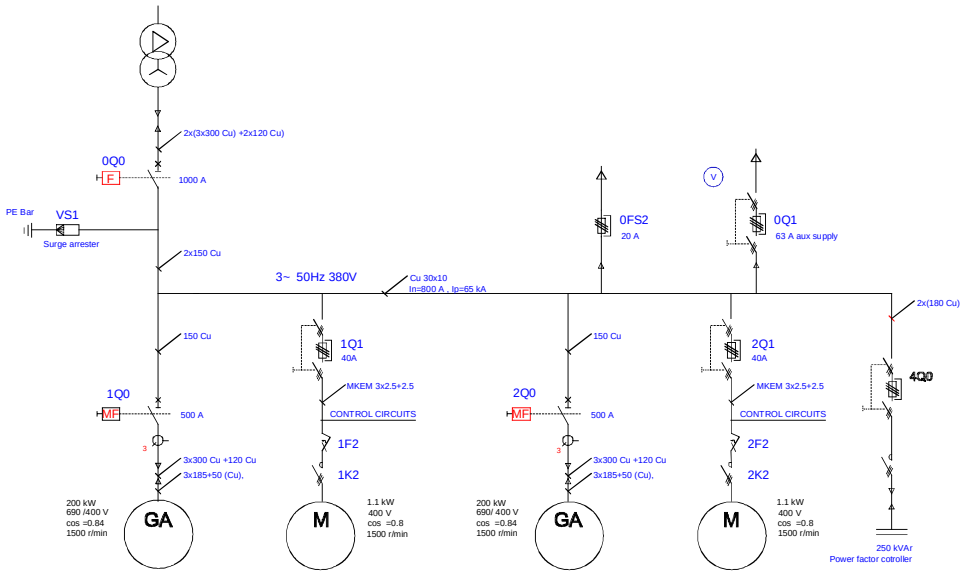

Figure 2.1. Main circuit of a small-scale hydropower plant (Lindh, 2002). The main components are two low voltage generators and a distribution transformer.

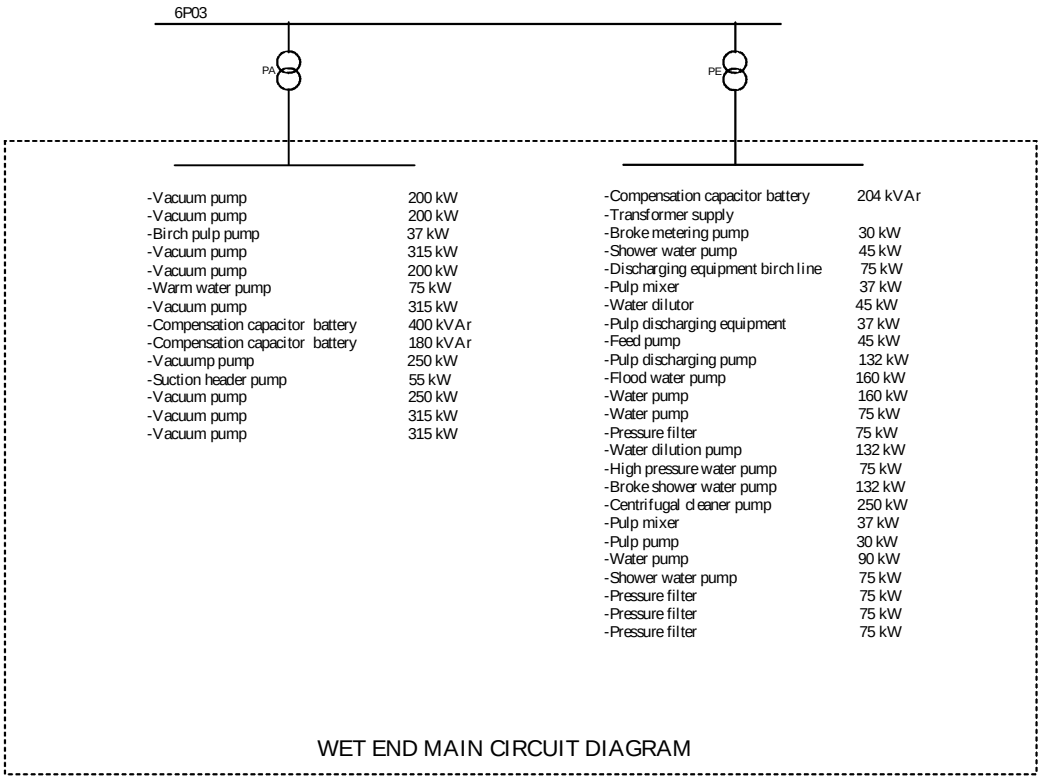

Figure 2.2. The most significant motor loads connected to two low voltage distribution transformers at a paper machine at StoraEnso in Varkaus, Finland. The motors represent a section of the paper machine. (Mäkinen, 1998)

Generally, a distribution network may be considered to be an unfavourable environment for communications. Power-lines are designed for the distribution of the electrical power. They are ideal for the distribution of high voltages at low frequencies. The data transmission generally uses high frequencies at low voltages, respectively. The power-line channel has a varying impedance, high attenuation and considerable noise. These properties easily cause small data transfer rates or big error percentages. For data transmission over any medium, it is necessary to determine the characteristics of the communications channel. When considering a communications channel, the interesting parameters are:

- Input impedance
- Signal attenuation
- Phase distortion
- Noise content

In the beginning of this chapter, the research carried out for public and domestic low voltage distribution networks is discussed. Next, the typical components belonging to industrial distribution networks are analysed, measured and modelled with respect to power-line communications at the frequencies up to 30 MHz.

The analysis, measurements and modelling of the distribution network components in this chapter focus on low voltage power cables and low voltage induction motors, which represent the main components in the target application environment. However, the characteristics of inverters and distribution transformers are also briefly analysed.

2.2 Characteristics of Indoor and Public Low Voltage Distribution Networks

There has not been carried out much research work that is focused on the high frequency characteristics of industrial low voltage distribution networks. Power-line communications research has been mainly concentrated on home automation, broadband indoor communications and broadband data transfer in a low voltage distribution network between home and transformer station. The topology of an industrial low voltage network differs from topologies of indoor and public low voltage networks. The indoor networks are single phase and the total length of the network is generally shorter than the length of the industrial low voltage distribution network. Additionally, the number of loads and noise sources is generally higher in indoor networks than in industrial networks. Correspondingly, public low voltage distribution networks are three-phased and their lengths are close to those of the industrial networks. However, the loads and the cables of public and industrial distribution networks are of a different type and the topology of these networks is different. The topology of the industrial network is typically radial. Each large load has its' own supply cable. Correspondingly, in the public low voltage distribution network loads are typically connected in chain. Despite of these differences, the research carried out in the fields of indoor networks and public low voltage distribution networks is a good starting point for the analysis of industrial low voltage distribution networks.

According to (Philipps 1999), the input impedance of a low voltage distribution network is dependent on location and frequency and is typically in the range of few ohms to few kilo-ohms. The impedance is influenced by the characteristic impedance of the cable as well as the topology of the distribution network and the connected electrical loads (Philipps, 2000). According to the statistical analysis of the measurements performed for a few hundred in-house power-line channels in the frequency band 0–30 MHz, the average input impedance of the distribution network is between 100 ohms and 150 ohms (Philipps, 2000). Due to the strongly frequency variant input impedance, coupling in and out and transmission losses are a common phenomenon (Philipps, 2000).

According to (Philipps, 1998), line loss, impedance mismatches, impedance discontinuities, low impedance loads and branch cables cause attenuation in a power-line channel. In addition, the power-line channel attenuation is highly frequency dependent containing multiple narrowband notches in the frequency space. These notches result from the multipath signal propagation caused by the impedance mismatches and by the topology of the distribution network. The signal attenuation in power-line channels is slightly increasing as a function of frequency and channel length (Philipps, 2000). However, the contribution of the cable to the total signal attenuation is quite small. The statistical analysis of the channel measurements introduced in (Philipps, 2000) shows that the average signal attenuation in the power-line channel increases in the frequency band 300 kHz – 5 MHz from 30 dB to 45 dB and in the frequency band 5–30 MHz from 45 dB to 50 dB.

Phase nonlinearities in the frequency response of the communications channel lead to variations in a group delay, which disturbs the data transmission. According to (Philipps, 1998), the phase responses of power-line channels are relatively linear with the phase decreasing as a function of frequency. Nonlinearities occur only in the frequency bands having a steep notch or peak in the amplitude response.

Besides signal attenuation and phase distortion, noise is an important factor that influences on the success of digital communications over a power-line channel. The power-line channel does not represent an additive white gaussian noise (AWGN) environment like many other communication channels (Zimmermann, 2000). Instead, it can be regarded as a fading multipath

channel with quasi-stationary frequency response. The frequency response of the channel varies as a function of time. However, it can generally be considered to be constant during a transmitted symbol. According to (Hooijen, 1998) and (Zimmermann, 2000), power-line noise can be classified into five categories:

1. Coloured background noise: This noise has a relatively low power spectral density, which is frequency variant. The noise is caused by numerous weak noise sources. The power spectral density of this type of noise varies in terms of minutes or hours.
2. Narrow band noise: This noise consists of sinusoidal signals with modulated amplitudes. The sources of the noise are broadcast stations and the noise level varies within the daytime.
3. Periodic impulsive noise that is asynchronous to the mains frequency: The impulses have a repetition rate generally from 50 kHz to 200 kHz. The noise is mostly caused by switching power supplies.
4. Periodic noise that is synchronous to the mains frequency: The impulses have a repetition rate of 50 Hz or 100 Hz and are synchronous to the mains cycle. The duration of impulses is short, generally in the order of microseconds. This noise is caused by power supplies that operate synchronously with the mains cycle.
5. Asynchronous impulsive noise: The noise is caused by switching transients in the distribution network. The impulses have a duration from some microseconds up to a few milliseconds. The power spectral density of this type of noise can have levels of more than 50 dB above the background noise.

In order to develop modulation techniques, power-line communication systems and network planning and simulation tools, channel models are required. The channel models proposed for power-lines are mostly based on the multipath propagation of a signal (Philipps, 1999), (Zimmermann, 1999). The models assume that due to imperfect terminations the impulse injected from the transmitter into the channel reaches the receiver propagating directly and indirectly from the source to the destination. The main signal is followed by a number of echoes. In other words, the multipath nature of the channel spreads energy send by the transmitter in the time-space. The presented models generally require the measurement of the transfer function or impulse response of the channel. They are formed by taking into account the most significant reflections and their amplitudes from the impulse response of the channel. The multipath channels and their characteristics are discussed in (Proakis, 1989).

2.3 High Frequency Characteristics of Low Voltage Power Cables

The low voltage power cable acts as a transmission line for the power-line communications system under research. In Finnish industry, the average cable length from a mains switching board to a motor or a generator are typically 70-80 metres (Ahola, 2001). However, there are installed cables with lengths of more than 200 metres. The use of long cable lengths is based on the tradition that the electric equipment should be separated from the process. In many cases this is necessary, because the electrical equipment, such as relays and inverters cannot withstand the hostile process environment.

Nowadays, mostly shielded and symmetrical low voltage power cables are installed as low voltage motor cables. This is necessary, especially with variable speed drive controlled motors, in order to avoid electromagnetic interference caused by the high speed switching of the power transistors and to minimise bearing currents (Bartolucci, 2001). In Europe, MCMK type low voltage power cables are widely used with motors directly connected to the supplying grid and with motors controlled by variable speed drives (figures 2.3 and 2.4). The MCMK cable has both the symmetrical structure of the phase conductors and the protective screen around the

phase conductors, which acts also as a neutral conductor. MCMK cables are rated for the nominal voltage $U_n = 1$ kV . The most common insulation material of low voltage power cables is polyvinyl chloride (PVC). When higher temperature grading is needed, insulation material polyethylene is used in the power cables. The insulation materials and conductor materials have a significant role in determining the high frequency characteristics of the power cables. However, it is not possible to define the general dielectric characteristics of PVC, because those depend heavily on the factors like temperature, frequency and the composition of insulation material (Dostert, 2001). The relative dielectric constant ε_r and the dissipation factor $\tan\delta$ of a PVC material are presented in figure 2.5 as a function of frequency. Correspondingly, in (Harper, 1975), the dielectric parameters of the different types of flexible PVC at the frequency 1 MHz are given: PVC filled ($\varepsilon_r = 3.5 - 4.5$, $\tan\delta = 0.09 - 0.1$) and PVC unfilled ($\varepsilon_r = 3.3 - 4.5$, $\tan\delta = 0.04 - 0.14$). According to (Harper, 1975), the dielectric characteristics of polyethylene are $\varepsilon_r = 2.25 - 2.35$ and $\tan\delta > 0.0005$. Both dielectric constant and dissipation factor of polyethylene remain relatively constant as a function of frequency and temperature. The conductors and the screen of the MCMK cable are made of copper. The resistivity of the copper is $\rho_{Cu} = 1.72 \cdot 10^{-8}$ Ωm (Alatalo, 1975).

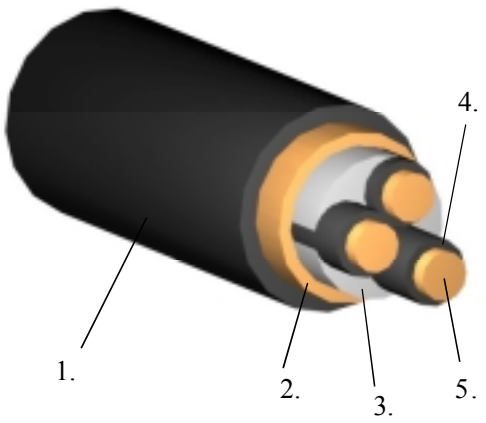

Figure 2.3. Structure of MCMK low voltage power cable (the cross-sectional area of the phase conductor 2.5-16 mm^2). The cable consists of following parts: 1. PVC outer jacket, 2. Screen (PE), which acts also as neutral conductor (N), 3. Plastic filling, 4. PVC insulation, 5. Phase conductor.

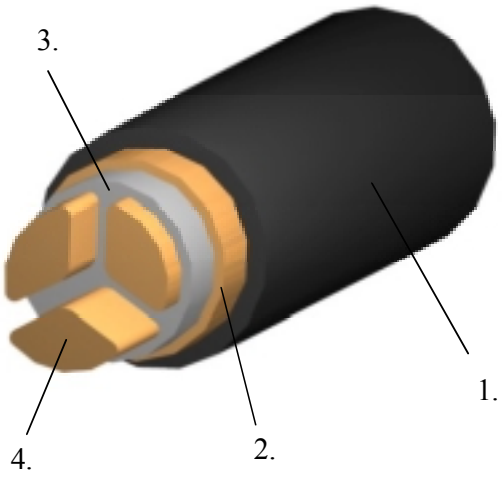

Figure 2.4. Structure of MCMK low voltage power cable (the cross-sectional area of the phase conductor 25-240 mm^2). The cable consists of following parts: 1. PVC outer jacket, 2. Screen (PE), which acts also as neutral conductor (N), 3. PVC insulation, 4. Phase conductor.

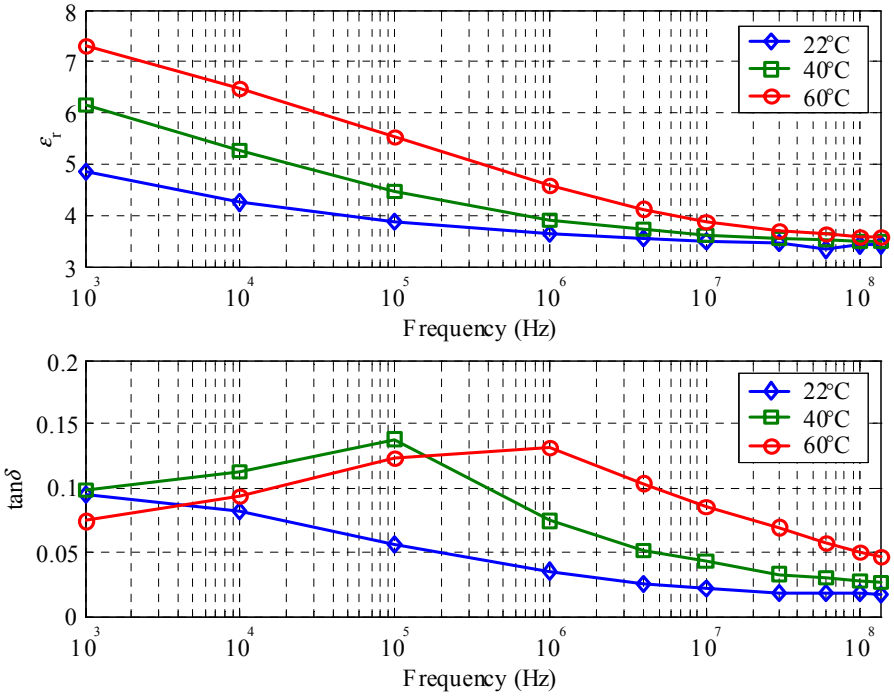

Figure 2.5. Measured dielectric characteristics of PVC insulation material as a function of frequency in the frequency band 1 kHz – 135 MHz (Lin, 1991).

2.3.1 Low Voltage Power Cable as Transmission Line

Three-phase low voltage power cables are multiconductor transmission lines (MTL). The number of conductors in MCMK low voltage power cables is four. An example of applying MTL equations for the four-conductor cable is introduced in (Sartenaer, 2001). In order to solve the currents and voltages in each point of the transmission line the following three-step procedure has to be carried out (Paul, 1994):

1. Determine the per-unit length parameters of inductance, capacitance, conductance and resistance for the given line
2. Solve the resulting MTL equations
3. Incorporate the terminal conditions to determine the unknown coefficients in the general form of the solution.

According to (Paul, 1994), the determination of the per-unit length parameters may be performed using analytical or numerical methods. The analytical methods are generally suitable for simple cross-sectional structures. Generally, the cross-section of the conductor has to be circular. The line conductors have to be relatively widely spaced and immersed in a homogenous surrounding medium. Otherwise, numerical methods, such as FEM (finite element method) are required in order to approximate the per-unit length parameters. The approximation of multiconductor per-unit length parameters for MCMK power cables requires a numerical method. The cross-section of the phase conductor is not always circular, the space between the conductors is narrow compared to the conductor diameter and the medium surrounding of the conductors is not necessarily homogenous. In addition, the dielectric characteristics of the insulation materials used in MCMK cables are, generally, unknown and they depend on different factors, such as manufacturer of the insulation, temperature and humidity of the insulation. Due to the manufacturing tolerances, the cross-sectional geometry of the cable also varies causing variations to the per-unit length parameters. Some per-unit parameters calculated for MCMK cables with FEM are presented in (Ahola, 2001).

In order to solve the currents and the voltages in each point of the transmission line, also the terminal conditions have to be known. In case of MCMK low voltage power cable in industrial application, this means that all load impedances and sources have to be modelled with three phases and protective earth. This modelling may be difficult, because the phases of the appliances cannot be generally considered to be independent of each other. Therefore, the complexity of the models containing three phases and earth is greater than the complexity of two-port models. In addition, generally in industrial plants, the topology of the distribution network is known, but there do not exist cable and appliance parameters that are required to create sophisticated simulation models.

When low voltage power cables are evaluated with respect to power-line data transfer, signal attenuation is the most important parameter. It defines the maximum data transfer distance, when the network topology and required signal to noise ratio at the receiver is known. The other important parameter is the propagation speed of the electromagnetic wave in the cable, which is determined at high signal frequencies by electromagnetic characteristics of the insulations material. If a low loss cable is terminated by a strongly mismatched load, at certain frequencies the input impedance of the cable will drop close to the zero. In case of a branch cable, this causes steep notch in the frequency response of the communication channel and spike in the group delay. Generally, these frequencies are unfavourable for data transfer.

Due to these factors, instead of the MTL analysis, the two-conductor transmission line analysis is selected for the modelling of MCMK cables. When applying the two-conductor analysis, the

crosstalk with the conductors not used in the signalling is neglected. The two-conductor model analysis is simpler than the MTL analysis. Despite of its simplicity, the two-conductor analysis models the signal attenuation in the cable as well as the propagation velocity of the electromagnetic wave in the cable and the characteristic impedance of the cable. The two-conductor transmission line parameters of a cable may be determined performing two input impedance measurements. In addition, in selecting the two-conductor analysis also the modelling of the termination impedances may be performed by using two-port models. On the other hand, considering that power-line modems use two conductors in signalling, the use of two-port models may be justified. Since it is selected the two-port model, the characteristic impedance referred and discussed later in this work actually denotes the impedance between the conductors used in the signalling.

In this work, the purpose of the cable research is to develop an attenuation model and to determine two-conductor transmission line parameters for the researched cables in various signal couplings in the frequency band 100 kHz – 30 MHz. The cable research is performed by combining the transmission line theory and measurements. The target of this research is to provide helpful means for the planning of power-line communications in industrial low voltage distribution networks and to determine the applicability of the researched cables for the power-line data transfer. The primary frequency band of interest is 95 kHz – 148.5 kHz (GENELEC B, C and D) due to the current regulations in European countries.

2.3.2 Transmission Line Equations for the Two-Conductor Transmission Line

The transmission line model describes the propagation of an electromagnetic wave in a transmission line. The model assumes that the signal injected into the transmission line propagates along the line as a TEM wave (transverse electromagnetic). When the length of the cable is short compared to the wavelength of the electromagnetic wave, the transmission line analysis is not necessary. Instead, the line may be modelled e.g. by using a simple model consisting of distributed components. In case of a short transmission line, the distribution of current and voltage in the transmission line may be assumed to be constant. Generally, the transmission line is short if the electrical length of the line is less than $l < \lambda/16$ (Tomasini, 2001) or $l < \lambda/8$ (Huloux), where λ is the wavelength of the signal. The electrical length of the transmission line is dependent on the signal frequency and the propagation velocity of electromagnetic wave. The signal frequency f and the wavelength λ are linked together by equation:

$$\lambda = \frac{v_p}{f}, \tag{2.1}$$

where v_p is the propagation speed of the electromagnetic wave in the transmission line. In other words, the same transmission line can be considered to be either electrically long or short depending on the used signal frequency. The TEM wave has electric and magnetic fields that are transversal to each other and transversal to the propagation directions. The finite conductivity of the waveguiding conductors gives also an electric field component at the propagation directions of the wave. In real cables, the actual field structure is almost TEM and is called quasi-TEM. The differential length Δx of the transmission line is described with the equivalent circuit (figure 2.6).

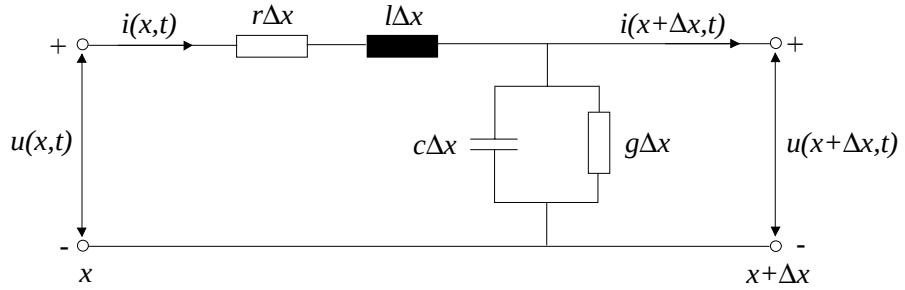

Figure 2.6. Equivalent circuit of a differential length Δx of a two-conductor transmission line. The quantities $u(x,t)$, $u(x+\Delta x,t)$, $i(x,t)$ and $i(x+\Delta x,t)$ denote the instantaneous voltages and currents at locations x and $x+\Delta x$.

The transmission line equations are derived from the equivalent circuit (figure 2.5). The voltage and the current in the transmission line may be presented with the coupled partial differential equations:

$$\frac{\partial u(x,t)}{\partial t} = -ri(x,t) - l\frac{\partial i(x,t)}{\partial t} \tag{2.2}$$

$$\frac{\partial i(x,t)}{\partial t} = -gu(x,t) - c\frac{\partial u(x,t)}{\partial t}, \tag{2.3}$$

where r, l, g and c are the distributed resistance, inductance, conductance and capacitance of the transmission line. The variables x and t denote place and time. The solution for this differential pair with sinusoidal and stationary voltage and current is:

$$\mathbf{U}(x) = \mathbf{U}^{+}e^{-\gamma x} + \mathbf{U}^{-}e^{\gamma x} \tag{2.4}$$

$$\mathbf{I}(x) = \frac{1}{\mathbf{Z}_0}\left(\mathbf{U}^{+}e^{-\gamma x} - \mathbf{U}^{-}e^{\gamma x}\right), \tag{2.5}$$

where $\mathbf{U}$ and $\mathbf{I}$ are the sinusoidal voltage and current, $\mathbf{Z}_0$ is the characteristic impedance and γ is the propagation constant. The electromagnetic wave propagates both $+$ and – directions along the transmission line length x. The positive propagation direction is defined to be from the generator to the load. The propagation constant γ determines the propagation speed and attenuation of the electromagnetic wave. The equation for the propagation constant is given by:

$$\gamma = \sqrt{(r + j\omega r)(g + j\omega c)} = \alpha + j\beta, \tag{2.6}$$

where α is the attenuation coefficient and β is the propagation coefficient. The characteristic impedance of the transmission line is:

$$\mathbf{Z}_0 = \sqrt{\frac{r + j\omega l}{g + j\omega c}}. \tag{2.7}$$

In case of a lossless $(r = 0, g = 0)$ or distortionless transmission line, the equation of the characteristic impedance is simply:

$$Z_0 = \sqrt{\frac{l}{c}} \,. \tag{2.8}$$

In case of a lossless and distortionless transmission line, the propagation speed of the electromagnetic wave v_p is:

$$v_\mathrm{p} = \frac{1}{\sqrt{lc}} = \frac{1}{\sqrt{\mu_0 \mu_{\mathrm{r,i}} \varepsilon_0 \varepsilon_{\mathrm{r,i}}}} = \frac{\omega}{\beta}, \tag{2.9}$$

where both μ_0 and ε_0 are the permeability and permittivity of vacuum. The relative permeability $\mu_{\mathrm{r,i}}$ and permittivity $\varepsilon_{\mathrm{r,i}}$ are the parameters of the insulation material of the transmission line. The propagation speed is only dependent on the electromagnetic characteristics of the insulation material when the currents are flowing on the surfaces of the conductors. At low signal frequencies, the currents also flow inside the conductors because of the finite conductivity of the conductors. The current flowing inside the conductor causes an internal inductance, which increases the total distributed inductance of the transmission line. Correspondingly, the increase in the distributed inductance decreases the propagation velocity of the electromagnetic wave (equation 2.9) and increases the characteristic impedance (equation 2.7). The distribution of the current on the cross-sectional area of the conductor is described with a variable penetration or skin depth:

$$\delta = \frac{1}{\sqrt{\frac{1}{2} \omega \mu_0 \mu_{\mathrm{r,c}} \sigma_\mathrm{c}}}, \tag{2.10}$$

where ω is the angular frequency of the signal propagating in the transmission line, $\mu_{\mathrm{r,c}}$ is the relative permeability of the conductor material, and σ_c is the conductivity of the conductor material. The skin effect also affects the losses of the conductor. The current density on the surface of the conductor increases as a function of frequency increasing the resistive losses.

2.3.3 Effect of Transmission Line Discontinuity

When an electromagnetic wave bound to a transmission line reaches an impedance mismatch, part of the power delivered by the wave is reflected and the rest of the power passes through the interface. The impedance mismatch may be e.g. the load impedance connected to the end of transmission line or a change in the type of transmission line. As data communications is concerned, the reflection is harmful. It produces standing voltage and current waves in the transmission line. The standing waves increase the power losses and make the input impedance of the cable terminated by the load impedance frequency variant (Räisänen, 1993). The complex reflection coefficient $\mathbf{\Gamma}_\mathrm{R}$ for a transmission line expressed using the characteristic impedance $\mathbf{Z}_0$ and complex termination impedance $\mathbf{Z}_\mathrm{L}$ is:

$$\mathbf{\Gamma}_{\mathrm{R}} = \frac{\mathbf{Z}_{\mathrm{L}} - \mathbf{Z}_0}{\mathbf{Z}_{\mathrm{L}} + \mathbf{Z}_0} = \left|\mathbf{\Gamma}_{\mathrm{R}}\right| \cdot \mathrm{e}^{j\theta} . \tag{2.11}$$

The reflection coefficient is $\mathbf{\Gamma}_R = 0$, if the load impedance of the transmission line is perfectly matched or the length of transmission line is infinite. In any other case, part of the transmitted power is reflected back at the impedance mismatch (figure 2.7). The complex reflection coefficient also affects the relations of the voltage and current amplitudes on the load impedance.

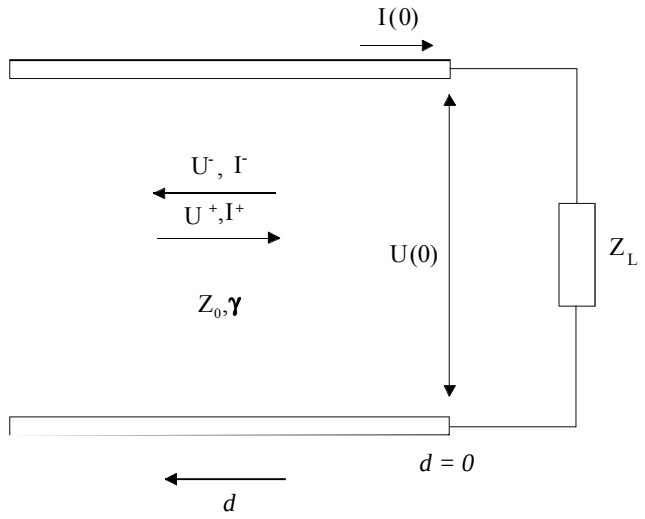

Figure 2.7. Power reflection at complex load impedance. The power reflection is caused by the impedance mismatch at the interface of the load and cable. Part of the power delivered by the wave is dissipated at the load and the rest of the power is reflected back.

The sinusoidal voltage and current in terms of the place *d* (figure 2.7) are:

$$\mathbf{U}(d) = \mathbf{U}^{+}\mathrm{e}^{j\gamma d}\left(1 + \mathbf{\Gamma}_{\mathrm{R}}\mathrm{e}^{-j2\gamma d}\right) \tag{2.12}$$

$$\mathbf{I}(d) = \frac{\mathbf{U}^{+}}{\mathbf{Z}_0}\mathrm{e}^{j\gamma d}\left(1 - \mathbf{\Gamma}_{\mathrm{R}}\mathrm{e}^{-j2\gamma d}\right). \tag{2.13}$$

The complex reflection coefficient either lengthens or shortens the electrical length of the transmission line. The amount of the impedance mismatch at the interface of the load impedance and transmission line may be expressed by using a single parameter standing-wave ratio (SWR). It describes the relation of the maximum and minimum current and voltage amplitudes in a transmission line. In case of a matched transmission line, the standing-wave ratio is $\mathrm{SWR} = 1$. The equation for the standing-wave ratio is given by:

$$\mathrm{SWR} = \frac{\left|\mathbf{U}_{\max}\right|}{\left|\mathbf{U}_{\min}\right|} = \frac{\left|\mathbf{I}_{\max}\right|}{\left|\mathbf{I}_{\min}\right|}. \tag{2.14}$$

The higher the SWR value is, the greater is the impedance mismatch between transmission line and load impedance.

2.3.4 Determination of Transmission Line Parameters by Input Impedance Measurements

The standing-wave ratio (SWR) measurement with a slotted line is traditionally used way to determine the characteristic impedance of an unknown coaxial air insulated transmission line or an unknown termination impedance of a known coaxial and air insulated transmission line in a laboratory environment (Nannapareni, 2000). The method is based on the measuring of voltage minimums, maximums and the places of the voltage minimums and maximums at the slotted coaxial cable. Due to the structure of the cable, the method is not suitable for low voltage multiconductor power cables. Hence, another method has to be applied. Another way to determine the characteristic impedance of a transmission line is to perform two input impedance measurements for the transmission line.

In order to determine the characteristic impedance and the propagation constant of the cable, the input impedance has to be measured when the cable end is open and short-circuited. When the cable end is short-circuited, the voltage at the end is zero and when the cable end is open, the current at the end is zero. The complex input impedance $\mathbf{Z}_{\text{ino}}$ for the cable with open end and with length L, is according to equations 2.4 and 2.5:

$$\mathbf{Z}_{\text{ino}} = \mathbf{Z}_0 \operatorname{cotanh}(\boldsymbol{\gamma} L). \tag{2.15}$$

When the end of the cable is short-circuited the equation for the input impedance $\mathbf{Z}_{\text{ins}}$ is:

$$\mathbf{Z}_{\text{ins}} = \mathbf{Z}_0 \tanh(\boldsymbol{\gamma} L). \tag{2.16}$$

The equation for the characteristic impedance may be formed combining equations 2.15 and 2.15:

$$\mathbf{Z}_0 = \sqrt{\mathbf{Z}_{\text{ins}} \mathbf{Z}_{\text{ino}}}\,, \tag{2.17}$$

and the solution for the propagation constant is:

$$\boldsymbol{\gamma} = \frac{1}{L} \operatorname{arctanh} \sqrt{\frac{\mathbf{Z}_{\text{ins}}}{\mathbf{Z}_{\text{ino}}}}\,. \tag{2.18}$$

The real part of the propagation constant is attenuation coefficient α and the imaginary part is propagation coefficient β. Distributed inductance l and capacitance c can be solved utilising the equations for the characteristic impedance and propagation constant (equations 2.17 and 2.18):

$$l = \frac{\operatorname{Im}\{\mathbf{Z}_0 \boldsymbol{\gamma}\}}{\omega} \tag{2.19}$$

$$c = \frac{\operatorname{Im}\{\mathbf{Z}_0 / \boldsymbol{\gamma}\}}{\omega}\,. \tag{2.20}$$

The attenuation coefficient α determines the losses of the cable. It consists of resistive losses of the conductors and the dielectric and the resistive losses of the insulation material. The attenuation coefficient may be solved from the propagation constant:

$$\alpha = \mathrm{Re}\{\gamma\}. \tag{2.21}$$

2.3.5 Input Impedance Measurements

A series of input impedance measurements was carried out for three MCMK low voltage power cables. The phase conductor cross-sectional areas of all the selected cables were different. In addition, two different cross-sectional geometries were represented in the test cable group. The selected cable types are generally used in industrial plants as motor cables. The measured cables and the lengths of the cables were:

- Reka EMCMK 3x16+16, 9.7 metres
- Pirelli MCCMK 3x35+16, 100 metres
- Reka EMCMK 3x120+70, 17.8 metres

The measured Pirelli cable was manufactured by Draka NK Cables Ltd. in Vantaa in Finland and Reka cables were manufactured by Reka Cables Ltd. In Hyvinkää in Finland. The cable lengths were not the same. The longest cable was 100 metres and the shortest 9.7 metres. Since the length of the measured cables varied rather significantly, the test environment was not exactly the same for all the cables. This inevitably has an effect on the results. For example, a bending of the cable may cause an impedance mismatch and power reflections, which affect the measurement results. However, at least in the GENELEC frequency band, which is used for the sensor level data transfer of the on-line condition monitoring system of electric motors, all measured cables are electrically short.

The cables were measured in the signal couplings: phase to protective earth (L1, PE), phase to phase (L1, L2), all phases together as signal conductor and protective earth as return conductor (L1+L2+L3, PE). Additionally, the signal coupling (L1, L2+L3) was measured for the cable MCCMK 3x35+16. It is a normal signal coupling when the electric motor is driven by a variable speed drive. One or two of the phases are switched to the upper branch of the DC-link circuit (direct current) and the other phases are connected to the lower branch. In each signal coupling, the input impedance was measured when the cable end was short-circuited and when the cable end was open. The measured frequency band was 100 kHz – 30 MHz and a linear frequency sweep was applied. The impedance analyser HP 4194A stored 401 data points (frequency, absolute value and phase) for each measurement.

Three of impedance measurements are illustrated in figures 2.8, 2.9 and 2.10. In all figures, the effects of the impedance mismatch at the cable end can be seen. There are frequently repeating slopes and peaks in the impedance curves. At the impedance peak, the cable looks like a parallel resonance circuit and at the impedance slope it looks like a serial resonance circuit. In case of a lossless cable, the input impedance should be infinite when the cable is in parallel resonance and the input impedance of the cable should be zero when the cable is in serial resonance. At the resonance frequency, the phase of the input impedance is always zero. The input impedance in the parallel resonances is hundreds of ohms when the signal frequency is low. When the signal frequency increases, the peaks get lower. This means that the losses of the cable increase as a function of frequency. At high signal frequencies and with long cables, the electromagnetic wave reflected back from the impedance mismatch in the cable end attenuates almost completely before it reaches the sending point again. Due to this property, the oscillation of the input impedance attenuates almost completely at high signal frequencies (figure 2.10).

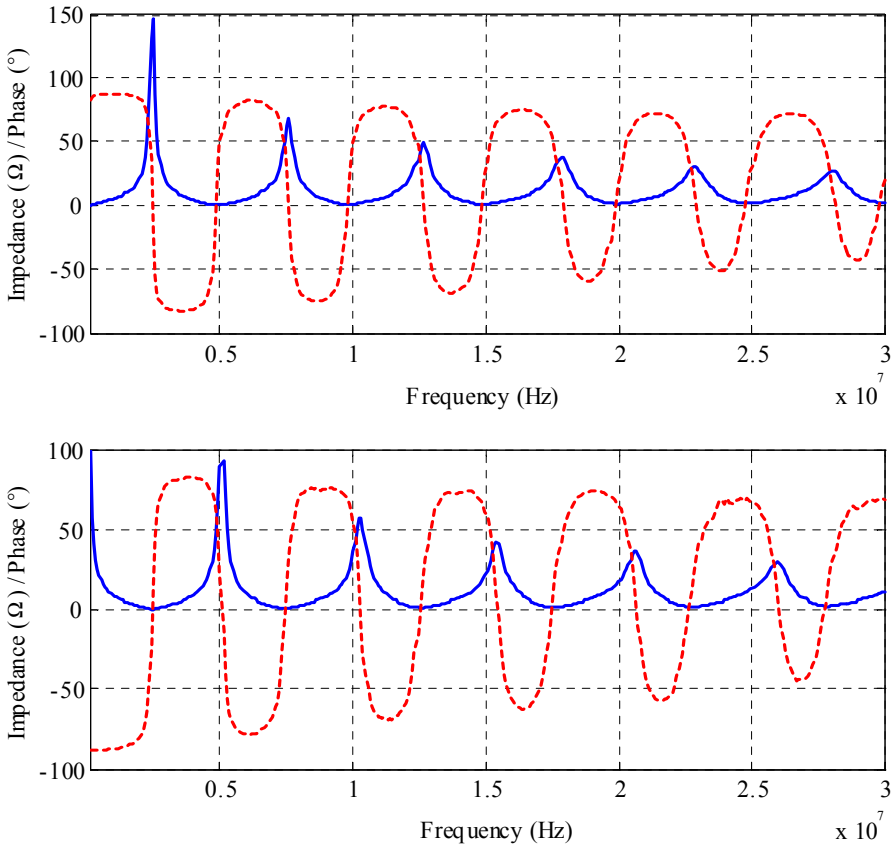

Figure 2.8. Input impedance (continuous line) and phase (dashed line) as a function of frequency for the low voltage power cable EMCMK 3x120+70. The signal coupling is (L1+L2+L3, PE) and measured frequency band is 100 kHz – 30 MHz. The upper figure is measured the cable end being is short-circuited and the lower figure is measured the cable end being open. The length of the cable is 17.8 metres.

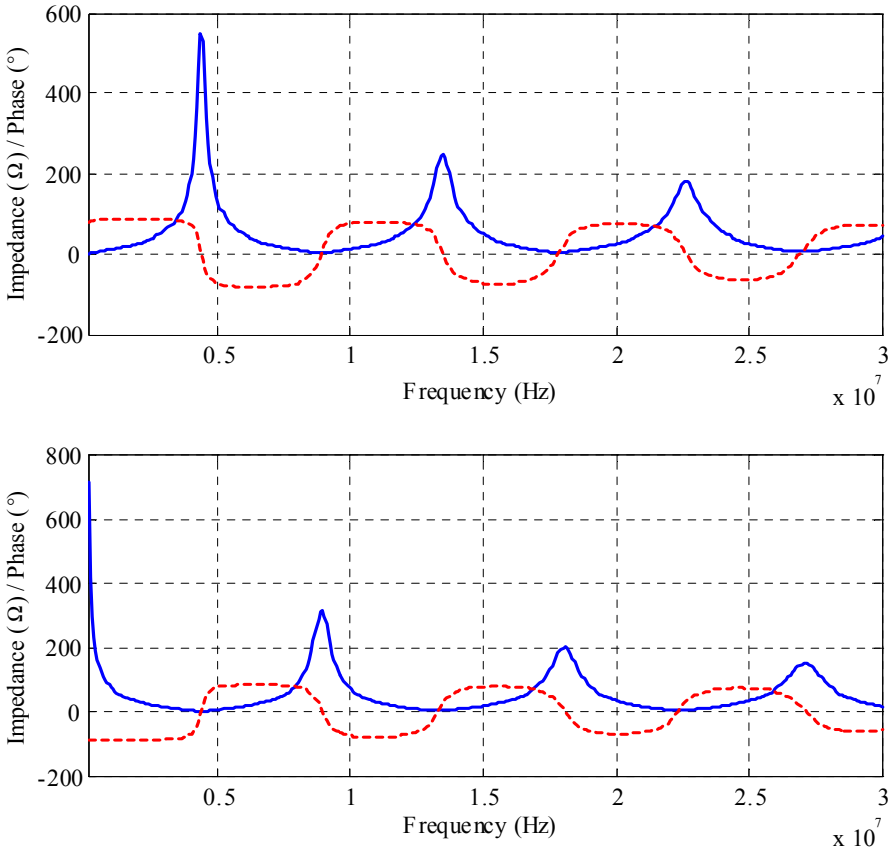

Figure 2.9. Input impedance (continuous line) and phase (dashed line) as a function of frequency for the EMCMK 3x16+16 cable. The signal coupling is (L1, PE) and length of the cable is 9.7 metres. The measured frequency band is 100 kHz – 30 MHz. The upper figure is measured the cable end being short-circuited and the lower figure is measured the cable end being open.

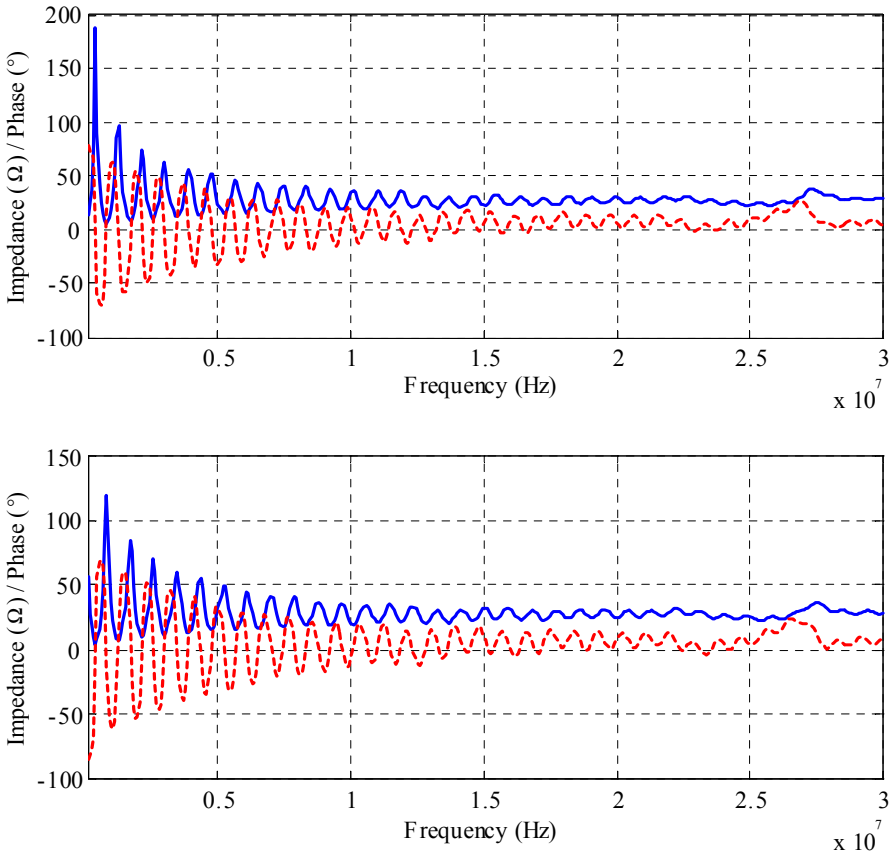

Figure 2.10. Input impedance (continuous line) and phase (dashed line) as a function of frequency for the MCCMK 3x35+16 cable. The signal coupling is (L1, L2) and the length of the cable is 100 metres. The measured frequency band is 100 kHz – 30 MHz. The upper figure is measured the cable end being short-circuited and the lower figure is measured the cable end being open.

2.3.6 Characteristic Impedance and Propagation Velocity

The characteristic impedance describes the relation between distributed capacitance and distributed inductance of a transmission line. Every transmission line and even a vacuum have a characteristic impedance. The importance of the characteristic impedance is based on the fact that it determines the relation of the reflected and absorbed power at the interface, where impedance mismatch occurs. Typical cross-sectional structures of low voltage MCMK power cables are illustrated in figure 2.11. A layer of insulation material between the phase conductors and phase conductor and protective earth conductor is thin in proportion to the cross-sectional dimensions of the conductors. In addition, the permittivity of the insulation material is higher than permittivity of the vacuum. These facts together form high distributed capacitance and low distributed inductance values, which make the characteristic impedances of the MCMK cables low.

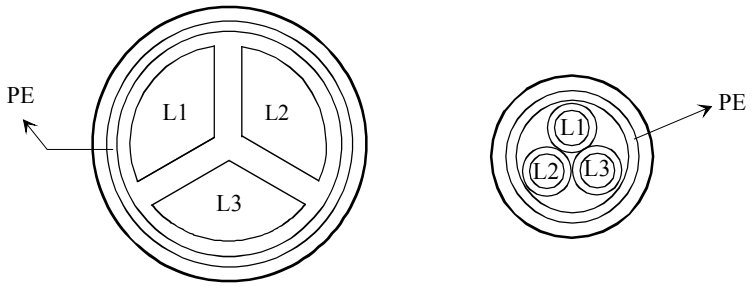

a) b)

Figure 2.11. Cross-sectional structures of MCMK type low voltage power cables.

The characteristic impedance is mainly dependent on the distributed capacitance and the distributed inductance of the cable. Additionally, also the distributed resistance and conductance exert an influence on the characteristic impedance (equation 2.7). Both the distributed capacitance and inductance are supposed to remain close to constant in the researched frequency band 100 kHz – 30 MHz. The internal inductance of the conductor is supposed to be insignificant. This assumption is based on the skin depth, which is at the frequency 100 kHz and with the copper conductor $\delta \approx 0.3\,\text{mm}$. Correspondingly, the cross-sectional conductor area of the phase conductor is $16\,\text{mm}^2$ or more including all the researched cables. In case of a circular cross-section, this corresponds the conductor radius of 2.26 mm. The internal inductance for the wire with circular cross-section and uniform cross-sectional current distribution is given by equation:

$$l_{\text{i,dc}} = \frac{\mu_0}{8\pi} = 0.5 \cdot 10^{-7}\ \text{H/m}\,. \tag{2.22}$$

Two characteristic impedance curves that are calculated using measurement data are illustrated in figures 2.12 and 2.13. In figure 2.13, there occurs oscillation in the calculated curves. These are probably caused either by crosstalk or measurement fixture. The signal injected into the conductors L1 and PE also couples with capacitive and inductive coupling into the floating conductors L2 and L3. The signal coupled into the conductors L2 and L3 affects the voltages and currents in the signalling conductors L1 and PE, respectively.

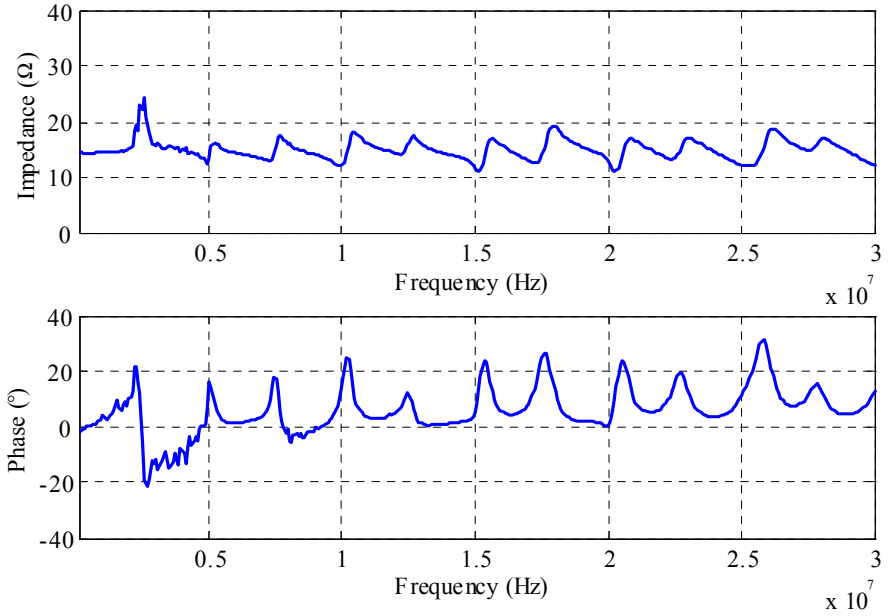

Figure 2.12. Calculated characteristic impedance and phase of the characteristic impedance for EMCMK 3x120+70 (length 17.8 meters) cable in the frequency band 100 kHz – 30 MHz. The signal coupling is (L1, PE). The curves are calculated using the measurement data.

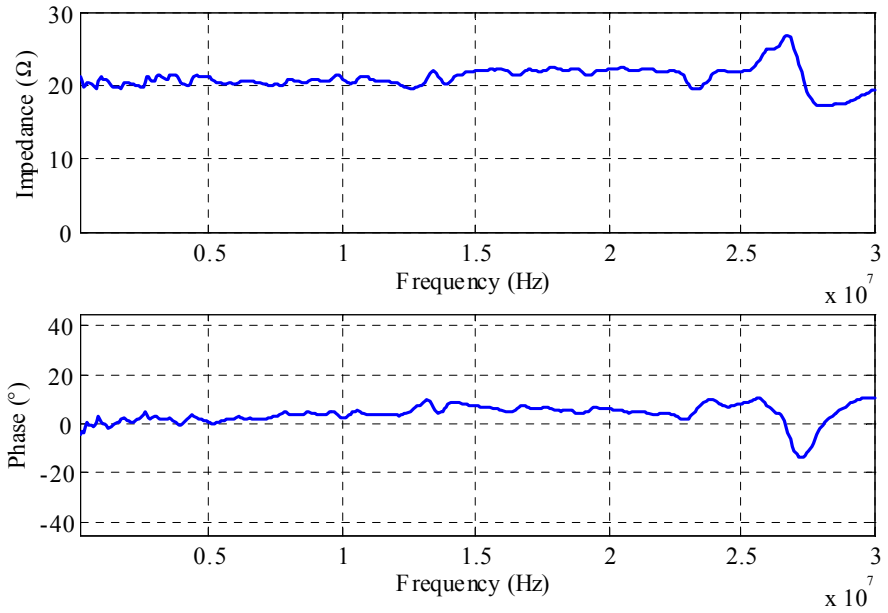

Figure 2.13. Characteristic impedance and phase of the characteristic impedance for MCCMK 3x35+16 cable (length 100 meters, signal coupling L1+L2, L3) in the frequency band 100 kHz – 30 MHz. The curves are calculated using the measurement data.

In order to verify the calculated characteristic impedance values, some additional measurements were performed. When a transmission line is terminated with a resistance equivalent to the characteristic impedance of the transmission line, the standing waves should not be formed into the transmission line. In other words, the input impedance of the cable should stay constant as a function of frequency. A sample input impedance measurement for an EMCMK 3x120+70 cable in the signal coupling (L1, PE), terminated by a resistor (15 Ω), is illustrated in figure 2.14. The selected termination impedance is close to the measured characteristic impedance of the cable. There are no visible impedance oscillations in figure 2.14. In other words, the measurement based characteristic impedance is close to the right value. The characteristic impedance (figure 2.14) increases slightly as a function of frequency due to the increase of the distributed resistance and decrease of the distributed capacitance as function of frequency. The decrease in the distributed capacitance is caused by the frequency variant electrical characteristics of PVC insulation material used in the cable (figure 2.5).

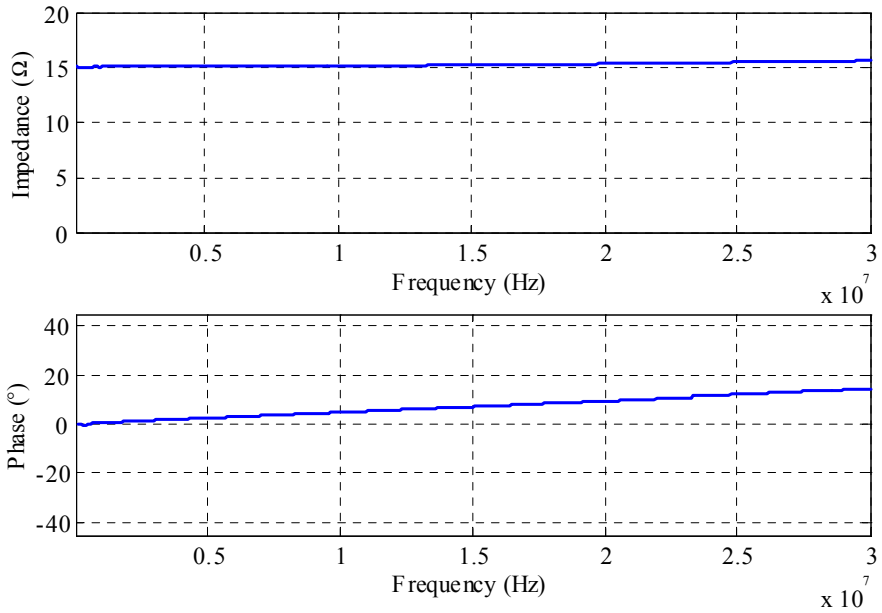

Figure 2.14. Measured input impedance and phase of the impedance for the EMCMK 3x120+70 (length 17.8 metres) low voltage power cable. The impedance is measured in the signal coupling (L1, PE) and the cable is terminated with a 15 Ω resistor. The measured frequency band is 100 kHz – 30 MHz.

The characteristic impedances, propagation velocities, distributed capacitances and distributed inductances that are calculated from the measurement data for all the measured cables and for all signal couplings are listed in table 2.1. The values given in table 2.1 are median values for the frequency band 100 kHz – 30 MHz. Each individual measurement consists of 401 linearly spaced data points. The median values are used in order to minimise the effect of disturbances mainly originating from the measurements. The procedure for the calculating parameters is presented in chapter 2.3.4.

Generally, the determined characteristic impedances are low compared to the characteristic impedances of the cables used in data transfer. For example, 120 Ω, 100Ω, 75 Ω and 50 Ω are typical characteristic impedance values for commonly used data transfer and signalling cables.

The impedance values (table 2.1) are close to the measured and calculated characteristic impedance values given for medium and low voltage power cables (Hensen, 1999), (Bostoen, 2000) and (Dostert, 2001). In (Dostert, 2001), the characteristic impedance for the MCMK type PVC insulated cable NYCY70SM/35 was calculated. The cable was coupled as a coaxial transmission line (signal coupling L1+L2+L3, PE) and analytical equations to solve the transmission line parameters of the coaxial cable were applied. The calculated characteristic impedance is about 7-8 Ω in the frequency band 1-20 MHz. In (Hensen, 1999), the characteristic impedance of a single conductor polyethylene insulated medium voltage power cable ABB NA2XS(FL)2Y 1x120RM/16 12/20 kV was measured. The measured characteristic impedance of the cable was 27 Ω. The measurement was taken up to the signal frequency 10 MHz.

The determined characteristic impedances (table 2.1) are close to each other with the cables EMCMK 3x120+70 and MCCMK 3x35+16 in each signal coupling. The phase conductors of both cables are sector-shaped and the relative cross-sectional dimensions for the conductors and insulation thickness are close to each others. The slight difference in the characteristic impedances may be explained by the permittivity of the insulation material. The difference in permittivity between these cables can be noticed from the propagation velocities (table 2.1). The cross-sectional geometry of the EMCMK 3x16+16 cable differs from the geometry of the two other measured cables. The phase conductors of EMCMK 3x16+16 are circular. Compared to the cables with sector-shaped phase conductors, the distributed inductance increases and the distributed capacitance decreases. This leads to larger characteristic impedance values than with the cables with sector-shaped phase conductors (equation 2.8).

Table 2.1. Characteristic impedance, propagation velocity, distributed inductance and distributed capacitance for MCMK type low voltage power cables. The values are calculated medium values from the impedance measurement data in frequency band 100 kHz – 30 MHz (Ahola, 2001)

Reka EMCMK 3x16+16				
Signal coupling	Z_0 (Ω)	v_p/c_0	l (nH/m)	c (pF/m)
L1+L2+L3, PE	16	0.58	89	372
L1, PE	30	0.58	173	191
L1, L2	42	0.57	245	138
Pirelli MCCMK 3x35+16				
Signal coupling	Z_0 (Ω)	v_p/c_0	l (nH/m)	c (pF/m)
L1+L2+L3, PE	8	0.66	39	656
L1, PE	16	0.66	83	313
L1, L2	27	0.64	141	190
L1,L2+L3	21	0.64	109	247
Reka EMCMK 3x120+70				
Signal coupling	Z_0 (Ω)	v_p/c_0	l (nH/m)	c (pF/m)
L1+L2+L3, PE	7	0.61	40	756
L1, PE	15	0.60	82	371
L1, L2	23	0.62	123	237

The propagation velocities of the electromagnetic wave in the measured cables are in the range of $0.57 - 0.66 c_0$ (table 2.1). (Bartolucci, 2001) introduced the approximate value of $0.5 c_0$ for the propagation velocity in a low voltage PVC insulated power cable. In order to verify the

calculated propagation velocity values, a separate propagation velocity measurement was carried out. The test arrangement is illustrated in figure 2.15. The surge wave was injected into the MCCMK 3x35+16 cable. The signal coupling (L1, L2+L3) was used and the signalling conductors were terminated by a resistor equivalent to the characteristic impedance of the cable in the applied signal coupling in order to avoid reflections due to the impedance mismatch at the cable end. The Hameg HM 8131-2 function generator was used as a surge wave source. The voltages were measured from the input end and output end of the cable. The ground of the oscilloscope probe in the output end was not connected in order to avoid current flowing through the ground of the oscilloscope probes. The measured propagation time of the pulse from the sending end to the receiving end was t_p =560ns. With the cable length of 100 metres, the corresponding propagation velocity is about $v_p = 0.6c_0$. The result is close to the calculated value $v_p = 0.64c_0$ based on the input impedance measurements (table 2.1).

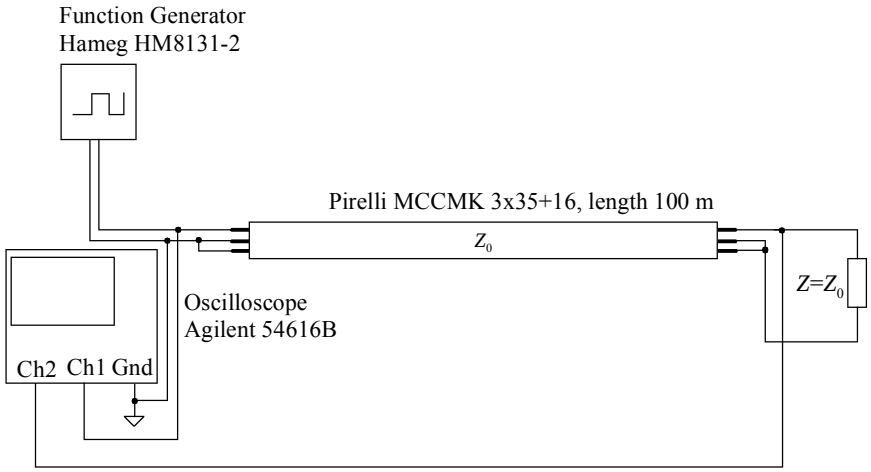

Figure 2.15. Test arrangement for the measurement of signal propagation velocity in a low voltage power cable with a surge wave test.

2.3.7 Signal Attenuation

The conductors and insulation materials of signalling and power cables are not ideal. Part of the power that the transmitter injects into the cable does not reach the receiver. The loss mechanisms are:

- Resistive losses of the conductors
- Dielectric losses of the insulation
- Radiation losses
- Coupling losses

The main loss mechanisms of low voltage power cables at signal frequencies used in power-line communications are the dielectric losses, resistive losses and coupling losses. The radiation losses are significant if the separation of the conductors is an appreciable fraction of the wavelength (Tomasini, 2001). With the cables researched and in the frequency band 100 kHz – 30 MHz this condition is not fulfilled.

Transmission line discontinuities, such as mechanical connections, changes in cable type or load appliances, cause coupling losses. The amount of coupling losses depends for example on the topology of the distribution network, the signal frequency, characteristics of cabling and

characteristics of devices connected to the distribution network. The resistive losses of the conductor are caused by the finite conductivity of conductors. At high frequencies, the current is forced to flow on the surface of the conductor due to the skin effect. The resistive losses increase as a function of frequency with relation of $r \sim \sqrt{f}$.

Dielectric losses occur in the insulation material. The polarised molecules inside the insulation material turn synchronised to the frequency of the electric field. The friction between the molecules causes power losses at each time when the electric field changes polarity. In addition, the resistivity of the insulation material is finite. Existence of leakage currents in the insulation material causes also losses. The losses of the insulation material are expressed by the term loss tangent or dissipation factor $\tan\delta$:

$$\tan\delta = \frac{\varepsilon_{\mathrm{i}}'' + \frac{\sigma_{\mathrm{i}}}{\omega\varepsilon_0}}{\varepsilon_{\mathrm{i}}'}, \qquad (2.23)$$

where $\varepsilon_{\mathrm{i}}'$ is the real part and $\varepsilon_{\mathrm{i}}''$ is the imaginary part of the relative complex permittivity of the insulation material and σ_{i} is the conductivity of the insulation material. Generally, in literature, the conductive losses are included in the imaginary part of the relative complex permittivity. The distributed conductance g for the transmission line model is given by:

$$g = \omega c \tan\delta . \qquad (2.24)$$

The attenuation coefficients for PVC insulated MCMK low voltage power cables were calculated from the impedance measurement data. The procedure to solve the attenuation coefficient is introduced in chapter 2.3.4. The attenuation curves are almost independent of the cross-sectional area of phase conductor and signal coupling (figures 2.16, 2.17 and 2.18). The cross-sectional area of the phase conductor of the smallest cable is 16 mm^2 and the cross-sectional area of the phase conductor of the largest cable is 120 mm^2. If the losses in the conductors are dominant, there should be a significant difference between the attenuation curves. According to the calculated results, it can be assumed that instead of the resistive losses, the dielectric losses are dominant in PVC insulated low voltage power cables in the frequency band 100 kHz – 30 MHz.

The signal attenuation coefficient of the measured cables increases as a function of frequency. However, the frequency relation of the attenuation coefficient is not linear. The reasons for the nonlinear behaviour of the attenuation coefficient are the dielectric characteristics of PVC insulation material and the skin effect. According to figure 2.5, both the dielectric constant and dissipation factor of PVC decrease as a function of frequency at frequencies higher than 1 MHz. These both affect directly the distributed conductance of the transmission line (equation 2.24) making it nonlinear as a function of frequency. The nonlinear distributed resistance and conductance together cause the attenuation coefficient to become nonlinear as a function of frequency.

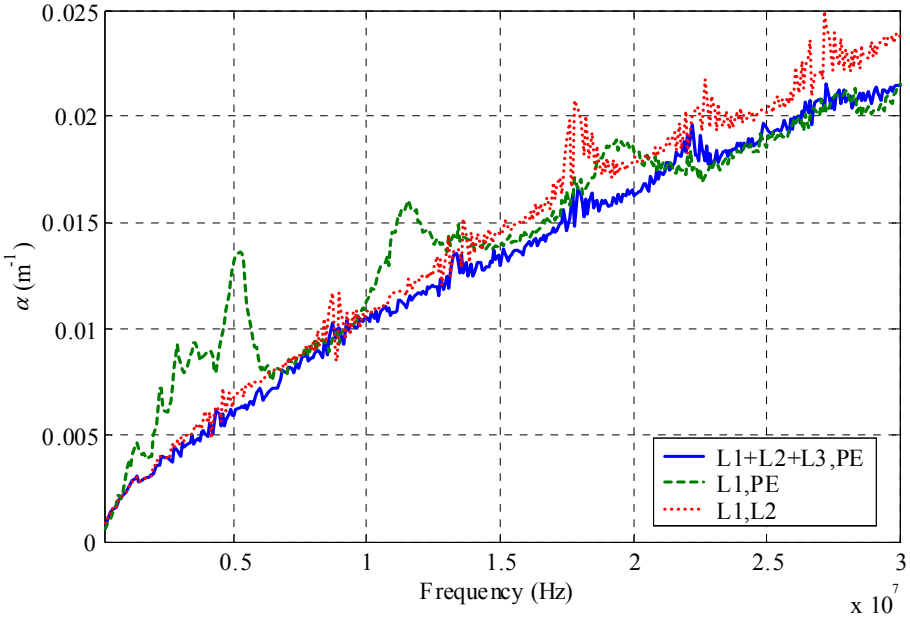

Figure 2.16. Attenuation coefficients for the EMCMK 3x16+16 cable as a function of frequency in the frequency band 100 kHz – 30 MHz. The values are calculated from the input impedance measurement data.

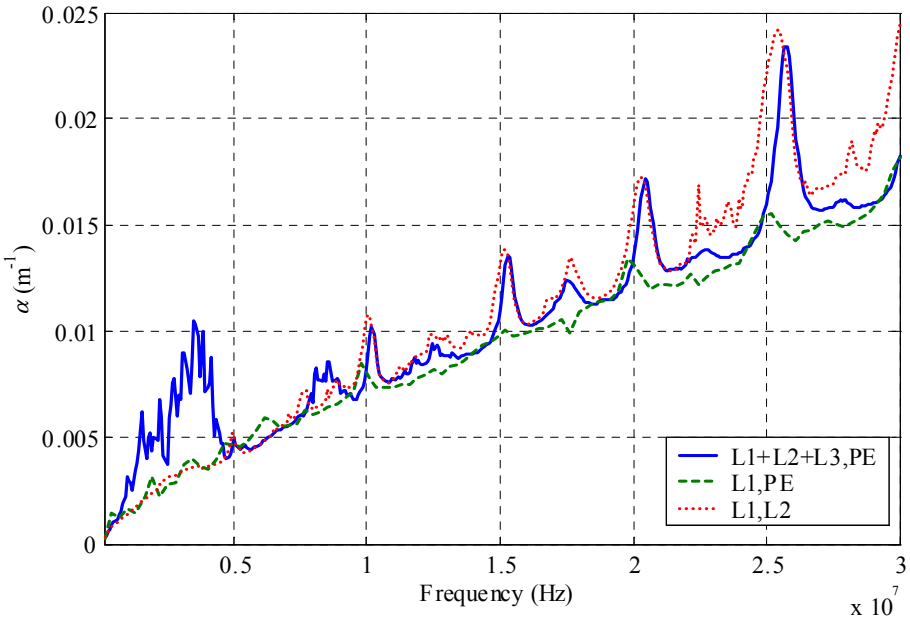

Figure 2.17. Attenuation coefficients for the EMCMK 3x120+70 cable as a function of frequency in the frequency band 100 kHz – 30 MHz. The values are calculated using the input impedance measurement data.

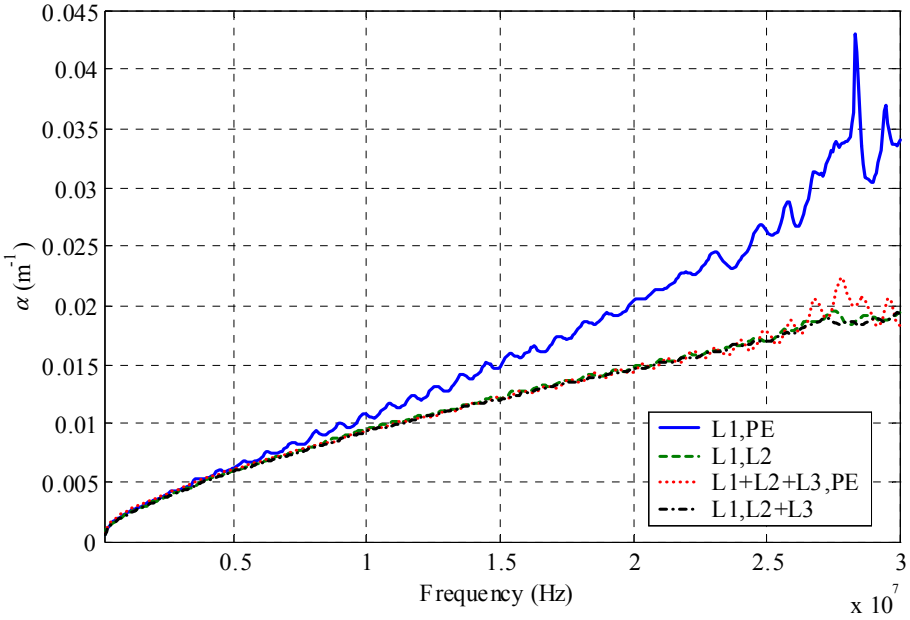

Figure 2.18. Attenuation coefficients for the MCCMK 3x35+16 cable as a function of frequency in the frequency band 100 kHz – 30 MHz. The values are calculated using the input impedance measurement data.

In order to verify the attenuation coefficient curves calculated from the impedance measurements, additional measurements were carried out. The attenuation of the cable MCCMK 3x35+16 (length 100 m) was measured. In each measured signal coupling, the cable was terminated by a resistor value equivalent to the characteristic impedance of the cable in the measured signal coupling. The termination resistor was added in order to make the transmission line matched. A sinusoidal signal was injected into the cable using a function generator and the voltages were measured with oscilloscopes at both ends of the cable. The attenuation coefficients were calculated using the measured peak-to-peak voltage values. The results are illustrated in figure 2.19. The upper frequency limit of the measurement was 15 MHz due to the limits of the Hameg HM 8181-2 function generator used in the measurement. The results are corresponding to the curves illustrated in figure 2.18. However, in both figures 2.18 and 2.19, the signal voltage attenuation in the signal coupling (L1, PE) is higher than in the other signal couplings.

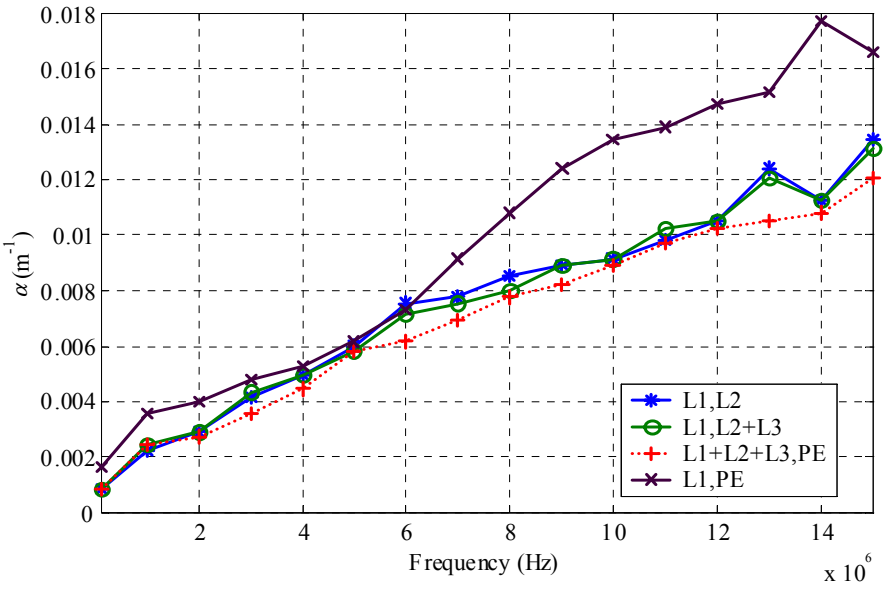

Figure 2.19. Measured attenuation coefficients for the MCCMK 3x35+16 cable as a function of frequency in the frequency band 100 kHz – 30 MHz. The measurements are performed in order to verify the results calculated from the input impedance measurement data.

Since the attenuation curves (figures 2.16, 2.17 and 2.18) are close to each other and behave similarly as a function of frequency, the general measurement based model for signal attenuation in MCMK type low voltage power cables was formed. The average attenuation coefficient was calculated for each measurement data point representing unique frequency. After that, a formula for the attenuation coefficient as a function of frequency was formed using the power curve fitting algorithm (Ahola, 2001):

$$\alpha(f) = 0.5 \cdot 10^{-6} \cdot f^{0.6}. \qquad (2.25)$$

Theoretically, there should also exist a constant in the attenuation formula (equation 2.25) describing the DC attenuation. However, in the frequency band 100 kHz – 30 MHz, the effect of DC attenuation is insignificant compared to the frequency related attenuation.

The attenuation coefficient given by (equation 2.25) is illustrated in figure 2.20 and presented in format (dB/m) in figure 2.21, which is more illustrative to engineers. The theory based signal attenuation curve for the MCMK type cable NYC70SM/35 in the frequency band 1-20 MHz is presented in (Dostert, 2001). The signal attenuation level introduced in (Dostert, 2001) is slightly lower than the attenuation level measured and determined for cables in this work. For example, at the signal frequency 5 MHz, the corresponding signal attenuation values are 0.03 dB/m and 0.044 dB/m. At the signal frequency 20 MHz, the respective values are 0.05 dB/m and 0.115 dB/m. The difference can be explained by the dissipation factor of PVC. In (Dostert, 2001), the dissipation factor was approximated to decrease from value 0.05 at 1 MHz to value 0.01 at 20 MHz. This is probably a too big drop at least for the cables measured in this work.

The comparison of signal attenuation between MCMK low voltage power cables and generally used data transmission cables is also interesting. The cable characteristics used in the comparison are acquired from (Farnell, 2002). At signal frequency 10 MHz the low cost coaxial cable

RG-59 ($Z_0 = 75\,\Omega$, polyethylene insulation) attenuates a signal 0.037 dB/m. The corresponding value for the MCMK power cable is 0.07 dB/m. The typical twisted pair cable (Category 5, polyethylene insulation) used in computer networks attenuates 0.09 dB/m at 20 MHz and the attenuation value for the MCMK power cable is 0.1 dB/m.

In low-cost data transmission cables, polyethylene is used as insulation material instead of PVC used in MCMK cables. Dielectric losses of PVC insulation material are about 50-100 times larger than those of polyethylene (Harper, 1975). On the other hand, due to the larger conductor diameter, the resistive losses of low voltage power cable conductors are smaller than the losses of cables designed for data transfer. The dielectric losses are the main loss mechanism at radio frequencies in PVC insulated low voltage power cables and the conductor losses are the main loss mechanism in commonly used data transfer and signalling cables.

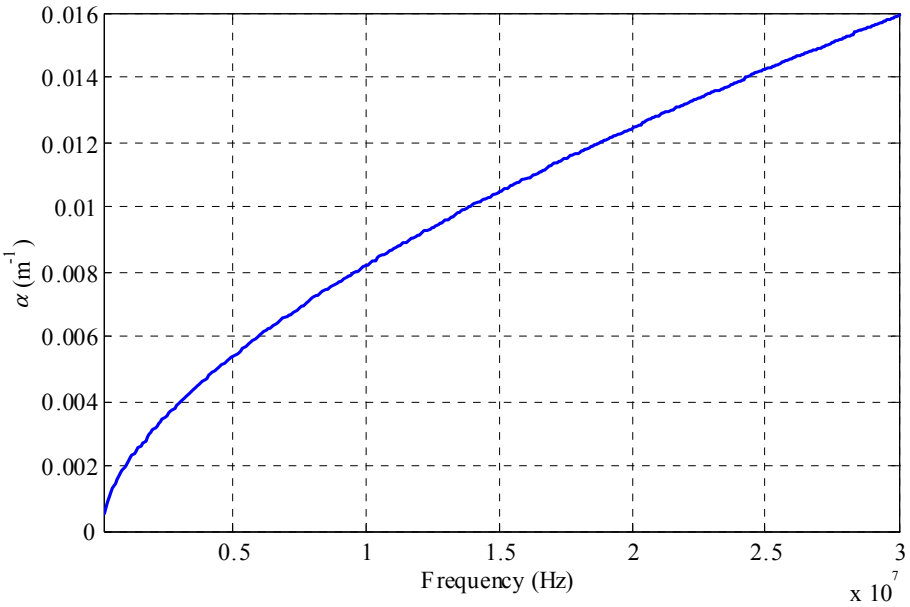

Figure 2.20. Signal attenuation coefficient as a function of frequency for the MCMK low voltage power cable in the frequency band 100 kHz – 30 MHz. The curve is calculated using the formed attenuation formula.

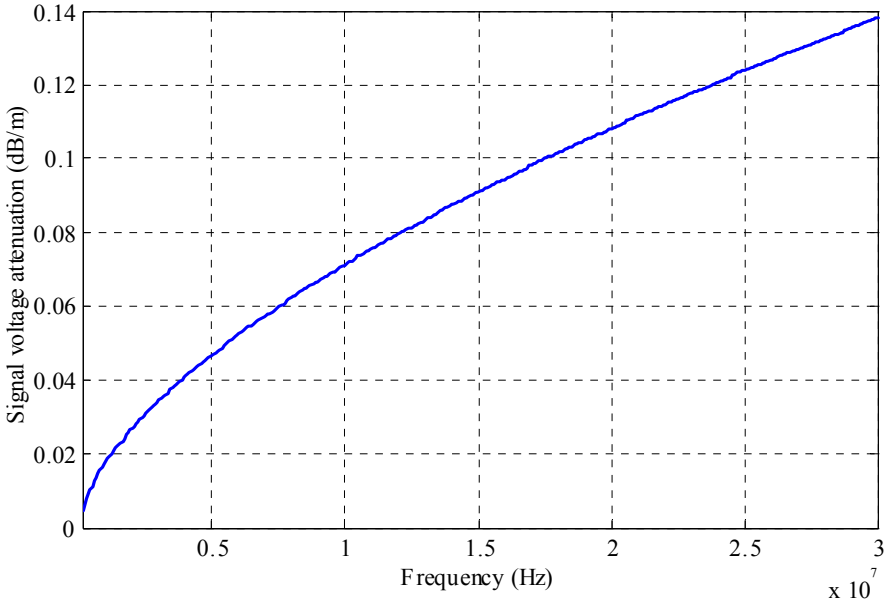

Figure 2.21. Signal voltage attenuation per-unit length in the MCMK low voltage power cable as a function of frequency in the frequency band 100 kHz – 30 MHz.

2.3.8 Applicability to Power-Line Communications

In chapter 2.3.5, three different MCMK power cables were measured. According to the measurements, two-conductor transmission line parameters l and c for the cables were determined in different signal couplings and in the frequency band 100 kHz – 30 MHz. In addition, the general signal voltage attenuation formula for the researched cables in the frequency band 100 kHz – 30 MHz was formed. Simulated and measured input impedances and the phases of the input impedances for a cable are illustrated in figure 2.22. The two-conductor transmission line model, measured cable parameters and developed attenuation formula (equation 2.25) were used in the simulation. In figure 2.22, both the simulated and measured curves behave similarly. At frequencies less than 2 MHz, the curves are visually corresponding. At higher frequencies, there is a difference in the simulated and measured phase curves. This difference is probably caused by the measurements.

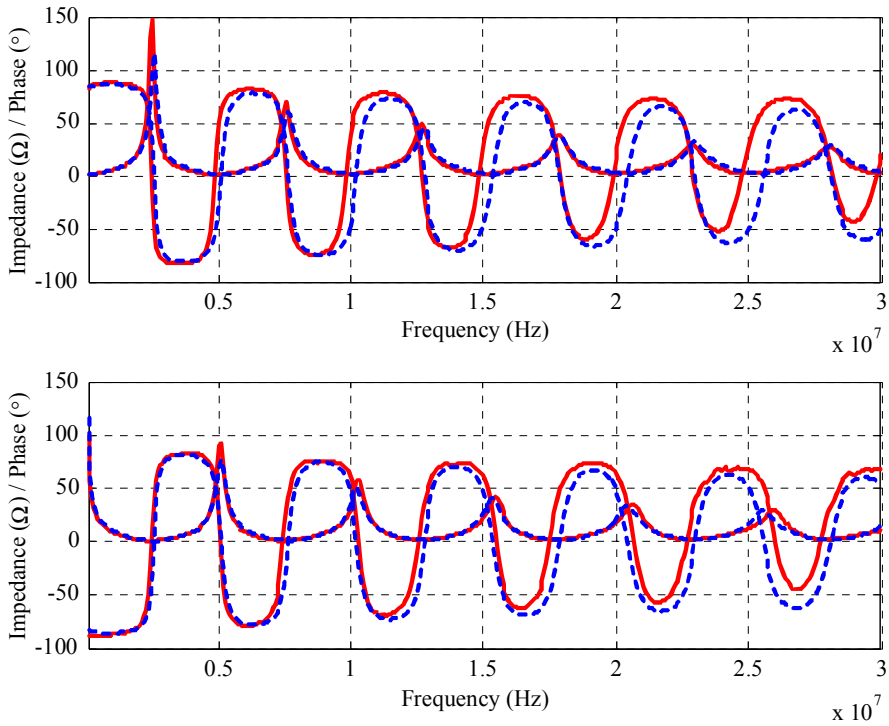

Figure 2.22. Measured (continuous line) and simulated (dashed line) input impedance and phase as a function of frequency for the low voltage power cable EMCMK 3x120+70. The signal coupling is (L1+L2+L3, PE) and the measured frequency band is 100 kHz – 30 MHz. The upper figure is measured the cable end being is short-circuited and the lower figure is measured the cable end being open. The length of the cable is 17.8 metres.

With respect to the power-line data transfer in the GENELEC B, C and D frequency bands (95-148.5 kHz), industrial distribution networks are generally electrically short and the signal attenuation is the most important of the cable parameters (figure 2.23). In this case, the characteristics of communication channel, such as input impedance and signal attenuation are determined by the attenuation of cabling and load impedances. In addition, the source impedance of the transmitter and the attenuation of the coupling interface affect the characteristics of the channel.

Generally, loads connected to the distribution network, such as electric motors and distribution transformers, can be considered to be high impedance cable terminations in the GENELEC frequency band. Hence, mainly the cable attenuation together with the transmitter output voltage and noise voltage at the receiver determine the performance of the data transfer. In addition, the receiver and the coupling interface characteristics have to be taken into account. The following parameters are selected:

- The modem circuit ST7537HS1 is used in data transfer. The bit error ratio of 10^{-3} is required. According to (ST, 1995), this requires signal to noise ratio S/N = 15 dB. The carrier frequency of the modem circuit is about 130 kHz.
- The signal is coupled between the phase conductors (L1, L2).

- Maximum required data transfer distance is 100 metres, which is assumed to be the maximum distance between PLC transmitter and receiver in the industrial low voltage distribution network.
- Transmitter maximum output voltage is 56 dB(mV) according to GENELEC specification (EN, 1991). The load impedance is assumed to be equivalent to the GENELEC test circuit.
- Noise voltage at the receiver is in the worst case 34 dB(mV) and in the best case –16 dB(mV) (figure 4.9)
- The attenuation of power-line coupling interface is 1.4 dB (figure 4.4).

The transmitter injects into the coupling interface carrier signal with voltage amplitude 56 dB(mV). The coupling interfaces attenuate the transmitted signal 2*1.4 dB = 2.8 dB. The signal voltage attenuation in the cable at frequency 130 kHz according to equations 2.4 and 2.25 is 0.0051 dB/m. This equals the total cable attenuation of 0.0051 dB/m*100 m = 0.51 dB. The carrier signal voltage at the receiver is 52.7 dB(mV). Hence, the signal to noise ratio at the receiver is in the worst case 18.7 and in the best case 68.7, respectively. According to this, at least in this case the required bit error ratio should be reached. In addition, the influence of the cable attenuation on the signal to noise ratio is small. A small inaccuracy in the cable attenuation formula or a small inaccuracy in the cable length will not affect the result. For example, in the worst case with the estimated attenuation level in the cable and with S/N = 15 dB at the receiver, the cable length could be more than 800 metres, which is very significant considering that, generally, 500 meters is assumed to be the practical limit for low voltage power cables.

The low voltage power cable offers several coupling possibilities for power-line communications. The simplest way of coupling into the mains is capacitive coupling between the phase conductors or between phase and protective earth conductor. The optimal way of coupling depends on the target distribution network topology and appliances that are connected to the target distribution network. At low frequencies, the using of protective earth as return conductor may be problematic, because there may be several return paths for the current. For example, devices, such as electric motors, inverters and pumps are generally connected to the ground potential.

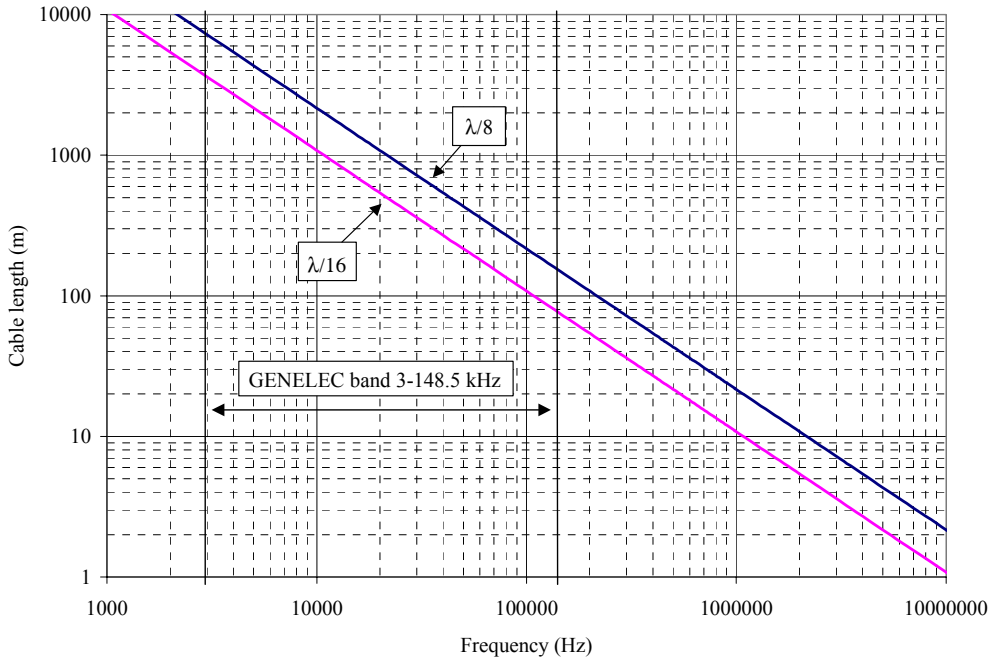

Figure 2.23. Electrical cable lengths $\lambda/8$ and $\lambda/16$ as a function of carrier frequency. The electrical length is calculated with the relative permittivity value of the insulation material $\varepsilon_{r,i} = 3$. With the used permittivity value, the propagation velocity of the electromagnetic wave is $0.58 c_0$.

2.4 Input Impedance of an Electric Motor

Previously, the input impedance of an electric motor has been an interesting parameter mainly in the closeness of the grid frequency (50/60 Hz). The importance of the input impedance at higher signal frequencies has increased due to the universal use of variable speed drives. The fast switching of power semiconductors of the inverter injects pulses with a wide frequency spectrum and high energy content into the motor feeder cable. The pulses cause problems in several ways. For example, they generate electromagnetic emissions, damage the winding insulation of the motor, cause problems for the control system of the inverter and generate bearing currents (Persson, 1991), (Saunders, 1996), (Takahashi, 1995), (Erdman, 1996). The occurrence of these problems is tightly related to the impedance mismatch between the motor feeder cable and motor. The electric motor also acts as a termination impedance when transmitting data in an industrial low voltage distribution network between the power-line modem installed in the motor and the receiver unit installed on the distribution transformer. Hence, the high frequency characteristics of an electric motor affect the high frequency characteristics of the power-line channel.

The input impedance of electric motor depends on many factors. At the frequencies close to the frequency of the supplying grid, the current injected into the terminals of motor flows through the stator windings. In such a case, the input impedance is dependent on the magnetisation inductance and leakage inductance of the stator coils, resistance of stator the coils, leakage inductance and resistance of the rotor and mechanical load of the motor. At higher signal frequencies, stray capacitances and other leakage inductances start to affect the input impedance of

the motor. Additionally, due to the skin effect all resistances of electric motor increase as a function of frequency. Some of the parasitic quantities that affect the input impedance behaviour of the electric motor at high frequencies are:

- Capacitance between the adjacent stator coil turns in the phase winding
- Capacitance between phase winding and stator frame
- Capacitance between the phase windings of two phases
- Mutual inductance between the adjacent stator coil turns in the phase winding
- Mutual inductance between the phase windings of two phases
- Resistance of the stator frame and the stator coils

(Zhong, 1995) and (Schlegel, 1999) introduced the input impedance models for simulation of electromagnetic emissions and voltage reflections. (Zhong, 1995) proposed a radio frequency model for a single phase-belt winding (figure 2.24). The complete input impedance model for an electric motor is formed by combining the multiple phase-belt winding models to form a complete phase winding for each phase. Correspondingly, the input impedance model proposed by (Schlegel, 1999) is illustrated in figure 2.25.

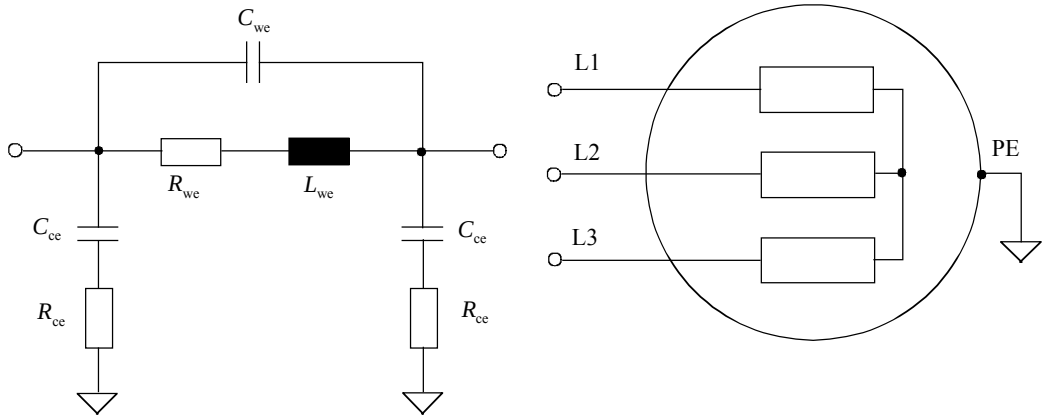

Figure 2.24. Model for a single phase-belt winding at radio frequencies (left). The model parameters are: the interturn capacitance between the coils C_{we}, the leakage inductance L_{we}, the resistive losses of the coil and the iron R_{we}, the capacitance between the winding and the stator frame C_{ce} and the losses in the path in which the current flows through the winding to the stator frame R_{ce}. The model of a complete electric motor (right) consists of the phase-belt winding models placed in series and in parallel. (Zhong, 1995)

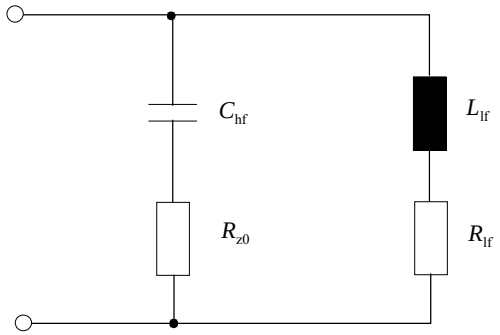

Figure 2.25. Differential input impedance model (signal coupling L1, L2+L3) for the simulation of voltage reflections in inverter-fed motors. The parameters of the model are: $L_{lf,}$ low frequency inductance describing the inductance of the stator coils, R_{lf} low frequency resistance describing the

resistance of the stator coils, C_{hf} high frequency capacitance and R_{z0} surge impedance. (Schlegel, 1999)

According to the experimental results presented in (Schlegel, 1999) and (Zhong, 1995), the input impedance of an electric motor has the following characteristics in differential mode (L1+L2, L3) and as a function of frequency in the frequency band 1 kHz – 1 MHz:

- The input impedance is inductive near to the frequency of the supplying grid and increases linearly as a function of frequency.
- The highest input impedance value is reached in the frequency band 10-100 kHz. The peak impedance value is about 1-10 kΩ depending on the motor. At the peak frequency, the electric motor behaves like a parallel resonant circuit.
- Beyond the resonant frequency, the input impedance of the motor becomes capacitive with the impedance magnitude rapidly decreasing to a few tens of ohms.

2.4.1 Input Impedance Measurements

In order to enhance experimental based knowledge of the input impedance behaviour of electric motors in the frequency band 10 kHz – 30 MHz, a test group was formed. The group (table 2.2) consisted of six induction motors manufactured by ABB (ABB Ltd., Zurich, Switzerland), Strömberg (Kymi-Strömberg Ltd., Helsinki, Finland) and Invensys (Invensys Ltd, United Kingdom). The sizes of the test group motors were at the range from 15 kW to 250 kW. The 33 kW induction motor was modified to a SR motor (synchronous reluctance) by replacing the old cage rotor with a new one developed in Lappeenranta University of Technology. The test group motors represent typical low voltage electric motors that are used in industrial applications. In addition, their sizes are interesting with the respect of the remote on-line condition monitoring. The objective of the measurement sequence was to answer the following issues:

- Estimation of the best signal coupling for power-line communications
- Behaviour of input impedance in the frequency band 10 kHz – 30 MHz
- Dependence of input impedance behaviour on signal coupling
- Dependence of input impedance behaviour on motor size
- Effect of rotor on the input impedance behaviour
- Possibility to model input impedance as a function of frequency with a simple model

The measurements for the test group motors were performed for the frequency band 10 kHz – 30 MHz with a HP 4194A impedance analyser and with a HP 41941A impedance probe. The signal couplings (L1, PE), (L1, L2), (L1, L2+L3) and (L1+L2+L3, PE) were measured. However, with respect to power-line communications the signal couplings (L1, PE) and (L1, L2) are the most interesting ones. The measured impedance curves are given in Appendix I.

Table 2.2. Technical data of the electric motors belonging to the test group.

Manufacturer	Type	I_N(A)	V_N(V)	P_N(kW)	r/min
ABB	M2AA160L4	30	400	15	1455
Invensys	T-01F160L4/01	28.5	400	15	1460
Strömberg	HXUR368G2B3	43	400	22	1460
ABB	M2BA200MLA4B3	56	400	33	1473
Strömberg	HXUR505G2(1)B3	100	400	55	1475
ABB	M2BA35532B3	410	400	250	2980

According to the input impedance measurements carried out, some main characteristics for the input impedance behaviour of an induction motor as a function of frequency can be found. These characteristics are reported in (Ahola, 2003).

The input impedance in signal couplings (L1, L2+L3) and (L1, L2) has two strong resonance frequencies (figure 2.26). The first one is a parallel resonance in the frequency band about 10-100 kHz. At the resonance frequency, the input impedance of the motor is about 1-10 kΩ. Below the parallel resonance frequency the input impedance is inductive and above the resonance frequency the input impedance becomes capacitive. The second strong resonance is a serial resonance in the frequency band about 1-20 MHz. At the serial resonance frequency the input impedance is about 1-10 Ω. Above the serial resonance frequency the input impedance becomes again inductive.

The input impedance in the signal couplings (L1, PE) and (L1+L2+L3, PE) has equivalent behaviour as a function of frequency (figure 2.27). There is only one strong resonance in the frequency band 10 kHz - 30 MHz. It is a serial resonance in the frequency band 1-20 MHz and depending on the motor and applied signal coupling. At frequencies lower than the serial resonance frequency, the input impedance is capacitive and above the serial resonance frequency it becomes inductive. At the serial resonance frequency the input impedance is purely resistive and the magnitude of the impedance is about 1-10 Ω.

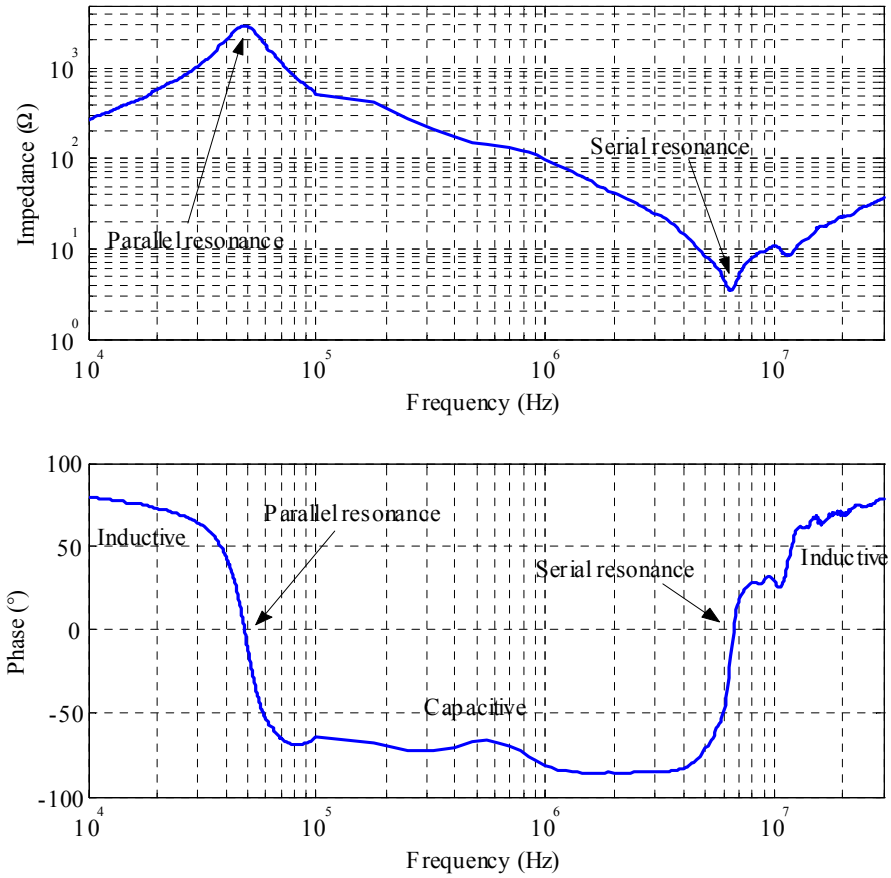

Figure 2.26. Typical behaviour of the input impedance of electric motor in the signal couplings (L1, L2), (L1, L2+L3) and in the frequency band 10 kHz – 30 MHz. The curves are measured for the induction motor (Invensys 15 kW, 4 poles). Signal coupling (L1, L2+L3) is used in the measurement.

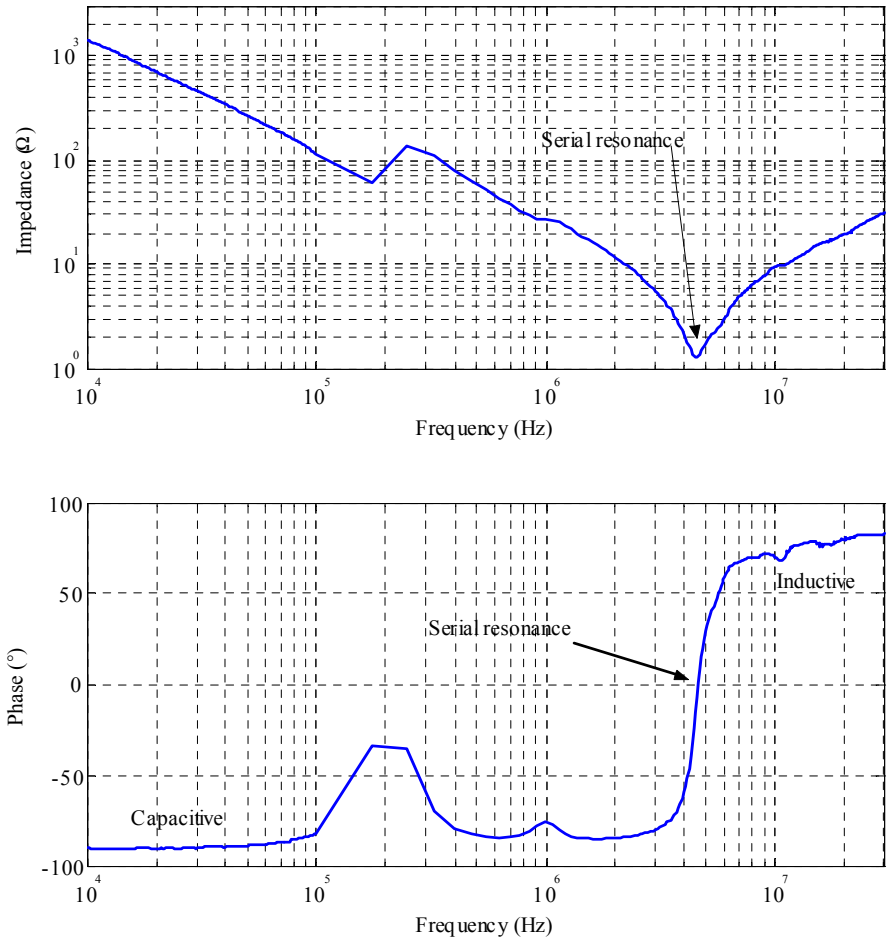

Figure 2.27. Typical behaviour of the input impedance of electric motor in the signal couplings (L1, PE), (L1+L2+L3, PE) and in the frequency band 10 kHz – 30 MHz. The curves are measured for the induction motor (Invensys 15 kW, 4 poles). Signal coupling (L1+L2+L3, PE) is used in measurement.

If only the frequency band 100 kHz – 30 MHz is observed, the input impedance of the electric motor behaves like a serial resonance circuit in all signal couplings. According to this property, the high frequency parameters for the measured electric motors were acquired. The high frequency resistance, inductance and capacitance for the serial resonance circuit were determined from the measurement data applying the following procedure:

1. The capacitance value was defined searching from the measurement data all the points, where the phase of the impedance was $\theta \leq -70°$. The circuit was supposed to consist of the serially connected resistance and capacitance. The capacitance value was calculated for all the selected data points and the median value was selected to be the capacitance value.
2. The inductance value was defined searching from the measurement data all the points, where the phase of the impedance was $\theta \geq 70°$. The circuit was supposed to consist of the

serially connected inductance and resistance. The inductance was calculated for all the data points and the median value was selected to be the inductance value.

3. The capacitive and inductive reactances compensate each other at the frequency of the serial resonance. Thus, the resistance value of the serial resonance circuit is the input impedance value measured at the serial resonance frequency.

Median values were used in the definition of the inductance and capacitance values in order to reduce the interference originating from the measurements. In addition, the parameters do not stay precisely constant as a function of frequency. Therefore, the median value was supposed to be a good estimate. The amount of values from which the median was determined was dependent on the motor and signal coupling. The total amount of data points in each measurement was 401 and the frequency spacing of the data points was linear. The determined high frequency parameters for all the signal couplings are listed in tables 2.3, 2.4, 2.5 and 2.6. The signal couplings (L1, PE) and (L1, L2) were measured for all the motors belonging to the test group.

Table 2.3. Calculated parameters for the serial resonance circuit that models the behaviour of input impedance of the electric motor in the frequency band 100 kHz – 30 MHz. The signal coupling is (L1, PE) and all the motors are connected in delta.

Mf.	Type	I_N(A)	V_N(V)	P_N(kW)	r/min	L_{hf}(nH)	C_{hf}(nF)	R_{hf}(ohm)
ABB	M2AA160L4	30	400	15	1455	140	0.8	6
Invensys	T-01F160L4/01	28.5	400	15	1460	149	2.5	3
Strömberg	HXUR368G2B3	43	400	22	1460	141	1.6	6
ABB	M2BA200MLA4B3	56	400	33	1473	239	2.3	2
Strömberg	HXUR505G2(1)B3	100	400	55	1475	318	1.7	6
ABB	M2BA35532B3	410	400	250	2980	270	12.2	1

Table 2.4. Calculated parameters for the serial resonance circuit that models the behaviour of the input impedance of the electric motor in the frequency band 100 kHz – 30 MHz. The signal coupling is (L1, L2) and all the motors are connected in delta.

Mf.	Type	I_N(A)	V_N(V)	P_N(kW)	r/min	L_{hf}(nH)	C_{hf}(nF)	R_{hf}(ohm)
ABB	M2AA160L4	30	400	15	1455	127	0.8	12
Invensys	T-01F160L4/01	28.5	400	15	1460	198	1.7	5
Strömberg	HXUR368G2B3	43	400	22	1460	127	0.8	12
ABB	M2BA200MLA4B3	56	400	33	1473	266	1.4	5
Strömberg	HXUR505G2(1)B3	100	400	55	1475	335	1.2	3
ABB	M2BA35532B3	410	400	250	2980	329	7.7	2

Table 2.5. Calculated parameters for the serial resonance circuit that models the behaviour of the input impedance of the electric motor in the frequency band 100 kHz – 30 MHz. The signal coupling is (L1, L2+L3) and all the motors are connected in delta.

Mf.	Type	I_N(A)	V_N(V)	P_N(kW)	r/min	L_{hf}(nH)	C_{hf}(nF)	R_{hf}(ohm)
Invensys	T-01F160L4/01	28.5	400	15	1460	181	2.2	4
Strömberg	HXUR368G2B3	43	400	22	1460	78	1.2	7
ABB	M2BA200MLA4B3	56	400	33	1473	271	1.5	5
Strömberg	HXUR505G2(1)B3	100	400	55	1475	280	1.2	4

Table 2.6. Calculated parameters for the serial resonance circuit that models the behaviour of the input impedance of the electric motor in the frequency band 100 kHz – 30 MHz. The signal coupling is (L1+ L2+L3, PE) and all the motors are connected in delta.

Mf.	Type	I_N(A)	V_N(V)	P_N(kW)	r/min	L_{hf}(nH)	C_{hf}(nF)	R_{hf}(ohm)
Invensys	T-01F160L4/01	28.5	400	15	1460	153	6.9	1
Strömberg	HXUR368G2B3	43	400	22	1460	310	2	2
ABB	M2BA200MLA4B3	56	400	33	1473	212	6	1
Strömberg	HXUR505G2(1)B3	100	400	55	1475	143	4.9	2

According to the estimated parameter values, the following conclusions can be made for the test motor group:

- The high frequency inductance values within the test group are about 50–350 nH.
- When comparing all the motors and signal couplings the high frequency capacitance values in the test group are ranging from 0.8 to 12.2 nF. The motor frame size does not clearly correlate with the capacitance value. However, if a single motor is observed, there is a difference in capacitance between the signal couplings. The order of the magnitude in the capacitance values is: (L1+L2+L3, PE), (L1, PE), (L1, L2+L3) and (L1, L2).
- The high frequency resistance is generally small. Within the test group it is less than $12\,\Omega$ if all the signal couplings are compared. The resistance is smallest in the signal coupling (L1+L2+L3, PE).

The high frequency inductance of an electric motor is probably caused by several sources. Some of these sources could possibly be the mutual inductance between the stator coil turns in the phase winding, the mutual inductance between the stator coil and motor frame and the mutual inductance between the phase windings of two phases. The measured high frequency inductances are significantly smaller than the inductances of the electric motor close to the mains frequency. According to (Haataja, 2003), the magnetisation inductance of an induction motor L_m close to the mains frequency is given by:

$$L_m = 0.37 \cdot P^{-0.76} \tag{2.26}$$

and correspondingly, the leakage inductance of the stator coils L_s is:

$$L_s = 0.07 \cdot P^{-0.76}, \tag{2.27}$$

where P is the nominal power of the induction motor (kW). Equations 2.26 and 2.27 may be applied for four pole induction motors that are connected in delta. For example, according to equations 2.26 and 2.27, the magnetisation and leakage inductances for an induction motor (15 kW, 4 poles) are $L_m = 47.2\,\text{mH}$ and $L_s = 8.9\,\text{mH}$. The corresponding high frequency inductance for the electric motor (Invensys, 15 kW, 4 poles) in the same signal coupling (L1, L2+L3) is 181 nH (table 2.5).

The test motor group included two identical Invensys induction motors (15 kW, 4 poles). One of these was intact and the other was disassembled. The rotor and the end plates were removed. A series of input impedance measurements were carried out for both motors. The goal of the measurements was to determine whether the rotor and end plates affect the input impedance of

the electric motor in the frequency band 100 kHz – 30 MHz. Because the motors were identical, the input impedances of the intact motors were supposed to be close to each other in the measured frequency band. The impedance measurements for the signal couplings (L1, PE) and (L1+L2+L3, PE) are illustrated in figures 2.28 and 2.29. The impedance and phase curves are close to each other at the whole frequency band. There is a slight difference in the impedance curves in figure 2.28, but the curves are almost identical in figure 2.29.

The minimal effect of the rotor and the end plates on the input impedance at high signal frequencies can be easily explained. The rotor and the end plates form mainly a capacitance between stator winding and motor frame. The capacitance between stator winding and stator frame is significantly larger than the parallel capacitance between stator winding and rotor and the parallel capacitance between stator winding and end plates. The reasons for this are the distance from the stator winding to the rotor and the distance from the stator winding to the end plates. Additionally, the capacitances formed between stator winding and end plates and stator winding and rotor are primarily air insulated. In other words, the removal of the rotor and the end plates should not significantly affect the total capacitance between stator winding and stator frame. Thus, the input impedance as a function of frequency should also be independent of the electric machine type, when the structure of the stator and stator windings stays uniform. Therefore, the structure of the stator and the insulation materials of the stator determine the high frequency characteristics of the electric motor.

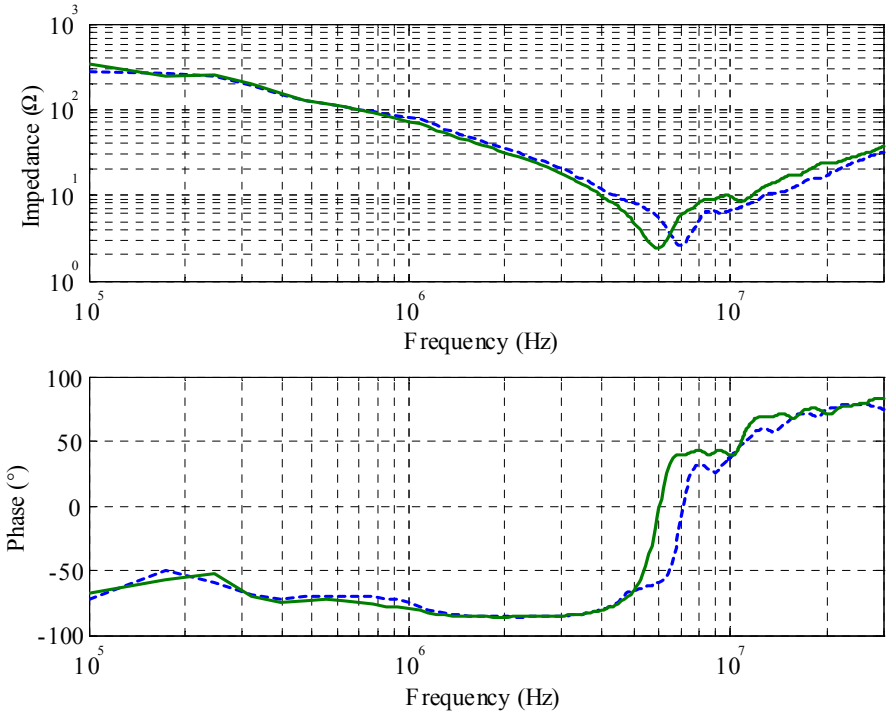

Figure 2.28. Effect of rotor on the input impedance of the Invensys 15 kW electric motor in the frequency band 100 kHz – 30 MHz. The signal is coupled between phase L1 and PE. The continuous line represents the intact motor and the dashed line represents the motor without rotor and end plates.

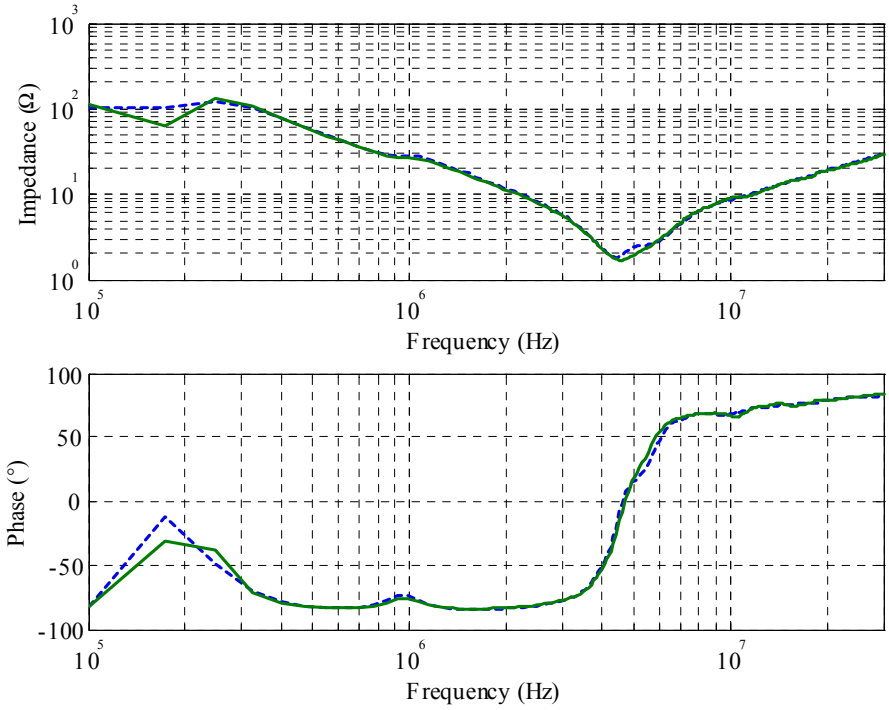

Figure 2.29. Effect of rotor on the input impedance of the Invensys 15 kW electric motor in the frequency band 100 kHz – 30 MHz. The signal coupling is (L1+L2+L3, PE). The continuous line represents the intact motor and the dashed line represents the motor without rotor and end plates.

2.4.2 Measurement Based Input Impedance Model for Power-Line Communications

Generally, electric motors are designed to operate near the frequency of the distribution network. Models that may be used to analyse the stationary and transient state behaviour of the electric motor are introduced in the literature treating the field of machines, e.g. (Kovacs, 1984). Correspondingly, (Schlegel, 1999), (Zhong, 1995) and (Skiblinski, 1994) propose experimental based models to model the reflected waves and electromagnetic interference of inverter-fed motor drives. The proposed models describe the electric motor as a frequency dependent termination impedance. For example, in (Tarkiainen, 2002), the termination impedance model is applied to form a simulation model for the cable oscillations of the PWM (pulse width modulation) drive. The same kind of simple termination impedance model could also be applied for the modelling and simulation of power-line communications.

Currently, there are no input impedance models for the electric motor, which are designed for the simulation and planning of power-line communications in industrial low voltage distribution networks. However, there is a need for this kind of model. The main requirement for the model is that it must describe the main characteristics of the input impedance of the electric motor in the frequency band 10 kHz – 30 MHz. These are the parallel and serial resonances, which were found for each measured motor. The main characteristics are important, because, in case of a branch cable, which is terminated with an electric motor, the input impedance of the branch cable becomes frequency variant due to the impedance mismatch at the interface of the cable and motor. Due to the low losses of the cable and strong impedance mismatch, the input impedance of the cable may be close to the zero at some frequencies. At these frequencies, there are

steep notches in the amplitude response of the power-line channel and distortion in the phase response. These frequencies are generally unfavourable for power-line data transfer. Due to the frequency variant input impedance, the motor cannot be modelled as open or short-circuited cable termination. On the other hand, the imaginary part of the input impedance of the electric motor affects the electrical length of the branch cable, which correspondingly affects the frequencies in which the notches are located. In addition to the general input impedance characteristics, the input impedance model has to be compatible with the two-conductor cable model. An accurate modelling of the impedance magnitude and phase is not required, because the exact high frequency characteristics of the motor cannot be evaluated based on the plate values. Instead, this requires input impedance measurements for the electric motor.

The input impedance models presented in (Schlegel, 1999) and (Zhong, 1995) are capable to model the input impedance characteristics of the electric motor up to the frequency 1 MHz (figures 2.24 and 2.25). However, they are not capable of modelling the behaviour of the input impedance at higher signal frequencies. The presented models do not describe the strong serial resonance that was found for each measured motor in each signal coupling in the frequency band 1–20 MHz.

The developed experimental based input impedance model is introduced in (Ahola, 2003) and illustrated in figure (2.30). It consists of two two-port models. The selection of the model is dependent on the applied signal coupling. The low frequency part in the developed model (figure 2.20) is the same as in the model proposed by (Schlegel, 1999) (figure 2.25). The improvements are made for the high frequency path of the model. In the developed model, the series connection of the high frequency capacitance C_{hf} and surge impedance R_{z0} forming a high pass filter is replaced with a serial resonance circuit consisting of: C_{hf} , L_{hf} and R_{hf} .

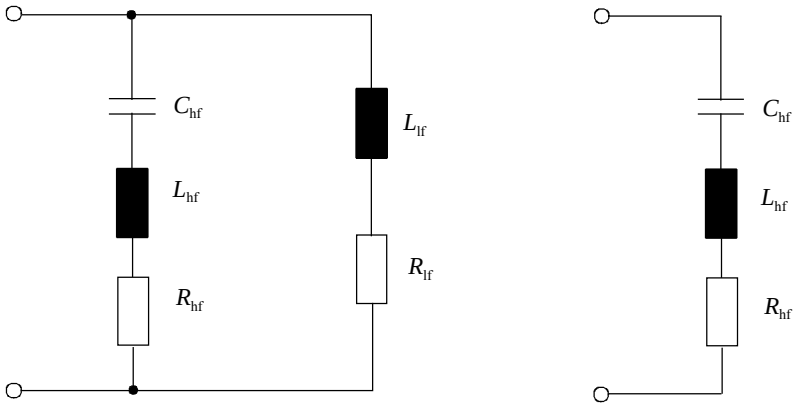

Figure 2.30. Developed two-port input impedance model for the simulation and modelling of power-line communications. The model consists of two submodels. The model (left) is for signal couplings (L1, L2) and (L1, L2+L3). The model (right) is for signal couplings (L1, PE) and (L1+L2+L3, PE).

The parameters of the model (figure 2.30) are:

L_{lf} = the low frequency inductance of the stator coils.

R_{lf} = the low frequency resistance of the stator coils.

C_{hf} = the capacitance of the high frequency current path.
L_{hf} = the inductance of the high frequency current path.
R_{hf} = the resistance of the high frequency current path.

The impedance equations for the submodels in the Laplace space (figure 2.30) are:

$$\mathbf{Z}_{in,1}(s) = \frac{sC_{hf}L_{hf} + s(C_{hf}R_{hf} + L_{lf}) + R_{lf} + 1}{s^2C_{hf}(L_{lf} + L_{hf}) + sC_{hf}(R_{lf} + R_{hf}) + 1}, \tag{2.28}$$

$$\mathbf{Z}_{in,2}(s) = \frac{s^2C_{hf}L_{hf} + sC_{hf}R_{hf} + 1}{sC_{hf}}. \tag{2.29}$$

The simulated and measured input impedance and phase curves for the electric motors are illustrated in figures 2.31, 2.32, 2.33 and 2.34. All the curves are for the frequency band 10 kHz – 30 MHz. The simulated impedance and phase curves were created applying the developed input impedance model (figure 2.30). The parameter values given in tables 2.3, 2.4, 2.5 and 2.6 are used in the simulations. The low frequency parameters of the input impedance model (figure 2.30) are estimated.

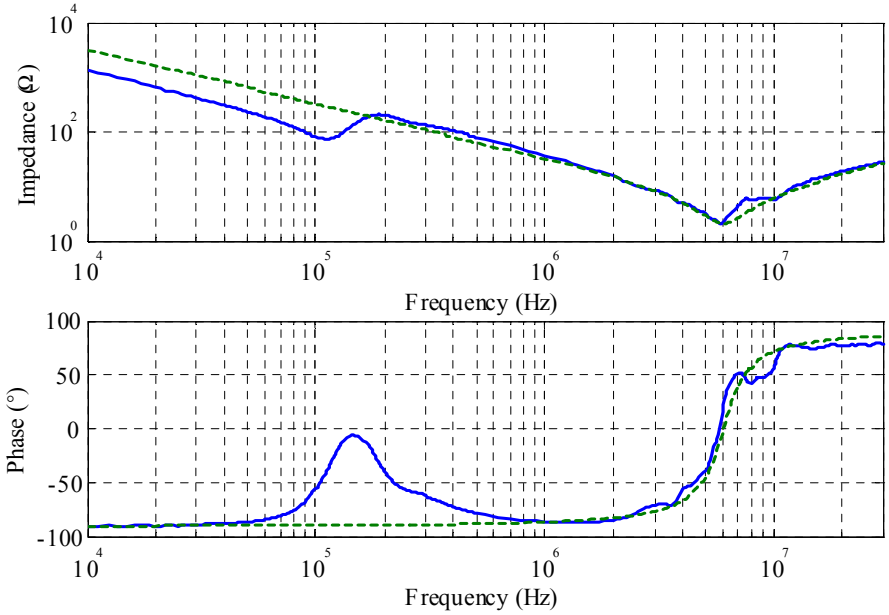

Figure 2.31. Measured (continuous line) and simulated (dotted line) input impedance and phase of the impedance of the induction motor (22 kW, 4 poles) in the frequency band 10 kHz – 30 MHz. The signal coupling is (L1+L2+L3, PE). The parameters used in the simulation model are: L_{hf}=145 nH, C_{hf}=4.9 nF and R_{hf}=2 Ω.

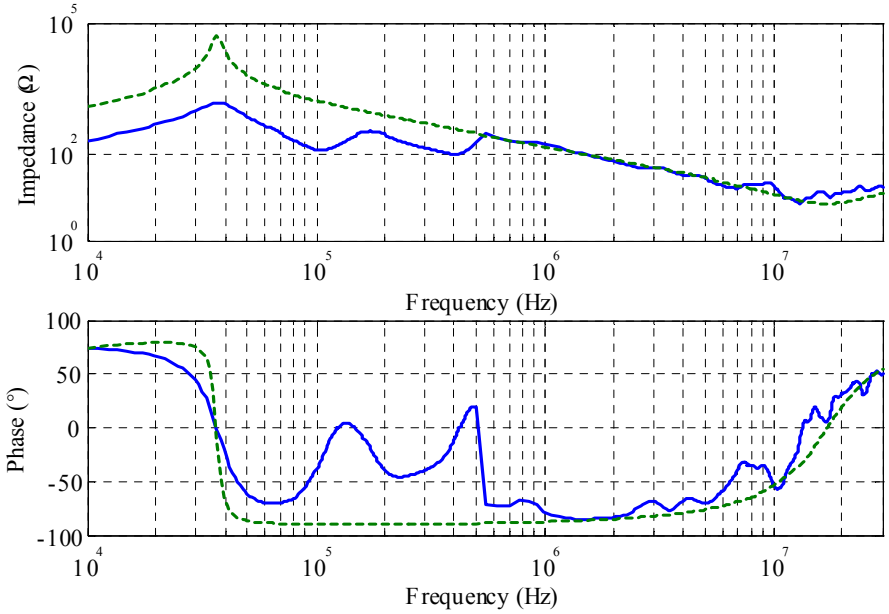

Figure 2.32. Measured (continuous line) and simulated (dotted line) input impedance and phase of the impedance of the induction motor (22 kW, 4 poles) in the frequency band 10 kHz – 30 MHz. The signal coupling is (L1, L2+L3). The parameters used in the simulation model are: L_{lf}=17 mH, R_{lf}=300 Ω, L_{hf}=78 nH, C_{hf}=1.1 nF and R_{hf}=7 Ω.

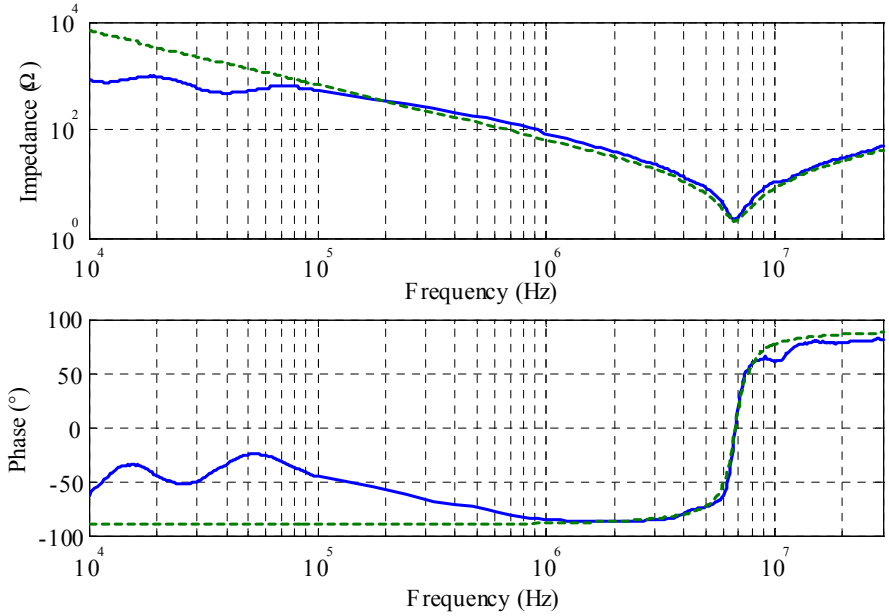

Figure 2.33. Measured (continuous line) and simulated (dotted line) input impedance and phase of the impedance of the SR motor (33 kW, 4 poles) at the frequency band 10 kHz – 30 MHz. The signal coupling is (L1, PE). The parameters used in the simulation model are: L_{hf}=239 nH, C_{hf}=2.3 nF and R_{hf}=2 Ω.

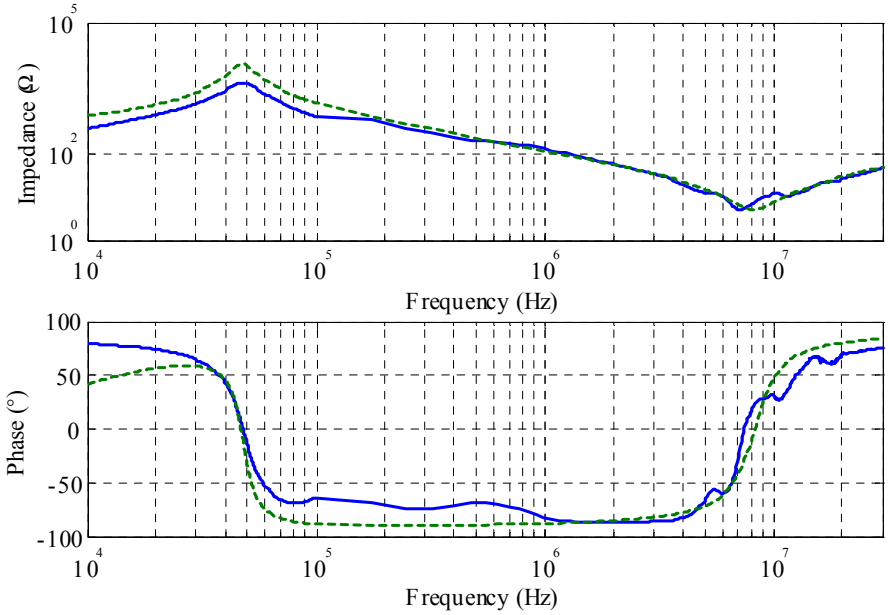

Figure 2.34. Measured (continuous line) and simulated (dotted line) input impedance and phase of the impedance of the induction motor (15 kW, 4 poles) in the frequency band 10 kHz – 30 MHz. The signal coupling is (L1, L2). The parameters used in the simulation model are: L_{lf}=7.8 mH, R_{lf}=500 Ω, L_{hf}=266 nH, C_{hf}=1.4 nF and R_{hf}=5 Ω.

According to figures 2.31, 2.32, 2.33 and 2.34, the proposed two-port input impedance model describes the main characteristics of the measured and simulated electric motors in the frequency band 10 kHz – 30 MHz. It is also possible to observe, that the simulated and measured impedance and phase curves are corresponding. Hence, the model fulfils the requirements that were set to the model earlier in this chapter (p. 67-68). Despite of the corresponding general impedance and phase characteristics, there are differences between the model and measurements. These result e.g. from:

- The structure of the stator windings and the electric motor is complicated. The presented model describes only the most dominant phenomena. In addition to the strong parallel and serial resonance, other weak resonance frequencies occur. In other words, there exits other parasitic components, such as stray capacitances and leakage inductances that are neglected when a simple model is used.
- Due to the size and structure of the electric motor, the parameters affecting the high frequency characteristics of the electric motor are distributed.
- The serial resistance of the stator coil is a frequency dependent parameter due to the skin effect. It is also obvious that there are also other frequency dependent parameters.

According to the simulations, there is difference between the simulated input impedance and measured input impedance in the frequency band 10 kHz – 1 MHz. Compared to the measurements, the simulations give higher input impedance values. However, when the motor is regraded as a termination impedance of a motor cable, there is no significant difference in the reflection coefficients at the interface of the motor and the cable between the simulation model and measurements. In both cases, the input impedance of the electric motor is about 100-1000 times larger than the characteristic impedance of the motor cable. This has as a result that the reflection coefficient becomes almost $|\mathbf{\Gamma}_R| \approx 1$ in both cases (equation 2.11) and the electric

motor looks like open cable end. When operating in the GENELEC frequency band and in industrial low voltage distribution networks, the cables are generally electrically short. Hence, in the GENELEC band the difference between the model and measurement can be noticed in network impedance levels. The load impedances given by the input impedance model are generally larger than measured values. Due to the source resistance of the practical modems and coupling interface, this will cause slight difference between measured and simulated channel attenuation.

The developed input impedance model can be applied to electric motors with slotted stator in the frequency band 10 kHz – 30 MHz. The model is simple and the parameters for the motor can be determined by a series of impedance measurements or even estimated based on the measurement data given in chapter 2.4.1. The developed model is computationally light compared to e.g. the distributed model presented in (Zhong, 1995). Despite of its simple structure, it models the most dominant resonances of the electric motor. In addition, its application for power-line communications, the developed measurement based model may be used at least for the simulating and modelling of inverter feeder cable oscillations.

2.4.3 Effect of Electric Motor on Power-Line Communications

The electric motor acts as a termination impedance, when the data are transferred in an industrial distribution network using power-line communications. The input impedance of an electric motor is frequency variant. According to the results presented in chapter 2.4.1, the absolute value of the input impedance typically varies in the frequency band 10 kHz – 30 MHz between the values 1 Ω - 10 kΩ and is mainly either almost purely capacitive or almost purely inductive. The characteristic impedances of low voltage power cables are typically in the range of 5 Ω to 50 Ω. Hence, there occurs an impedance mismatch at the interface of the cable and the motor in the whole frequency band 10 kHz – 30 MHz. This leads to power reflection at the interface of the cable and motor.

The simulated reflection coefficients and the phases of the reflection coefficients at the interface of an induction motor and low voltage power cable are illustrated in figure 2.35. The curves are simulated using equation 2.11. The measured input impedance curves for the electric motor and measured cable parameters are used in the simulation. According to the simulation (figure 2.35), there exists impedance mismatch ($|\boldsymbol{\Gamma}_R| \neq 0$) in the whole frequency band 10 kHz – 30 MHz. In addition, the phase of the reflection coefficient is not constant as a function of frequency. In the target GENELEC frequency band (95-148.5 kHz), the electric motor can be considered to be an open cable end ($|\boldsymbol{\Gamma}_R| \approx 1,\ \theta \approx 0°$). However, the industrial cable lengths are short compared to the wavelength of the electromagnetic wave. Hence, at the target GENELEC frequency band, the effect of the cable on the input impedance of the cable-motor combination can be considered to be small. Instead, the electric motor is a load impedance having a large impedance value.

Due to the impedance mismatch at the interface of the cable and electric motor, the input impedance measured from the input of the cable becomes frequency variant. The frequency dependent input impedance is problematic for the power-line data transmission. A branch cable terminated with an electric motor can be considered to be a load impedance that is connected in parallel to the power-line channel. Due to the almost perfect power reflection at the interface of the cable and motor and due to the low losses of the cable, at certain frequencies the input impedance of the cable drops close to zero. This almost short-circuits the power-line channel causing steep notches to the frequency response and distortions to the phase response. Branch

telephone cables with open end cause similar problems for VDSL (very high speed digital subscriber line) channels (Im, 1997).

Figure 2.36 illustrates the sequential pikes and slopes in the simulated and measured impedance curves. These attenuate as a function of frequency due to the increasing attenuation of the cable. The curve simulated with the developed motor and cable model corresponds the laboratory measurement. However, the cable attenuation in the measured curve at high frequencies is higher than in the simulated curve. The impedance value at the peaks is lower and at slopes higher in the measurement than in the simulation. The simulations carried out with the developed cable model with open cable end and with short-circuited cable end are added in figure 2.36. According to figure 2.36, the simulated and measured input impedances of the cable-motor combination drop close to zero for the first time at the frequency about 1.8 MHz. The zero impedance frequencies given by the simulations with open and short-circuited cable ends differ from the previous ones. Hence, it can be noticed that the input impedance model for the motor is required at frequencies higher than the GENELEC band.

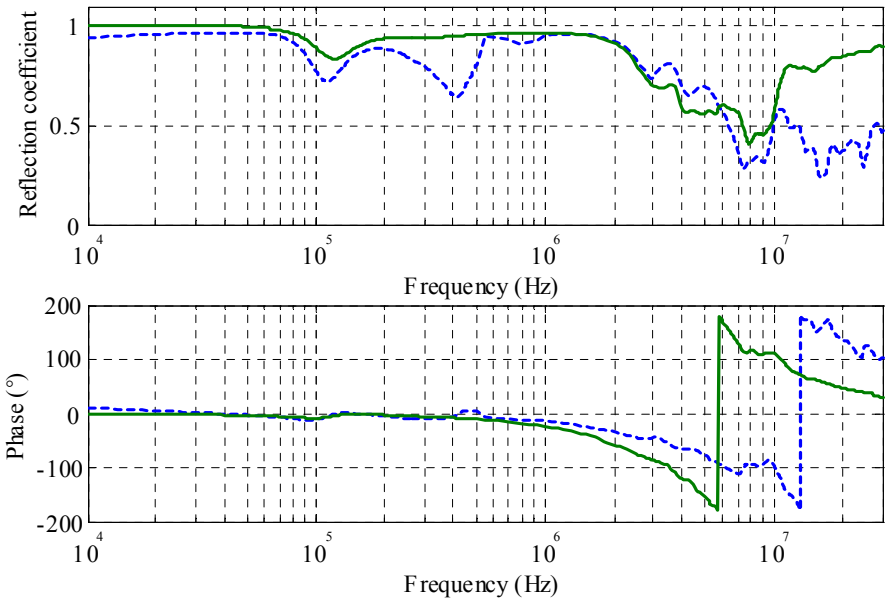

Figure 2.35. Simulated complex reflection coefficient and phase of the reflection coefficient as a function of frequency at the interface of the induction motor (22 kW 4 poles) and low voltage power cable (MCCMK 3x35+16). The continuous line represents the signal coupling (L1+L2+L3, PE) and the dashed line the signal coupling (L1, L2+L3). The simulated frequency band is 10 kHz – 30 MHz.

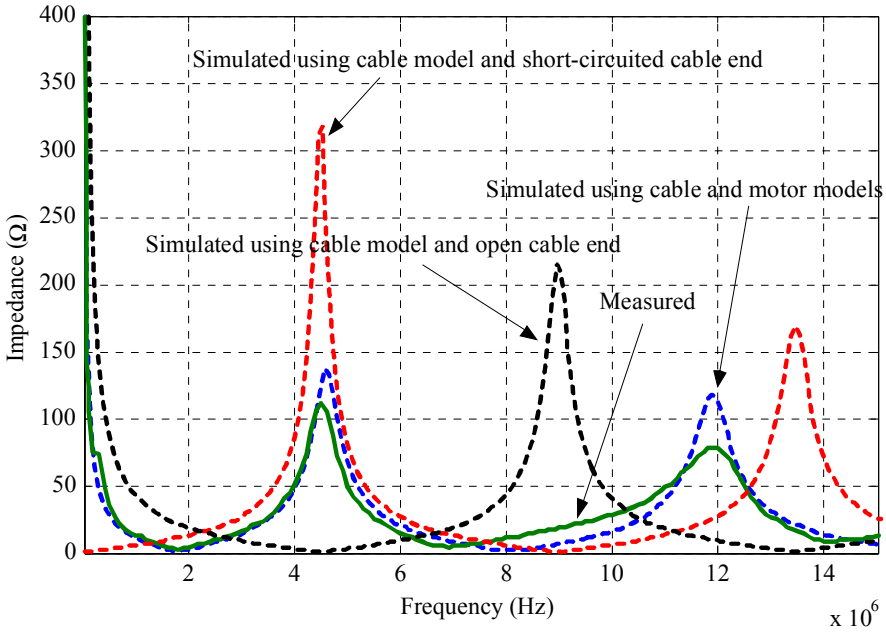

Figure 2.36. Measured and simulated input impedances of the cable (MCCMK 3x16+16, length 9.7 m) in the frequency band 10 kHz – 15 MHz. The cable is terminated by the induction motor (15 kW, 4 poles), short-circuited and open ended. Signal coupling is (L1+L2+L3, PE).

2.5 Characteristics of DC-Voltage Link Inverter

Nowadays, inverters are commonly used electrical devices in industrial low voltage distribution networks. Due to the controllability and energy saving aspects, the amount of electrical drives equipped with an inverter continues to increase. The use of inverters offers several advantages over the use of conventional direct electric drives. However, it also creates new problems, especially for power-line communications. The operation of the inverter generates high frequency noise with a wide frequency spectrum that spreads out into the distribution network. In addition, a rectifier unit with DC–link capacitors makes the input impedance of the inverter time variant and nonlinear. The general structure of a DC-voltage link inverter is illustrated in figure 2.37. The main components of an inverter are:

1. Mains EMI filter
2. Rectifier unit
3. DC-link inductor and capacitor
4. Inverter stage
5. Output filter

The inverter structure is not always as complete as it is presented in figure 2.37. There is necessarily no mains EMI filter or output filter in low-cost inverters.

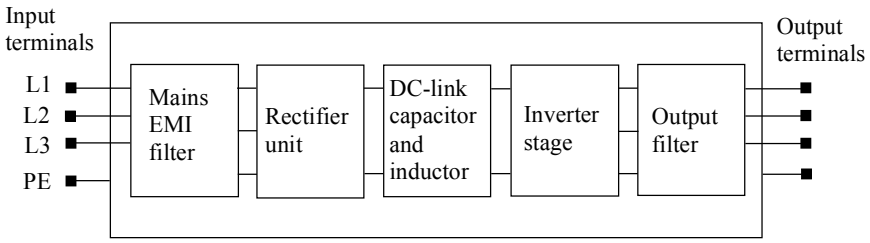

Figure 2.37. General structure of a DC-voltage link inverter.

The operation of the inverter chiefly generates two types of disturbances into a low voltage distribution network:

1. Conducted noise generated by the inverter operation
2. Time varying and nonlinear input impedance of the inverter

Both phenomena have harmful effects on power-line communications. They shrink the maximum data rate achievable by increasing the noise power in the communications channel. In the worst case, the disturbances can prevent the whole process of power-line communications.

2.5.1 Noise Generated by the DC-Voltage Link Inverter

The DC-voltage link inverter is an effective source of conducting disturbances that spread out into the supplying network. The inverter produces noise that is synchronous to the frequency of the supplying grid and noise that is asynchronous to the frequency of the supplying grid. Correspondingly, the inverter can be considered to be both a source of impulsive noise and a source of harmonic noise. According to (Rhoades, 1995), the electromagnetic disturbances generated by the inverter operation originate mainly from two sources, which are the mains rectifier unit and inverter stage.

At the inverter stage, the high frequency switching and steep voltage rise times produce a high frequency noise. The noise couples through the rectifier unit into the supplying network. The output voltage rise and fall times of a PWM inverter may be with modern insulated gate bipolar transistors (IGBT) in the order of 0.1-10 μs (Bartolucci, 2001). Nowadays, the switching frequencies of PWM inverters vary in the range of 2 - 20 kHz. According to (Silventoinen, 2001), with respect to the supplying network, the inverter stage acts mainly as a common mode emission source at the frequency range 9 kHz – 30 MHz. The noise generated by the inverter stage is impulsive and asynchronous to the frequency of the supplying network. The impulsive disturbance is injected into the supplying network each time when a single IGBT is switched on/off. According to (Silventoinen, 2001), the noise power generated by the inverter can be significantly reduced with a proper mains side filtering. However, normally these filters are sold separately and they are still rarely used.

Another significant noise source of the DC-voltage link inverter is the rectifier unit. The rectifier unit generates mainly harmonic currents and voltages into the supplying network since the phase currents of the rectifier unit are far from sinusoidal. The harmonic components are generated into phase voltages and currents every time when the DC-link capacitor is charged through the rectifier bridge. The frequency content of the harmonic components is dependent on the size of the DC-link capacitor, the size of the DC-link inductor and the load of the inverter. In addition to the harmonic noise, the commutation of the rectifier unit generates impulsive noise spikes with a wide frequency spectrum. Compared to the noise caused by the nonsinusoidal phase currents and voltages the frequency content of the commutation noise is in a significantly

higher frequency band and close to the frequencies used in power-line communications. Thus, the effect of commutation noise in power-line communications is more harmful than the effect of the harmonic components. According to (Silventoinen, 2001), the rectifier unit is an effective source of conducted emissions in the frequency band 9 kHz – 2 MHz and the measurements indicate that the emissions are mainly in differential mode. The noise generated by the uncontrolled rectifier unit is synchronous to the frequency of the supplying network.

The high frequency noise generated by the inverter was measured in the laboratory using an Agilent 54622D digital oscilloscope. The measurement sequence was performed for the ABB ACS 200 inverter that was not equipped with a mains side EMI filter. The inverter was feeding a 15 kW induction motor. Due to the lack of the mains side EMI filtering, the inverter could be considered to be a very effective noise source. All the measurements were carried out with the band pass filter designed to function as a coupling interface of the power-line modem. The purpose of this was to remove the frequencies close to supply frequency and to achieve a good resolution of the noise that exists at the carrier frequencies used in power-line communications. On the other hand, the noise passing through the filter is the actual noise that disturbs the data transmission. The filter used in the measurements was fourth order band pass filter with a centre frequency of the pass band 130 kHz. The attenuation of the filter at frequency 50 Hz was about 100 dB. The gain and the phase curves for the filter are illustrated in figure 4.4 in chapter 4.2.

The noise measured from the mains side of the inverter in the signal coupling (L1, PE) is illustrated in figure 2.38. The upper subfigure in figure 2.38 illustrates the measured noise of the supplying network the inverter being in idle state. The noise voltage floor is only some millivolts, but there are periodic impulsive disturbances that arise from the commutation of the rectifier unit. The lower subfigure in figure 2.38 illustrates the noise generated by the ACS 200 inverter when it is feeding a 15 kW induction motor. The noise voltage level increases significantly. It can be clearly noticed that the inverter stage acts as the main noise source. The same measurements for the signal coupling (L1, L2) are illustrated in figure 2.39. The synchronous noise spikes generated by the rectifier unit have about the same maximum amplitude as those in the signal coupling (L1, PE). Correspondingly, the noise generated by the inverter stage has a smaller amplitude level in the signal coupling (L1, L2) than in the signal coupling (L1, PE). The inverter stage mainly injects common mode noise into the supplying network. On the other hand, the impedance level of the distribution network is probably lower in the signal coupling (L1, L2) than in the signal coupling (L1, PE).

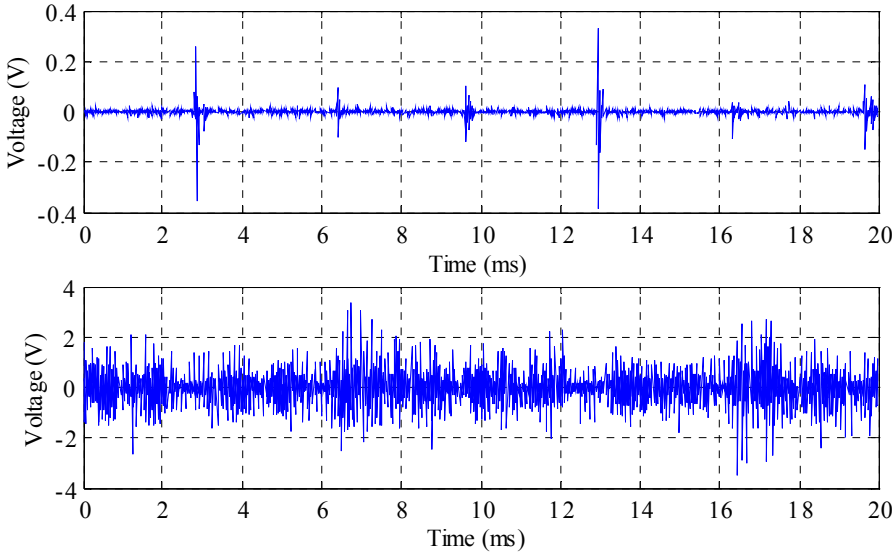

Figure 2.38. Noise of the distribution network measured through the power-line coupling interface in the ACS 200 inverter in the signal coupling (L1, PE). The upper subfigure is measured with the inverter being in idle state. The lower subfigure is measured with the inverter stage being active.

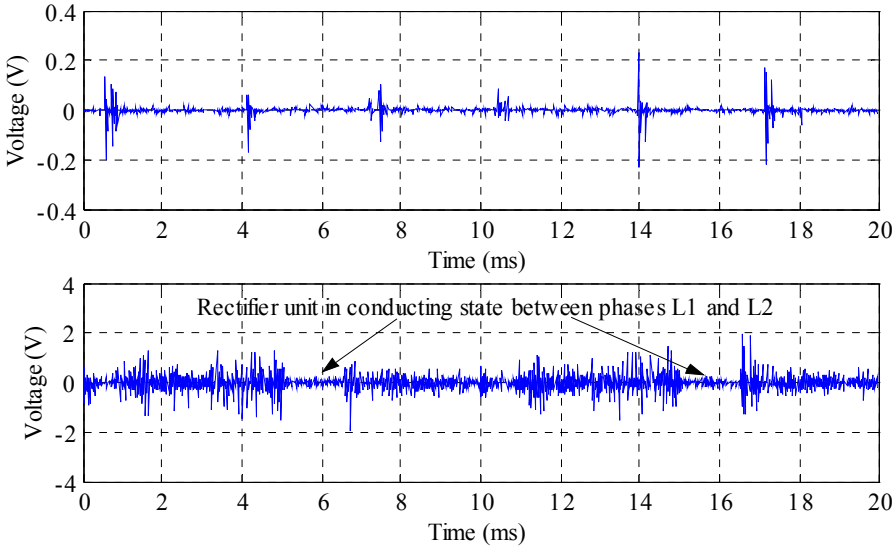

Figure 2.39. Noise of the distribution network measured through the coupling interface in the ABB ACS 200 inverter in the signal coupling (L1, L2). The upper subfigure is measured with the inverter being in idle state. The lower subfigure is measured the inverter stage being active. The noise level drops twice during a period of supply frequency. At these moments, phases L1 and L2 are coupled by the rectifier bridge to charge the DC-link capacitor of the inverter

The moments the DC-link capacitor of the ACS 200 inverter is charged from the phases L1 and L2 can be found in the lower subfigure in figure 2.39. It happens twice during a single period of

the supply frequency. At these moments, the noise level of the supplying network drops due to the drop of the impedance level of the distribution network.

2.5.2 Input Impedance of the DC-Voltage Link Inverter

In the previous chapter, the noise generated by the DC-voltage link inverter was described. The inverter generates also other kind of problems that disturb power-line data transfer in the distribution network. The time variant and nonlinear input impedance of the inverter forms an inappropriate property. In industrial three-phase low voltage distribution networks, this problem is mainly linked to the case in which the power-line modem is coupled between two phases. The input impedance of the inverter in the signal coupling (L1, PE) stays high all the time, because the DC-voltage link is not bound to the potential of the earth.

The inverter input impedance observed between two phases is time variant and nonlinear due to the structure of the inverter. When a diode pair in the rectifier unit is conducting, the conducting phases are directly coupled into the DC-voltage link. The input impedance measured between the conducting phases becomes low due to the low impedance of the large DC-link capacitor (figure 2.40). Thus, the impedance of the supplying network between the phases steeply drops each time the rectifier unit between the phases starts conducting. Correspondingly, the impedance level of the distribution network steeply rises when the diode bridge stops conducting. This mechanism turns the input impedance of the inverter time variant.

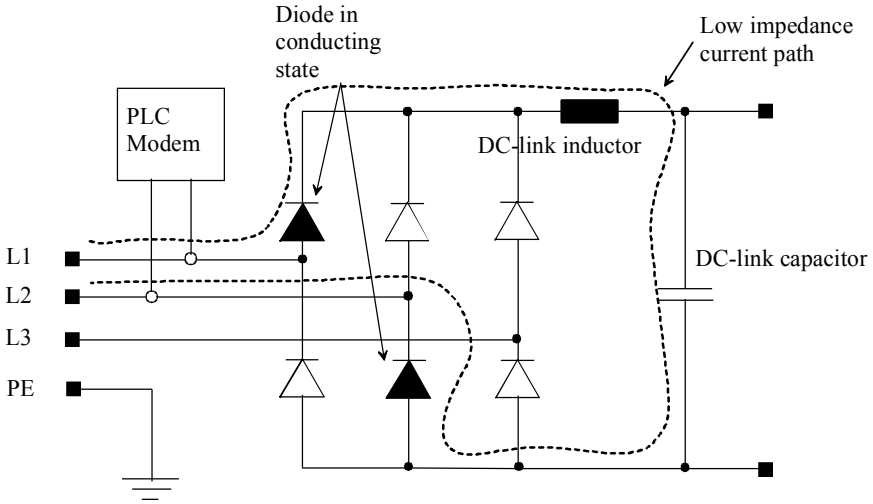

Figure 2.40. The inverter input impedance is time variant and synchronous to the frequency of the supplying network. The input impedance level observed between phases L1 and L2 drops each time the diode bridge between these phases starts conducting.

In addition to the time variance, the inverter input impedance observed between two phases is nonlinear. The diodes of the rectifier unit are nonlinear devices and therefore the rectifier unit of inverter operates as a complex amplitude modulator. When a diode pair between two phases is conducting, it performs a rectangular wave modulation to the carrier signal. The frequency of the modulating wave is equal to the frequency of the carrier wave. The voltage level of the carrier wave drops close to zero when the carrier wave has a positive polarity. This is caused by the low impedance of the DC-voltage link capacitor. Correspondingly, when the polarity of carrier wave is negative, the impedance of the rectifier bridge increases. Thus, the attenuation of the carrier wave decreases. Due to the modulation performed by six-pulse rectifier bridge, the

voltage amplitude of the carrier wave decreases and new harmonic frequencies are generated. The measured attenuation caused by the modulation and impedance changes for the carrier frequency is shown in figure 2.41. The phase voltage waveforms are added to figure 2.41. In figure 2.41, the carrier signal is attenuated each time the rectifier unit starts conducting.

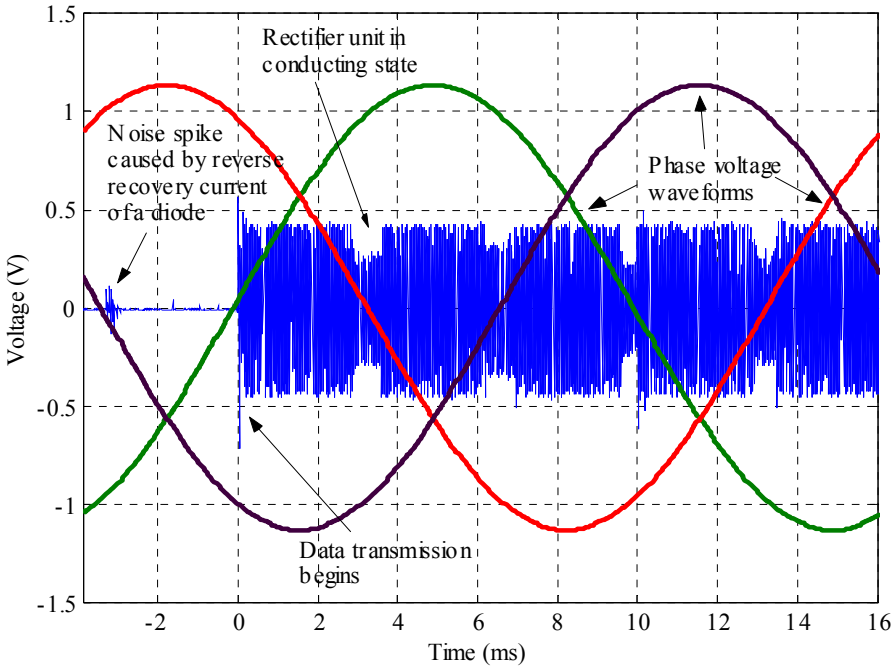

Figure 2.41. The rectifier unit of the ABB ACS 200 inverter both modulates and attenuates the carrier signal which is injected into the distribution network between phases L1 and L2. The inverter is in idle state. The DC-link capacitor of the inverter is loaded six times during a period of supply frequency. The measurement is performed using the power-line interface of a power-line modem as a coupling device.

2.5.3 Effect of the DC-Voltage Link Inverter on Power-Line Communications

Generally, the inverter can be considered to be a harmful device for the power-line communications system operating in the same distribution network. The inverter is an effective source of conducting noise as well as nonlinear load that distorts the signals injected into the distribution network. The high frequency noise generated by the inverter is mainly impulsive and it results from the rectifier unit and inverter stage. The inverter primarily generates four types of disturbances into the supplying network:

1. Noise generated by the rectifier unit and inverter stage
2. Time variant input impedance that is synchronous to the frequency of the supplying network
3. Complex amplitude modulation of carrier signal performed by the rectifier unit
4. Power reflection caused by the impedance mismatch at the interface of inverter input and the low voltage power cable.

According to the results, the sudden drop or rise in the input impedance is the most serious problem caused by the inverter and it can prevent from the transferring data with power-line data transfer in the distribution network. However, this problem can be effectively avoided. The

easiest means of avoiding this problem is to connect the power-line modem between phase and protective earth. The DC-voltage link is isolated from the protective earth. Thus, the operation of the rectifier unit will not significantly affect the impedance level the modem experiences. Another way to avoid or minimise problems is to transmit the data only at those moments the DC-link is not charged through the phases that are used for communications. The noise generated by the inverter decreases the achievable data transfer rate and increases the number of data transfer errors.

2.6 Input Impedance of the Distribution Transformer

The distribution transformer also acts as a termination impedance to the power-line data transfer system as well as electric motors, inverters and other appliances that are connected to the low voltage distribution network. For this reason, an insight into the high frequency characteristics of the transformer is required.

The input impedances of single and three phase power transformers were measured in (Liu, 1992) at the frequency range of 50 Hz to 1 MHz. The measurements were carried out for the signal coupling between phase and transformer frame. According to (Liu, 1992), the input impedance of the distribution transformer is a function of a frequency and consists of sequential parallel and serial resonances. The first resonance is a parallel resonance and it is found at a frequency below 80 kHz. At the first parallel resonance, the input impedance of the transformer is about 1–10 kΩ. In (Liu, 1992), it is also indicated that the iron core of the transformer starts to appear like an air core at frequencies around 50 kHz. The high frequency characteristics of power transformers were modelled in article (Popov, 2001), where a lumped parameter model was formed for the simulation of transients caused by switching surges.

Some laboratory tests were carried out to measure the input impedance of the distribution transformer (France Transfo, 50 kVA, 20 kV/400 V). The measurements for the signal couplings (L1, PE) and (L1, L2) are illustrated in figures 2.42 and 2.43. During the measurements, the high voltage side of the transformer was open. However, according to (Dostert, 2001), in the frequency range above 20 kHz, the distribution transformers are almost perfect barriers. Hence, the impedance level on the high voltage side of the transformer should not affect the input impedance measured from the low voltage side.

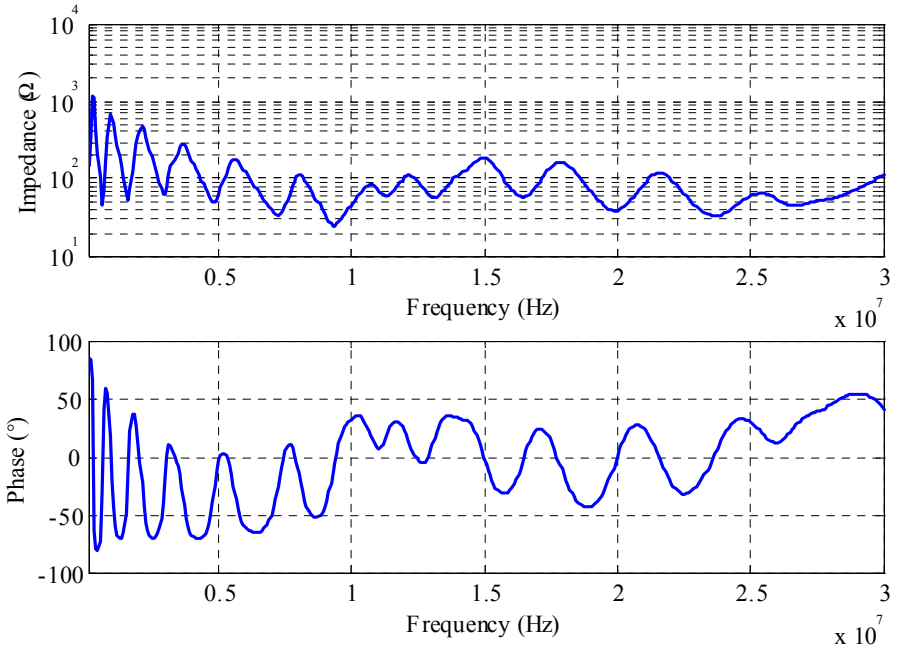

Figure 2.42. Input impedance of the distribution transformer (50 kVA, 20 kV/400V) measured from the low voltage side and in the signal coupling (L1, PE) and in the frequency band 100 kHz – 30 MHz.

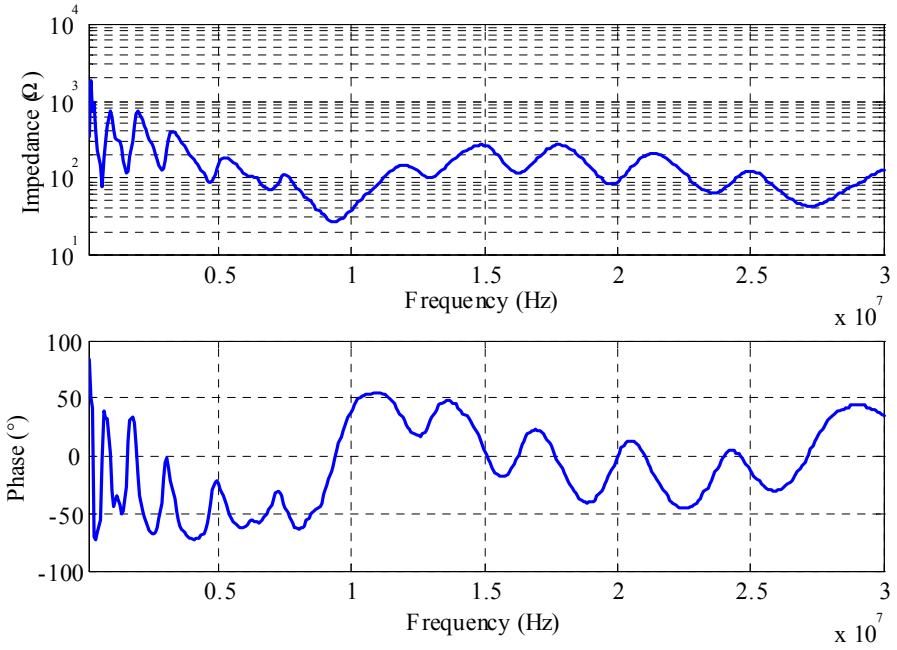

Figure 2.43. Input impedance of the distribution transformer (50 kVA, 20 kV/400V) measured from the low voltage side and in the signal coupling (L1, L2) and in the frequency band 100 kHz – 30 MHz.

The sequential serial and parallel resonances reported by (Liu, 1992) are also shown in figures 2.42 and 2.43. The absolute value of the impedance varies in both measurements between 10 Ω and 1 kΩ. According to the measurements and research carried out earlier, the following conclusions about the characteristics of distribution transformer can be made:

- The input impedance of the distribution transformer is frequency variant consisting of sequential parallel and serial resonances.
- With respect to power-line communications, the distribution transformer is mismatched load, which causes power reflections and multipath signal propagation when transmitting a signal in the distribution network.
- Although the input impedance of the transformer may be close to the characteristic impedance of the power cable, the input impedance is either capacitive or inductive.
- The impedance level at the high voltage side should not affect the impedance level at low voltage side.

3. Characteristics of the Pilot Distribution Network

3.1 Introduction to Chapter 3

In chapter 2, the high frequency characteristics of individual distribution network components were measured, modelled and analysed. The selected network components, cables, electric motors, inverters and distribution transformers are the main components of a typical industrial low voltage distribution network. In order to analyse the high frequency characteristics of a complete distribution network and the effect of individual components on the characteristics, a pilot network was constructed (figure 3.1).

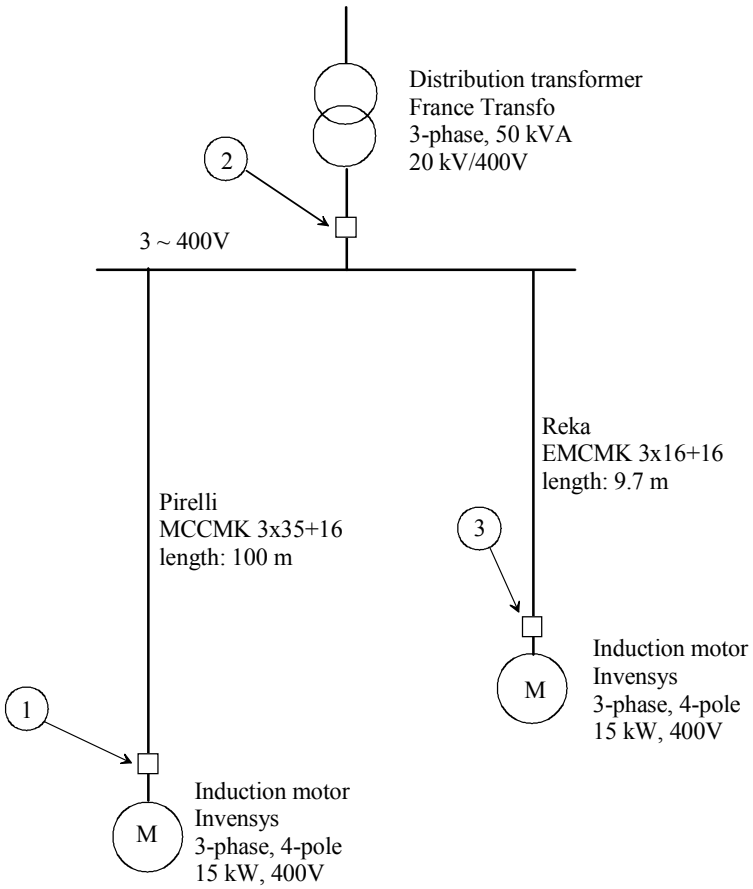

Figure 3.1. Topology of the pilot environment. The pilot environment is a simple industrial three-phase low voltage distribution network. The markings in the figure represent the test points, which are used for the injecting of signals into and measuring of signals in the pilot environment.

The pilot environment (figure 3.1) is a simple industrial low voltage distribution network, in which the motors could be monitored with the remote diagnostics system (figure 1.5). The components of the network are selected such that the distribution transformer is capable to feed the motors and the cables are capable to safely carry the current drawn by the motors. Due to the simple topology, the effects of individual components on the characteristics of the distribution network may possibly be observed and the frequency responses of the network can be

modelled utilising the models developed for the cables and electric motors. Since there is not available any transformer model, the input impedance measurement data for the distribution transformer are used directly in simulations.

In the beginning of this chapter, the modelling of power-line channels is discussed and the method used in this work is introduced. After this, the simulation models are formed for the pilot environment and the simulation results are compared with the frequency response measurements carried out for the pilot environment. Next, noise current measurements are performed for the pilot environment and the channel capacity analysis is carried out. Finally, the characteristics of the pilot environment with respect of power-line communications are analysed and summarised.

3.2 Modelling the Power-Line Channels

In order to simulate a communications channel, a channel model is required. There exist two alternatives of approaching for the modelling of power-line channels. The first one applies the methods used for the modelling of radio channels. The power-line channel is assumed to be a multipath propagation environment. The parameters of the channel are acquired based on the topology of the distribution network or based on the channel measurements and optimisation algorithm. This kind of channel models are presented e.g. in (Zimmermann, 1999) and (Philipps, 1999). The transmitted signal arrives in the receiver via the N signalling path. On path v the arriving signal is delayed by the time τ_v and attenuated by the complex attenuation factor $\boldsymbol{\rho}_v$:

$$\boldsymbol{\rho}_v = \left|\boldsymbol{\rho}_v\right| \cdot e^{j\varphi_v}, \tag{3.1}$$

where φ_v is the phase of the complex attenuation factor. The impulse response of the channel $h(t)$ can be written as a sum of the delayed and attenuated Dirac pulses:

$$h(t) = \sum_{v=1}^{N} \left|\boldsymbol{\rho}_v\right| \cdot e^{j\varphi_v} \cdot \delta(t - \tau_v), \tag{3.2}$$

where $\delta(t)$ is the Dirac pulse. The other alternative applies the methods used to model electricity distribution networks. These approaches are introduced e.g. in (Banwell, 2001) and (Esmailian, 2002). Both approaches have their advantages and disadvantages. In this work, the later method has been chosen, because the topology of the pilot distribution network is known and the high frequency characteristics of the individual network components were modelled and measured earlier. The basics of the applied modelling method are discussed below.

The transmission or chain parameter matrices can be applied for the modelling the transfer function of a communications channel. The analysis is applicable for TEM waves. The relation between input voltage and current and output voltage and current of a two-port network can be described (figure 3.2) as:

$$\begin{bmatrix} \mathbf{V}_1 \\ \mathbf{I}_1 \end{bmatrix} = \begin{bmatrix} \mathbf{A} & \mathbf{B} \\ \mathbf{C} & \mathbf{D} \end{bmatrix} \begin{bmatrix} \mathbf{V}_2 \\ \mathbf{I}_2 \end{bmatrix}, \tag{3.3}$$

where **A**, **B**, **C** and **D** are frequency dependent coefficients.

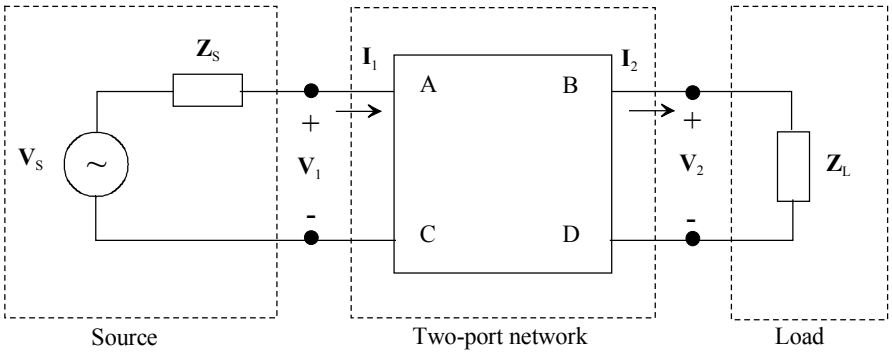

Figure 3.2. Two-port network connected to a voltage source and load. The signal source consists of a voltage source and the serially connected internal impedance.

The frequency dependent input impedance of the two-port network (figure 3.2) can be calculated by equation:

$$\mathbf{Z}_{\text{in}} = \frac{\mathbf{A}\mathbf{Z}_{\text{L}} + \mathbf{B}}{\mathbf{C}\mathbf{Z}_{\text{L}} + \mathbf{D}}. \tag{3.4}$$

Respectively, the amplitude and phase at a certain signal frequency is given by equation:

$$\mathbf{H} = \frac{\mathbf{V}_2}{\mathbf{V}_{\text{S}}} = \frac{\mathbf{Z}_{\text{L}}}{\mathbf{A}\mathbf{Z}_{\text{L}} + \mathbf{B} + \mathbf{C}\mathbf{Z}_{\text{L}}\mathbf{Z}_{\text{S}} + \mathbf{D}\mathbf{Z}_{\text{S}}}. \tag{3.5}$$

The coefficients of the transmission matrix are dependent on the type of the load. The transmission matrix for the transmission line is:

$$\begin{bmatrix} \mathbf{A} & \mathbf{B} \\ \mathbf{C} & \mathbf{D} \end{bmatrix} = \begin{bmatrix} \cosh(\gamma L) & \mathbf{Z}_0 \sinh(\gamma L) \\ \dfrac{1}{\mathbf{Z}_0}\sinh(\gamma L) & \cosh(\gamma L) \end{bmatrix}. \tag{3.6}$$

The transmission matrix for the serially connected impedance $\mathbf{Z}_{\text{S}}$ is given by:

$$\begin{bmatrix} \mathbf{A} & \mathbf{B} \\ \mathbf{C} & \mathbf{D} \end{bmatrix} = \begin{bmatrix} 1 & \mathbf{Z}_{\text{S}} \\ 0 & 1 \end{bmatrix}, \tag{3.7}$$

and the transmission matrix for the parallel connection of load impedance $\mathbf{Z}_{\text{P}}$ is:

$$\begin{bmatrix} \mathbf{A} & \mathbf{B} \\ \mathbf{C} & \mathbf{D} \end{bmatrix} = \begin{bmatrix} 1 & 0 \\ 1/\mathbf{Z}_{\text{P}} & 1 \end{bmatrix}. \tag{3.8}$$

The branch cable terminated by the load impedance $\mathbf{Z}$ can be considered to be equivalent load impedance $\mathbf{Z}_{\text{eq}}$:

$$\mathbf{Z}_{eq} = \mathbf{Z}_0 \frac{\mathbf{Z} + \mathbf{Z}_0 \tanh(\gamma L)}{\mathbf{Z}_0 + \mathbf{Z} \tanh(\gamma L)}. \quad (3.9)$$

The channel from a source to a load may consist of several network sections having different cabling, branch cables and loads connected in parallel. Each section can be described with a single transmission matrix. The sections are serially connected. The transmission matrix **T** from the source to the load can be formed applying the chain rule:

$$\mathbf{T} = \prod_{i=1}^{n} \mathbf{T}_i , \quad (3.10)$$

where n represents number of network sections. Figure 3.3 illustrates an example of a channel model formed using the transmission matrices for the pilot environment (figure 3.1).

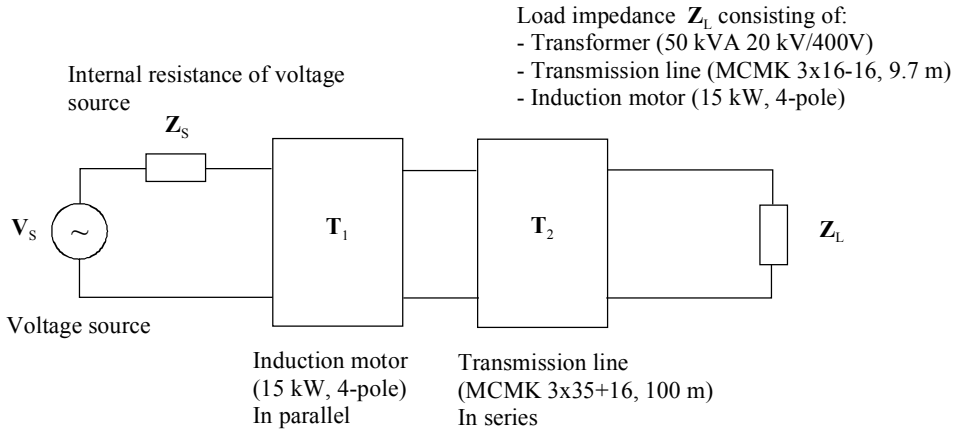

Figure 3.3. Example of channel model that is formed for the pilot environment using transmission matrices. The model represents the channel from (figure 3.1, point 1) to (figure 3.1, point 2).

3.3 Amplitude and Phase Responses of the Pilot Environment

Both the amplitude and phase response are significant parameters for a communications channel. The amplitude response determines the signal voltage attenuation, when the signal propagates through the channel from a transmitter to a receiver. Furthermore, the signal attenuation together with a signal to noise ratio and with the available bandwidth determine the maximum data transfer rate that can be theoretically attained. In addition to the amplitude response, the phase response is also an important parameter when considering the quality of the channel for digital communications. For the channel the linear phase response is desirable characteristics. Due to the phase nonlinearities, the waveform of the transmitted symbol changes when propagating through the channel from the sending point to the receiving point. This easily leads to synchronisation errors if data are transmitted parallel using the multicarrier data transfer methods, as e.g. OFDM (orthogonal frequency division multiplexing). The linearity of the phase response is described by a term group delay or envelope delay τ_g:

$$\tau_g(f) = -\frac{1}{2\pi} \frac{d\theta(f)}{df}, \quad (3.11)$$

where θ describes the signal phase. With linear phased channel the group delay should be constant. The group delay is interpreted as the propagation time of a signal frequency component from the input to the output of the system (Proakis, 1996).

Simulation models were formed for the power-line channels of the pilot environment using the procedure and methods described in chapter 3.2. An example procedure is presented in appendix II. The simulation results were verified by performing a series of amplitude response measurements for the pilot environment. The measurements were carried out by injecting the signal into the pilot distribution network using a function generator and measuring signal voltages with two oscilloscopes, one in the transmitting point and the other in the receiving point. The simulated and measured amplitude responses, the simulated phase responses and group delays are illustrated in figures 3.4–3.9.

In figure 3.4 the simulated and measured amplitude responses are illustrated for the channel from (figure 3.1, point 1) to (figure 3.1, point 2) in the frequency band 100 kHz – 20 MHz and in the signal coupling (L1, PE). The simulated phase response and group delay for the same channel are presented in figure 3.5. In figure 3.6, respectively, the simulated and measured amplitude responses are illustrated for the power-line channel (figure 3.1, point 3) to (figure 3.1, point 2). The signal coupling was (L1, PE) and the frequency band ranging from 100 kHz to 15 MHz. The simulated phase response and group delay for the same channel are presented in figure 3.7. The simulated and measured amplitude and phase responses for the frequency band 10–100 kHz are illustrated in figures 3.8 and 3.9. The channel was from (figure 3.1, point 1) to (figure 3.1, point 2) and the signal coupling (L1, PE).

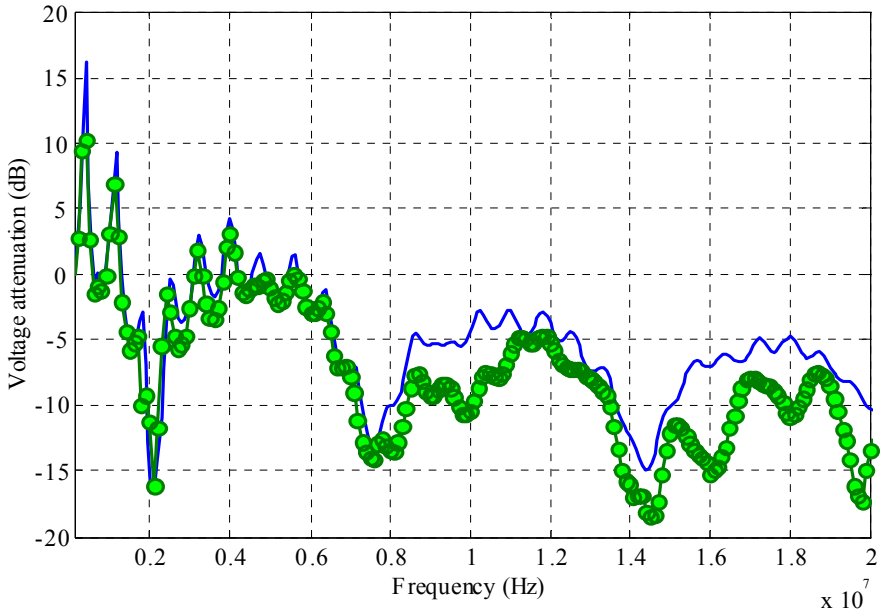

Figure 3.4. Simulated (solid line) and measured (marked with circles) amplitude response for the frequency band 100 kHz – 20 MHz. The distance between receiver and transmitter is 100 metres and the signal coupling is (L1, PE). The simulated curve models relatively accurately the measured curve. The notches and peaks in the amplitude response curves result from the impedance mismatches between cabling and loads connected to the distribution network.

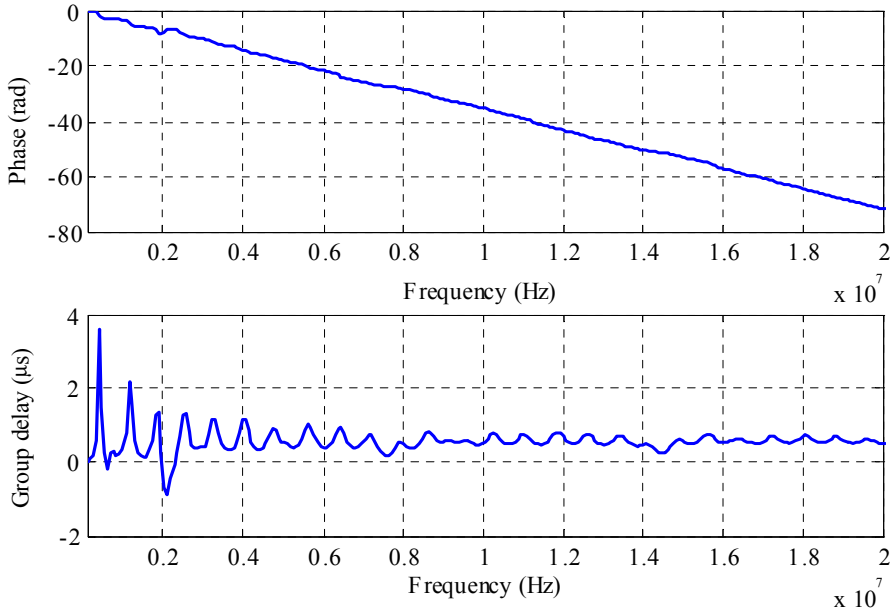

Figure 3.5. Simulated phase and group delay for the frequency band 100 kHz – 20 MHz. The signal coupling is (L1, PE) and the distance between receiver and transmitter is 100 m.

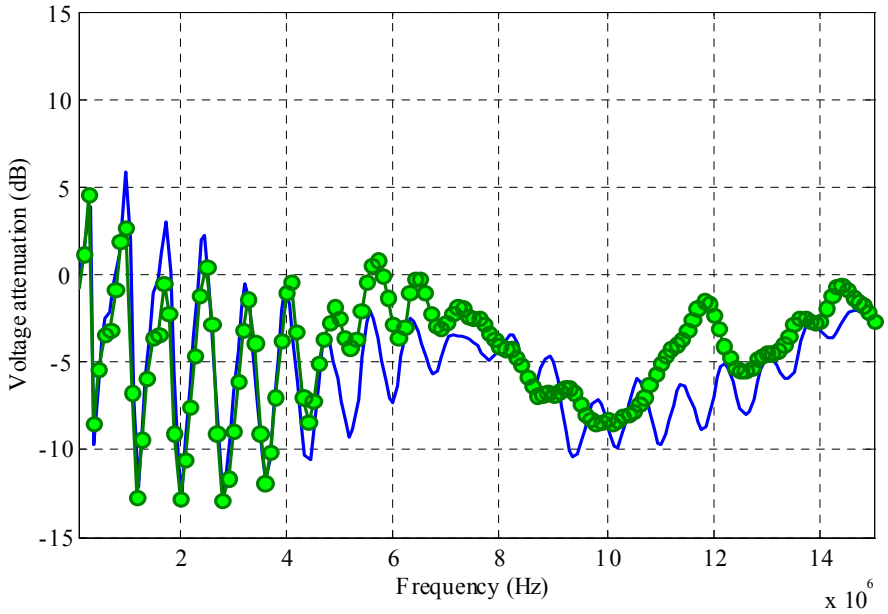

Figure 3.6. Simulated (solid line) and measured (marked with circles) amplitude response for the frequency band 100 kHz – 15 MHz. The distance between receiver and transmitter is 9.7 metres and signal coupling is (L1, PE).

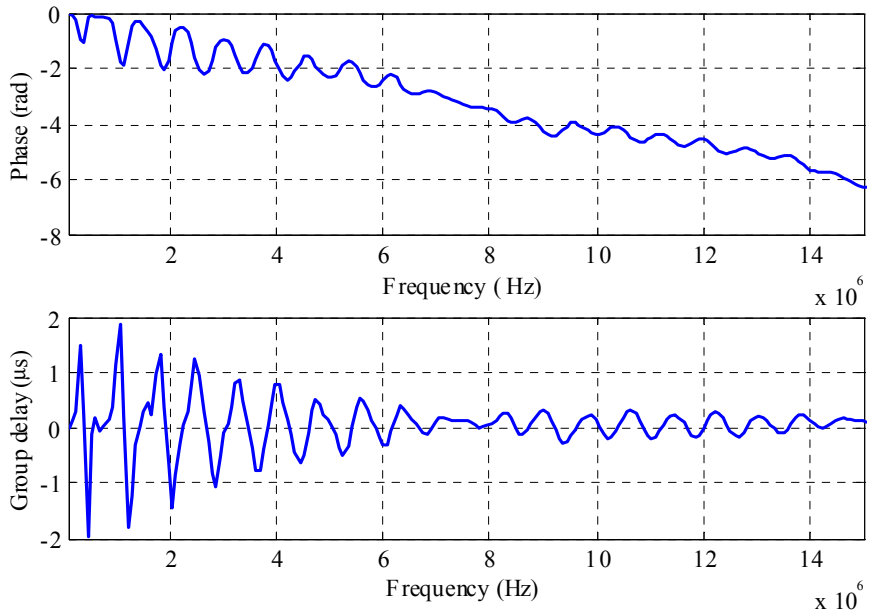

Figure 3.7. Simulated phase and group delay for the frequency band 100 kHz – 15 MHz. The signal coupling is (L1, PE) and the distance between receiver and transmitter is 9.7 m.

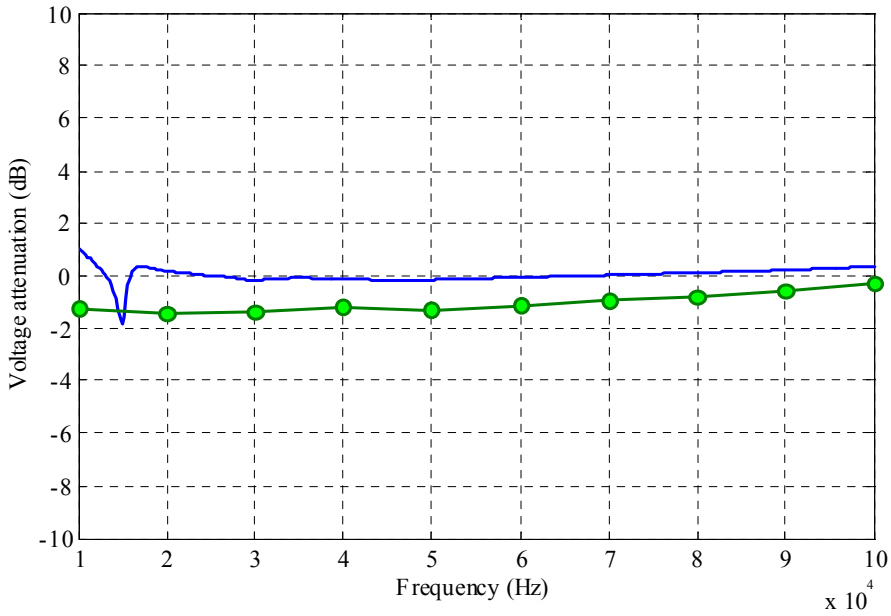

Figure 3.8. Simulated and measured amplitude responses for the frequency band 10-100 kHz. The distance between receiver and transmitter is 100 metres and signal coupling is (L1, PE). The notch at frequency 15 kHz in the simulated curve is caused by the serial resonance of the transformer. The voltage attenuation of the measured amplitude response is slightly higher compared to the simulated curve. The difference results mainly from the too high impedance of the input impedance model of the motor at frequencies less than 100 kHz.

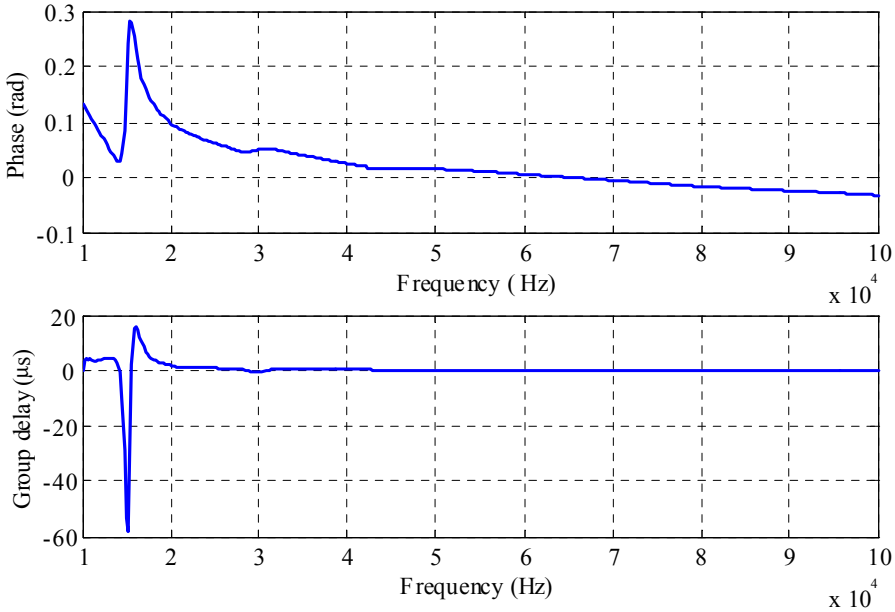

Figure 3.9. Simulated phase and group delay for the frequency band 10-100 kHz. The signal coupling is (L1, PE) and the distance between receiver and transmitter is 100 m.

It is possible to observe, that the simulations and the measurements correspond each other. The notches and peak are at the same frequencies. In addition, the attenuation levels both in the simulations and measurements are corresponding. This leads us to the conclusion that the formed cable and motor models have to be valid at least in the pilot environment and at least up to the signal frequency 15 MHz. However, it is probable that at higher frequencies there may be differences between the simulated and measured amplitude responses.

The distributed capacitance value of the cables was modified during the simulations. The value was increased about 10-40% in order to match the notches and the peaks in the simulations with measurements. The main reason for this is that the permittivities of the PVC insulation materials used in the researched cables seems to be larger than the values determined by the input impedance measurements. The surge wave test presented in (figure 2.15) supports this indication.

The impulse response of the communications channel can be formed from the frequency response of the channel by performing the inverse discrete Fourier transform (IDFT) for the simulated frequency response:

$$\mathbf{x}(n) = \frac{1}{N}\sum_{k=0}^{N-1}\mathbf{X}(k)\mathrm{e}^{j2\pi kn/N} \quad n = 0,1,2,\ldots,N-1, \tag{3.12}$$

where $\mathbf{x}(n)$ is the discrete time series representing the impulse response of the channel and $\mathbf{X}(k)$:s are the coefficients of discrete Fourier transform (DFT) representing N point frequency response of the channel. In figure 3.10, the normalised amplitude of impulse response is illustrated for the channel (figure 3.1, point 1) to (figure 3.1, point 2). The multipath propagation characteristics of power-line channel can be clearly seen. The power injected from the transmit-

ter is spread in the time space due to the multipath propagation caused by the impedance mismatches and branches in the channel. The total length of the impulse response is about $2\,\mu s$ (figure 3.10). The main impulse sent from the transmitter propagates to the receiver in about $0.6\,\mu s$. The distance between transmitter and receiver is 100 metres. This corresponds to the propagation velocity of the electromagnetic wave $0.56c_0$. Part of the transmitted power is dissipated in the transformer, part is reflected back in the direction of the transmitter and part continues in the direction of the second electric motor (figure 3.1, point 3). When the impulse reaches the interface of the cable and the motor (figure 3.1, point 3), part of the power carried by the impulse is dissipated and the rest is reflected back due to the impedance mismatch. The first echo in figure 3.10 represents the power reflected back from the motor (figure 3.1, point 3). The time space between main impulse and first echo is about $0.15\,\mu s$. This corresponds to the propagation distance of the electromagnetic wave $2*9.7\,m$ at speed $0.43c_0$. The second echo in figure 3.10 results also from the power reflection in (figure 3.1, point 3) and the third echo results from the second power reflection in (figure 3.1, point 1).

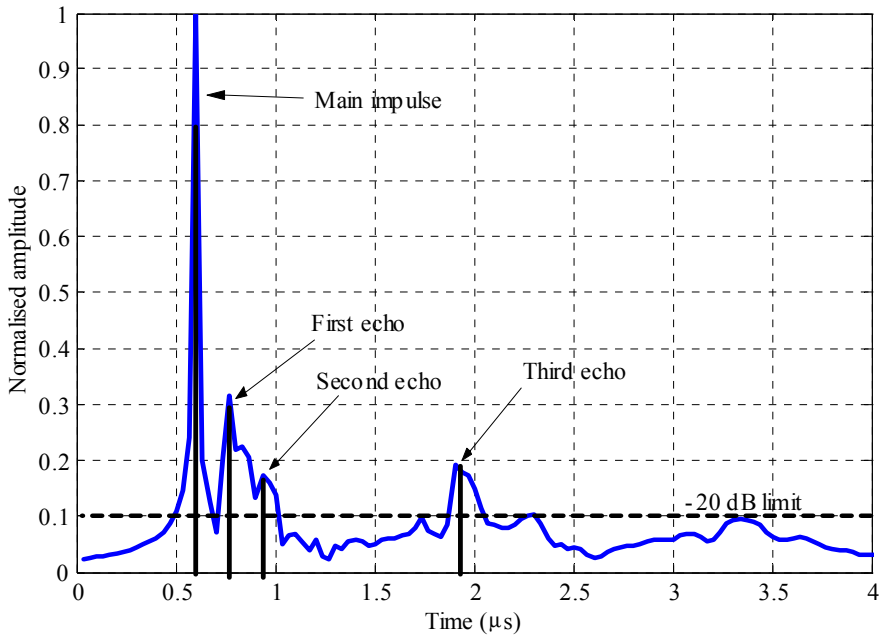

Figure 3.10. Normalised amplitude of the impulse response calculated from the simulated frequency response. The most significant impulses caused by power reflections are marked in the figure with arrows. The length of the impulse response is about 2 µs.

3.3.1 Characteristics of the Pilot Environment in the Frequency Band 3 – 148.5 kHz

In the GENELEC frequency band (3–148.5 kHz) and with industrial cable lengths the attenuation caused by the cabling can be considered to be low. Typically, the voltage attenuation of the carrier signal in a power-line channel is less than -10 dB (figure 3.8) and the phase response is relatively linear (figure 3.9). In addition, the number of notches in the amplitude response is small. The notches in the amplitude response are primarily caused by the serial resonances of the distribution transformers and other appliances connected to the distribution network. The

occurrence of notches and peaks in the frequency response generated by standing waves is rare due to the relatively short network lengths compared to the wavelength of the electromagnetic wave. However, the occurrence of standing waves is limited only by the network length. The load impedances of the network are strongly mismatched with the cabling. The main parameters affecting the signal voltage attenuation in power-line channels and in the GENELEC frequency band are:

- Number and type of loads connected to the distribution network
- Topology of the distribution network
- Branch cables

3.3.2 Characteristics of the Pilot Environment in the Frequency Band 148.5 kHz – 30 MHz

In the frequency band 148.5 kHz – 30 MHz the signal attenuation in the pilot environment is also relative light, but it is significantly higher than in the frequency band 3 – 148.5 kHz. The maximum attenuation level is less than –20 dB and the channel has lowpass characteristics due to the frequency dependent attenuation of the cables (figures 3.4 and 3.6). The electric motor is an imperfect cable termination, which makes the input impedance of the cable and motor combination frequency variant. Due to this fact, frequently repeating peaks and notches occur in the amplitude response and in the group delay. The signal voltage amplitude on the load may be even larger than on the source. The oscillations in the amplitude responses attenuate as a function of frequency. The increasing attenuation of the cable primarily causes this phenomenon. The wave reflected from the interface of motor and cable attenuates significantly before reaching the transmitter again. The main factors that affect the signal voltage attenuation as it propagates through a communications channel are:

- Attenuation of cabling
- Number and type of loads connected to the distribution network
- Branch cables
- Topology of distribution network
- Signal frequency

At high signal frequencies, the signal voltage attenuation depends on many things and it cannot be dicovered straightforwardly, which is the voltage attenuation in a certain channel and frequency.

Also the phase response is an important parameter. According to the simulations, the absolute value of the phase increases as a function of frequency (figures 3.5 and 3.7). This is natural, since the propagation velocity of the electromagnetic wave is close to constant as a function of frequency. Thus, the higher the signal frequency is, the more wavelengths will fit into the same cable length. This means that phase of the transmitted signal increases as a function of frequency. In the frequency band 148.5 kHz – 30 MHz the variations of the group delay may cause problems for data transfer.

3.4 Channel Capacity Analysis and Bit Error Probability

The information capacity of a communications channel describes the number of independent symbols that can be transmitted through the channel in a given unit of time. The basic symbol in digital communications is the bit. In communication, the transmitter injects a signal into the channel (figure 3.11). The channel filters the transmitted signal and at the receiver noise is added to the transmitted signal.

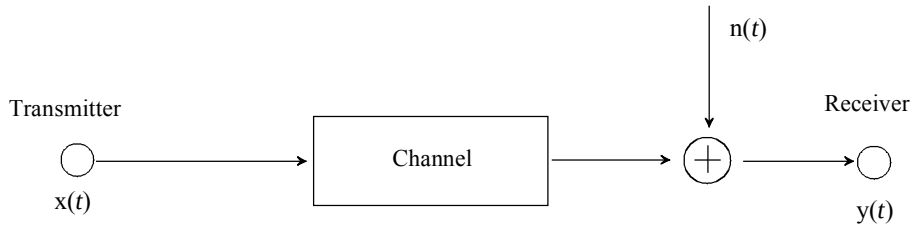

Figure 3.11. General communications channel model. The transmitter injects a signal into the communications channel, which filters the injected signal. Noise is added to the filtered signal at the receiver.

The capacity of the channel is dependent on the signal to noise ratio at the receiver and the bandwidth available for data transfer. C.E. Shannon from Bell Telephone Laboratories presented in 1948 the mathematical formula for the information capacity of a communications channel:

$$C = B\log_2\left(1+\frac{S}{N}\right), \tag{3.13}$$

where C represents the information capacity of the channel (bits/second), B is the available bandwidth and the symbols S and N represent the signal and the noise power at the input of the receiver. Shannon's theorem is not directly applicable for the capacity analysis of a power-line channel, because the signal to noise ratio is frequency variant with practical channels.

The output voltage amplitude of the transmitter $\left|\mathbf{U}_{\mathrm{tx}}(f)\right|$ can be presented with the output power of the transmitter $P_{\mathrm{tx}}(f)$ and the input impedance of the communications channel at the transmitter $\mathbf{Z}_{\mathrm{in,tx}}(f)$:

$$\left|\mathbf{U}_{\mathrm{tx}}(f)\right| = \left|\sqrt{\frac{P_{\mathrm{tx}}(f)}{\cos\varphi(f)}\cdot\mathbf{Z}_{\mathrm{in,tx}}(f)}\right|, \tag{3.14}$$

where $\cos\varphi(f)$ is the phase angle of the input impedance $\mathbf{Z}_{\mathrm{in,tx}}(f)$. The voltage amplitude of the received signal at the receiver $\left|\mathbf{U}_{\mathrm{rx}}(f)\right|$ can be written as:

$$\left|\mathbf{U}_{\mathrm{rx}}(f)\right| = \left|\mathbf{H}(f)\right|\cdot\left|\mathbf{U}_{\mathrm{tx}}(f)\right|, \tag{3.15}$$

where $\mathbf{H}(f)$ is the transfer function of the communications channel. The information capacity of the channel presented with the signal voltage and noise voltage amplitudes is:

$$C = \int_{f_l}^{f_h}\log_2\left[1+\left(\frac{\left|\mathbf{U}_{\mathrm{rx}}(f)\right|}{\left|\mathbf{U}_{\mathrm{n}}(f)\right|}\right)^2\right]df\ , \tag{3.16}$$

where $B = f_h - f_l$ and $|\mathbf{U}_n(f)|$ is the amplitude of the noise voltage at the receiver. The noise voltage amplitude can be calculated applying the noise current amplitude $|\mathbf{I}_n(f)|$ and the input impedance at the receiver:

$$|\mathbf{U}_n(f)| = |\mathbf{Z}_{in,rx}(f)| \cdot |\mathbf{I}_n(f)| . \quad (3.17)$$

Shannon's theorem gives the theoretical data transfer rate of the communications channel that can be achieved at a low probability of data transfer errors. Another quantity to estimate the quality of the communications channel and the receiver is the bit error ratio (BER). It describes the probability of error per received bit. Theoretically, the bit error ratio is dependent on the signal to noise ratio at the receiver and on the used modulation method. The bit error ratio for binary FSK can be estimated using equation:

$$\mathrm{BER} = \frac{1}{2}\mathrm{erfc}\left(\sqrt{\frac{\gamma_b}{2}}\right), \quad (3.18)$$

where γ_b is the signal to noise ratio per received bit and

$$\mathrm{erfc}(x) = \frac{2}{\sqrt{\pi}} \int_x^\infty \mathrm{e}^{-t} dt . \quad (3.19)$$

3.4.1 Noise Measurements and Channel Capacity Estimation

The theoretical data transfer capacities of the power-line channels in the pilot environment are estimated in this chapter. The estimation is performed for the frequency bands GENELEC (3-148.5 kHz) and 3 kHz – 30 MHz. Estimation of the capacity requires noise voltage spectrum at the receiver. The noise voltage spectrum at the receiver can be estimated if both the noise current spectrum at the receiver and the input impedance at the receiver are known. The input impedance at the receiver can be estimated using the simulation model for the pilot environment introduced previously. Thus, only noise current spectrum measurements are required.

The noise current measurements were performed with a Rohde & Schwarz EHSHS 30 EMI Test Receiver and with a Rohde & Schwarz EZ-17 current probe. The test receiver was set to peak detect mode and the intermediate filter of the receiver was set to bandwidth 10 kHz. The noise current was measured from a single phase. The measured frequency bands were 9 kHz – 30 MHz and 9–150 kHz (figures 3.12 and 3.13). The noise current measurements were obtained when the ABB ACS 200 inverter connected to the pilot environment was both in idle and in operational state. To carry out the noise current measurements, the pilot environment was connected to the supplying network of the laboratory. Thus, the actual impedance levels may be a bit different from the levels in the pilot environment without supply voltage.

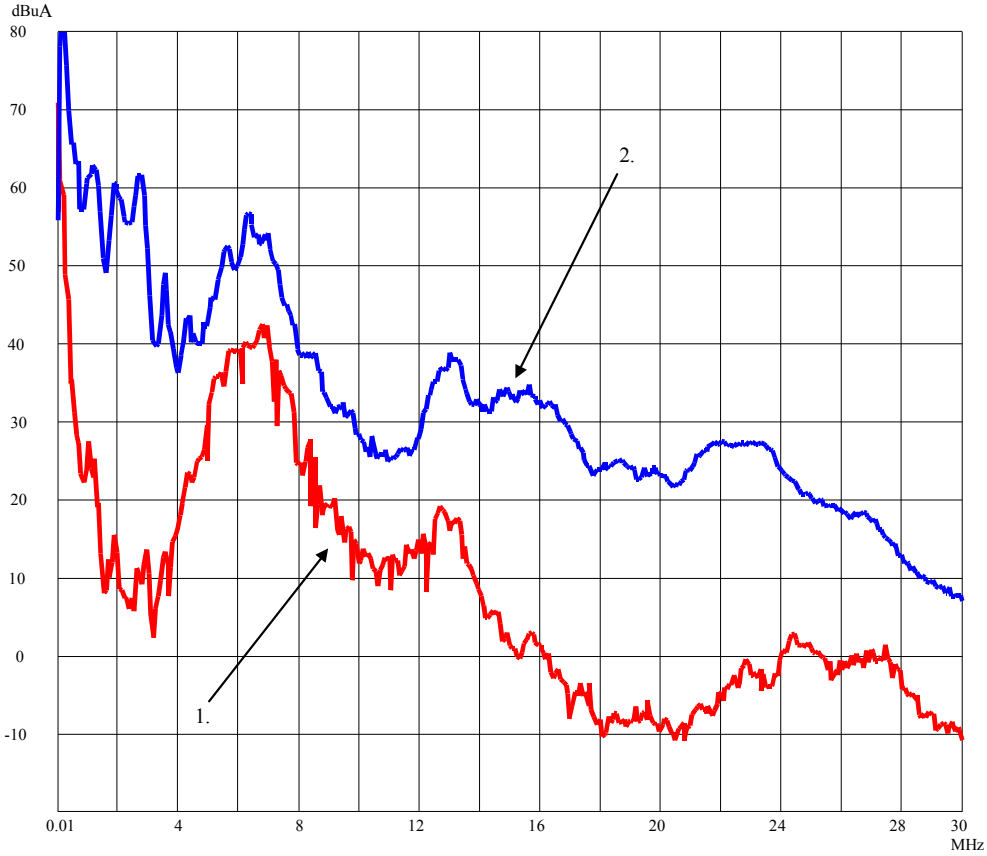

Figure 3.12. Noise current measurement in the frequency band 9 kHz – 30 MHz in the pilot environment connected to the distribution network of the laboratory. The measurement is carried out with a Rohde & Schwarz EHSHS 30 EMI Test Receiver and with a Rohde & Schwarz EZ-17 current probe from a single phase. The curve denoted with (1.) is measured the inverter being in idle state and the curve denoted with (2.) is measured the inverter being active. The frequency stepping of the measurements is 9 kHz and intermediate filter with a bandwidth of 10 kHz is used.

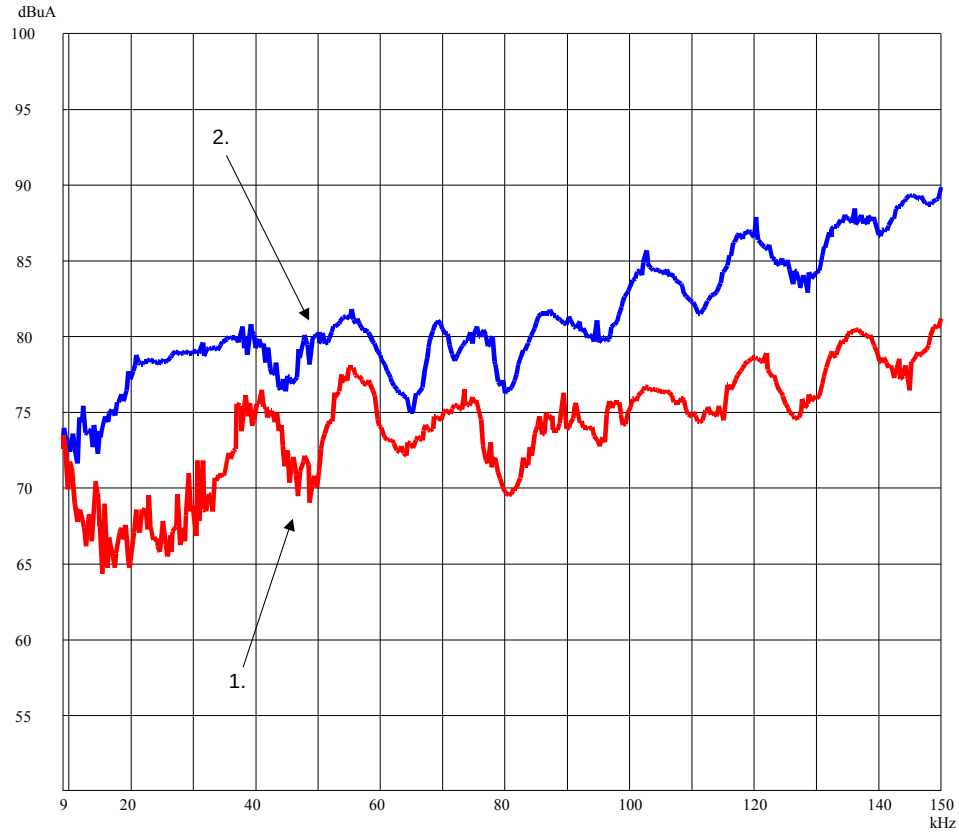

Figure 3.13. Noise current measurement in the frequency band 9-150 kHz in the pilot environment connected to the distribution network of the laboratory. The measurement was carried out with Rohde & Schwarz EHSHS 30 EMI Test Receiver and with Rohde & Schwarz EZ-17 current probe from a single phase. The curve denoted with (1.) is measured the inverter being in idle state and in the curve denoted with (2.) is measured the inverter being active.

According to the noise current measurements (figures 3.12 and 3.13), the activity of the inverter has a strong effect on the noise current levels in the distribution network. It increases the noise current levels from 10 dB to 50 dB depending on the frequency. The effect of the inverter on the noise current level is strongest in the frequency band 2-4 MHz. The trend of the noise current level is descending as a function of frequency (figure 3.12).

The EMI receiver used in the noise current measurements sampled the noise current by frequency stepping of 9 kHz searching a peak value for each frequency band. Thus, it performed the Fourier transform for the noise current with matched filters and with frequency a stepping of 9 kHz.

In order to estimate the data transfer capacity of the channel, the signal to noise ratio at the receiver should be known. Thus, the power spectrum of the transmitted signal at the receiver must be known. The power spectrum at the receiver is dependent on the power spectrum of the transmitted signal and the characteristics of the channel. Correspondingly, the power spectrum of the transmitted signal is dependent on the total transmitted power and the distribution of the transmitted power in the frequency space. In channel capacity estimations, the transmitted power varied in the range 0.2-20 mW. According to the GENELEC specification (EN, 1991), in

the frequency range from 95 kHz to 148.5 kHz, the maximum allowed output power of the power-line transmitter was estimated to be of the order of 10 mW. In this analysis, the transmitted power was distributed with a flat power spectrum. This is not an ideal solution, because the noise power spectrum and the channel characteristics are both frequency variants. The best theoretical channel capacity can be achieved by distributing the transmitted power according to the waterfilling distribution (Gallager, 1968). However, the main purpose of this analysis is to obtain the indicative estimate of the channel capacity.

According to the estimates, the theoretical capacities of the channels are depending on the transmit and noise power and are 10-300 Mb/s in frequency band 3 kHz – 30 MHz (figure 3.14). The spectral efficiency for a channel (length 100 metres) is illustrated in figure 3.15. It can be notified that the inverter is an effective noise source at frequencies below 10 MHz, where the spectral efficiency drops due to the noise generated by the inverter close to zero. According to the spectral efficiency (figure 3.15), the frequencies higher than 15 MHz at the frequency range from 3 kHz to 30 MHz seem to be favourable for power-line communications.

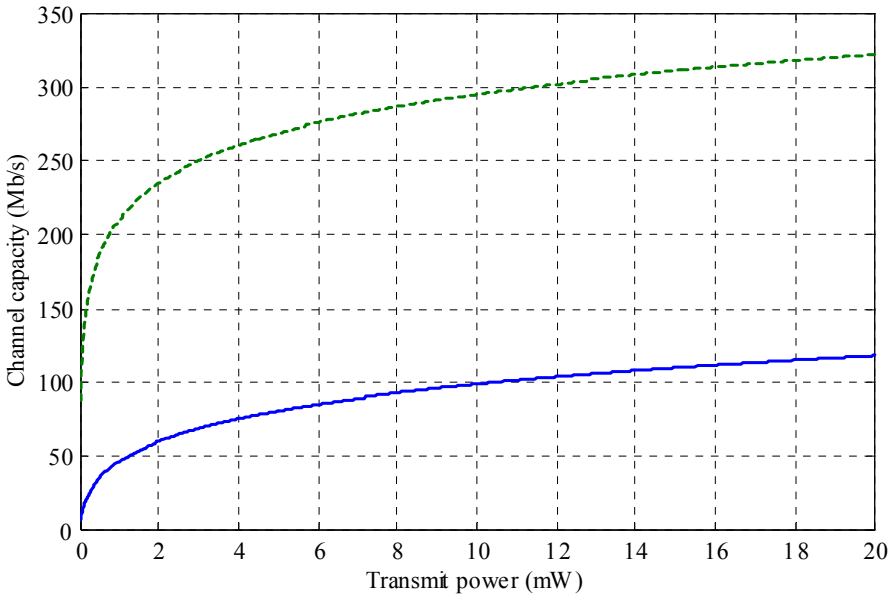

Figure 3.14. Estimated channel capacity of the pilot environment as a function of transmit power and in the frequency band 3 kHz – 30 MHz. The distance between transmitter and receiver is 100 metres and the signal coupling is (L1, PE). The inverter connected to the pilot environment is inactive (dashed line) and active (solid line).

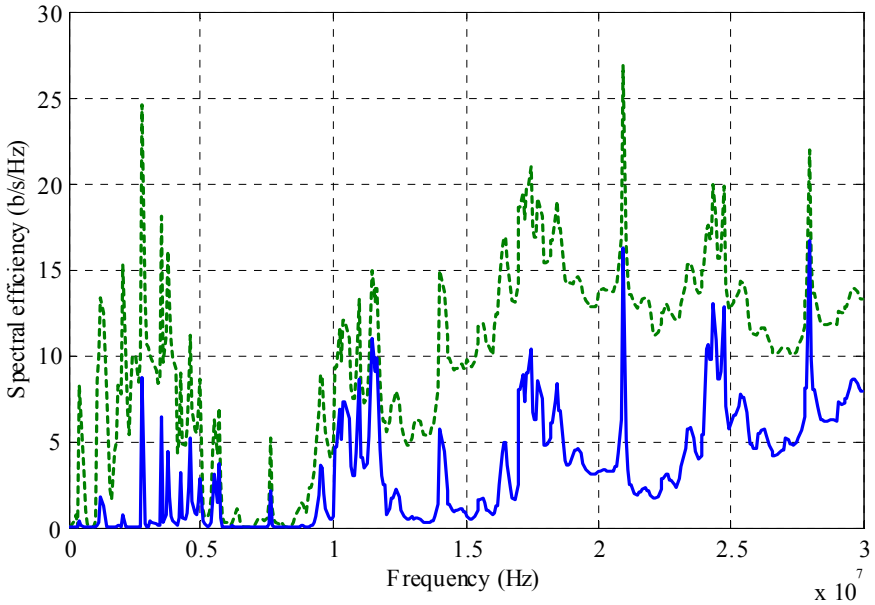

Figure 3.15. Estimated spectral efficiency in the frequency band 3 kHz – 30 MHz. The distance between transmitter and receiver is 100 metres and the total transmit power is 10 mW with flat power spectral density. Signal coupling is (L1, PE). The inverter is switched off (solid line) and the inverter is switched off (dashed line).

The theoretical capacity of communications channel in the frequency band 3–148.5 kHz is much lower than the channel capacity in the frequency band 3 kHz – 30 MHz, although the total transmit power is the same in both cases. However, the theoretical capacity is still on the average more than 1 Mb/s (figure 3.16). The effect of noise generated by the inverter on the channel capacity is smaller than in the previous case. Although the inverter increases the noise level, the signal to noise ratio remains still relatively high due to the small bandwidth to which the transmit power is distributed.

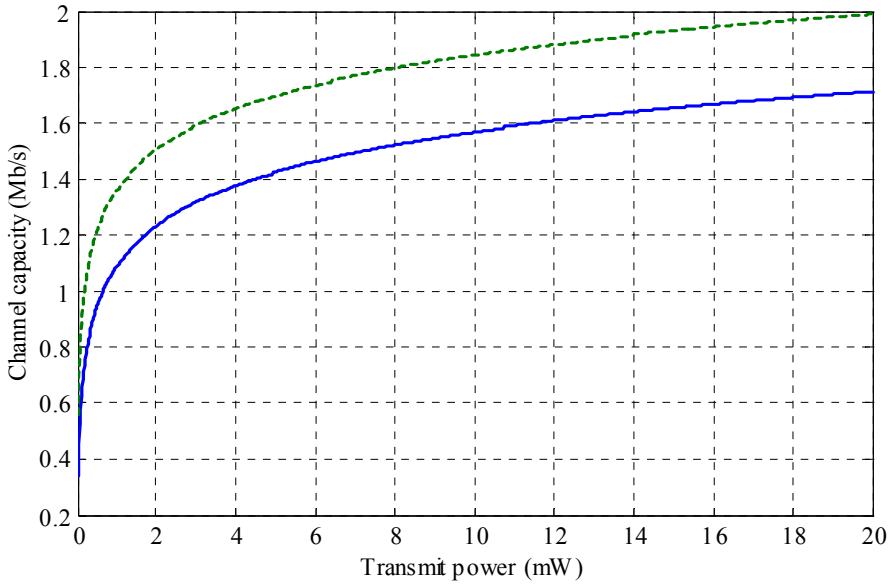

Figure 3.16. Estimated channel capacity for pilot environment as function of transmitting power and in the frequency band 3 kHz – 148.5 kHz. The distance between transmitter and receiver is 100 metres and signal coupling is (L1, PE). The inverter connected to the pilot environment is inactive (dashed line) and active (solid line).

According to the channel capacity estimation, the capacity of the pilot environment is 10-300 Mb/s in the frequency band 3 kHz – 30 MHz and about 1-2 Mb/s in the frequency band 3 kHz – 148.5 kHz at total transmit power 1-20 mW. However, the results are too optimistic. For example, they do not take in the consideration the signal distortion that is caused by nonlinear loads connected to the distribution network. Additionally, in the capacity analysis multipath signal propagation in the power-line channel is not taken into the consideration.

In order to obtain data rates that are even close to those given by Shannon's theory, modems with sophisticated modulation techniques should be used. Data rates that are close to one third of Shannon's limit can be reached with practical modems in the GENELEC frequency band using OFDM and QAM (quadrature amplitude modulation) (Polytrax, 2000). In the frequency band 3 kHz – 30 MHz, it is ever harder to reach this limit. The amount of digital signal processing required for modulation and demodulation increases significantly, which automatically brings an increasing of the implementation costs of a practical system.

The theoretical channel capacity of power-line channels is changing all the time due to the changing noise content and channel characteristics. Thus, the results should be critically evaluated. It is also difficult to estimate the capacity differences between different power-line channels. In this analysis, the losses resulting from the coupling and decoupling signal into the power-line channel were not taken into account. These also reduce the maximum attainable data transfer capacity. The amount of coupling and decoupling loss is dependent on the characteristics of the distribution network and of the coupling interface and, additionally, these cannot be assumed to stay constant as a function of frequency.

4. Data Transfer Tests and Test Equipment

4.1 Introduction to Chapter 4

This chapter introduces the design of a power-line modem and power-line coupling interface. The applicability of the equipment is tested by performing data transfer tests in the pilot environment. The power-line modem and the power-line interface are designed using standard electronics components. The modem uses in data transmission the GENELEC frequency band that is standardised for power-line communications in European countries. The basic principle of the design is to fulfil the data transfer requirements for on-line condition monitoring of electric motors. Finally, the results of the tests are analysed and the applicability of equipment is evaluated.

4.2 Equipment Build for Data Transfer Tests

Data transfer tests require a test equipment. There exist commercial power-line communications systems that could have been directly used in tests. However, the use of commercial devices was considered to be problematic, since the modem software of or the protocol that the modems use in data transmission is protected. Modifications are necessary when the reliability of data transfer is tested. In addition, in order to create statistic, a PC program that is capable to communicate with the modem is required. This is again difficult to develop if the user is not capable to modify the software embedded in the microprocessor of the modem. There are also other reasons for building the test equipment. It is possible to estimate the costs and to design the modem to serve the data transfer of predictive condition monitoring of electric motors. In addition, the characteristics of the power-line coupling interface can be controlled in the design phase.

The test equipment was designed for the GENELEC frequency band, because signalling in low voltage distribution networks is allowed in Europe only at the GENELEC band. On the other hand, there are commercial integrated modem circuits designed for home automation. These chips are in mass production. Hence, the price of the integrated circuit is low. Because of its' availability and technical characteristics, the modem chip ST7537HS1 (ST, 1995) was chosen for the test design. It complies with the GENELEC EN 50065 standard and operates in the GENELEC C frequency band (125-140 kHz). The chip uses binary FSK (frequency shift keying) modulation in data transmission, which has based on (Dostert, 2001) several advantages:

- Easy implementation
- Robustness to impulsive noise
- Robustness to amplitude variations

The bit states 0 and 1 are expressed by carrier frequencies 133.05 kHz and 131.85 kHz. The maximum data rate of the modem chip is 2400 bits/s. The modem chip requires an external power amplifier stage and supporting microcontroller. Manufacturer promises that the modem circuit will reach bit the error rate from 10^{-5} to 10^{-3} in signal reception when $S/N = 15\,\mathrm{dB}$ and $S = 10\,\mathrm{mV_{RMS}}$ and the noise is supposed to be white. Another widely available integrated modem chip is Philips TDA5051, which uses simple OOK modulation in data transmission (Philips, 1999).

Another main component of the developed power-line modem is the microcontroller that controls data transmission and provides an interface for the condition monitoring sensor. The

PIC16F876 microcontroller was selected (Microchip, 2000). It contains a digital I/O and integrated A/D converter that can be applied in connecting external sensors. The microcontroller contains also an in-circuit USART (universal synchronous asynchronous receiver transmitter) that can be used for serial communications between power-line modem and PC. The constructed test modem is illustrated in figure 4.1.

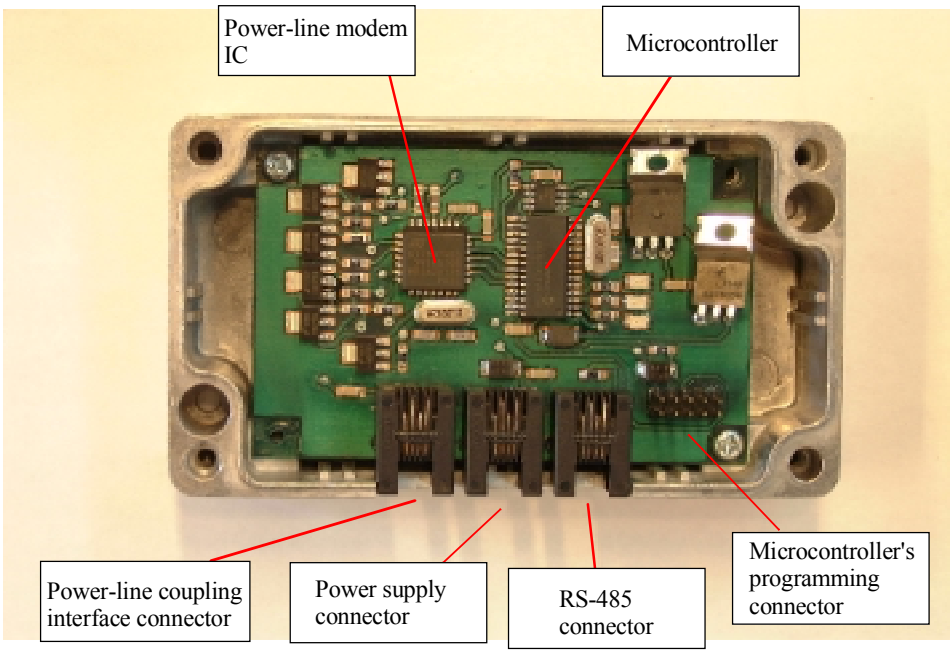

Figure 4.1. Structure of the test modem. The master and slave modules are identical. The difference between the modules is in the microcontroller software. The hardware is packed in an EMI shielded metal case.

The power-line interface is an apparatus between power-line modem and mains network. The interface has three main tasks:

1. To inject the transmitted signal with minor losses into distribution network
2. To filter the undesired portion from the signal at reception
3. To isolate galvanically the power-line modem from distribution network

According to (Dostert, 2001), the separation of transmitter and receiver side in the power-line interface is appropriate. The reason for separating is that weak signal coupling is enough for the receiver, but transmitter side requires strong coupling in order to enable effective injecting of the transmitted signal into the distribution network. However, in this work the both sides were combined because of the simpler implementation.

The power-line interface built is actually a band pass filter, which has a pass band at the carrier signal frequency. The circuit diagram of the designed interface is illustrated in figure 4.2 and the structure of the interface is illustrated in figure 4.3. The interface consists of two filters. There is a serial resonance circuit at the mains voltage side and a parallel resonance circuit at the low voltage side. In addition, the high and low voltage sides are galvanically isolated using a signal transformer. The minimum attenuation of the filter is at frequency 130 kHz and at frequency 50 Hz the filter attenuates about –100 dB (figure 4.4). The insertion loss of the designed

filter is less than –2 dB at the carrier frequency. Additionally, in the signal coupling between two phases, the current $4\,\mathrm{mA}_{\mathrm{RMS}}$ at the mains frequency 50 Hz passes through the filter.

Because of the low mains frequency current value, the power-line modem can be used when coupled between phase and protective earth without tripping of false current relay. In the industry, false current relays are generally set to trip fault currents $\geq 100\,\mathrm{mA}$.

The measured input impedance of the power-line interface is illustrated in figure (4.5). In the pass band of the interface, there is a resonance spike, which is mainly generated by the parallel connection of the 1 kΩ resistor and parallel resonance circuit formed by 47 nF capacitor and 33 µH inductor.

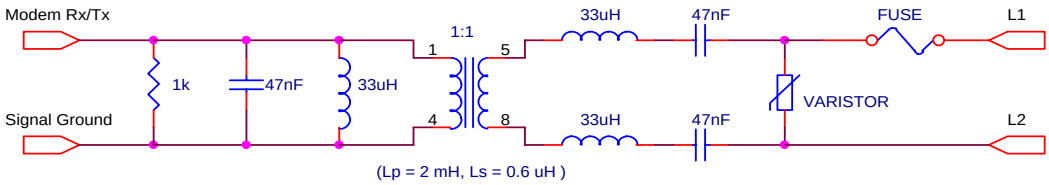

Figure 4.2. Circuit diagram of the designed power-line interface. The interface uses capacitive coupling. The modem side and distribution network side are galvanically isolated using an isolation transformer.

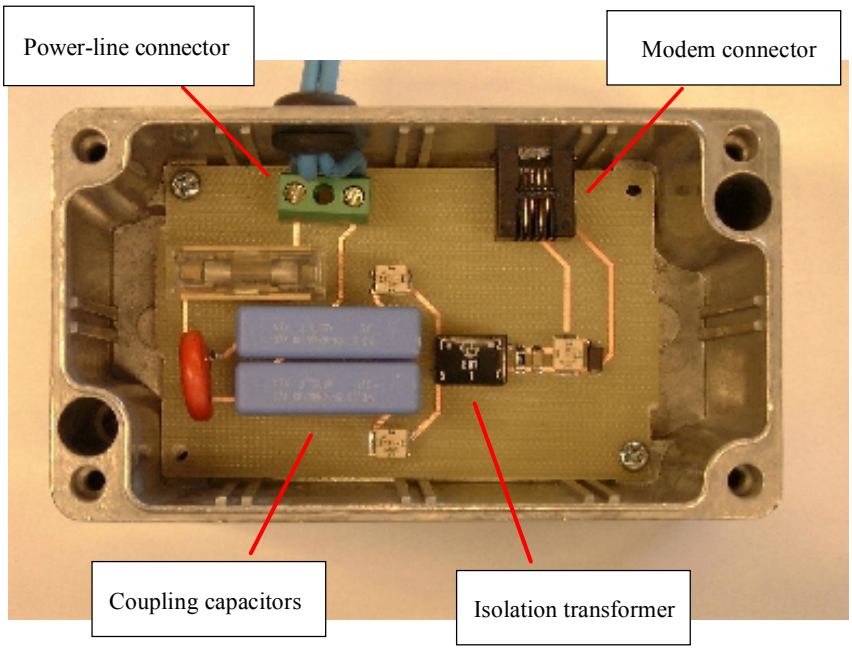

Figure 4.3. Structure of the designed power-line coupling interface.

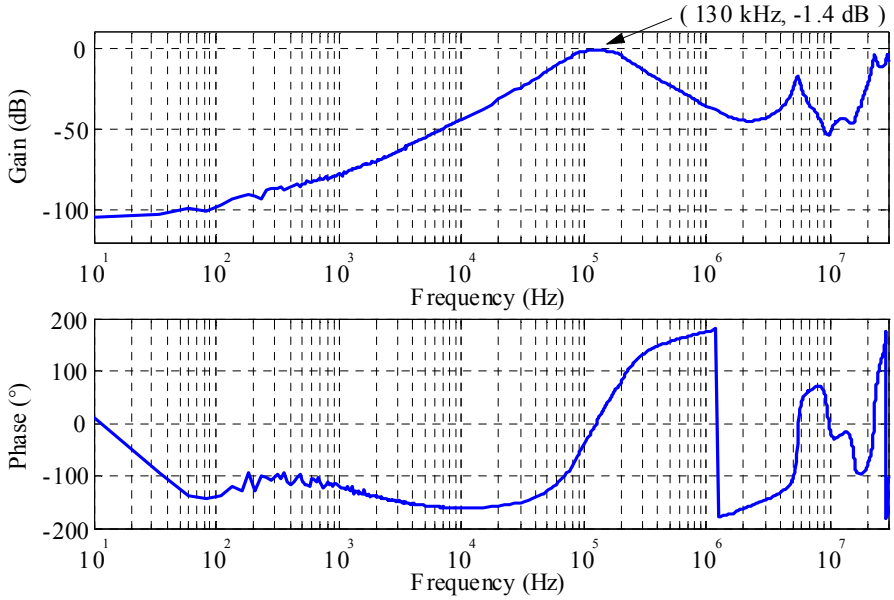

Figure 4.4. Gain and phase curves for the power-line interface in the frequency band 10 Hz – 30 MHz. The signal is injected from the mains voltage side and received from the modem side. An HP 4194A Impedance/Gain Phase Analyser is used in the measurement.

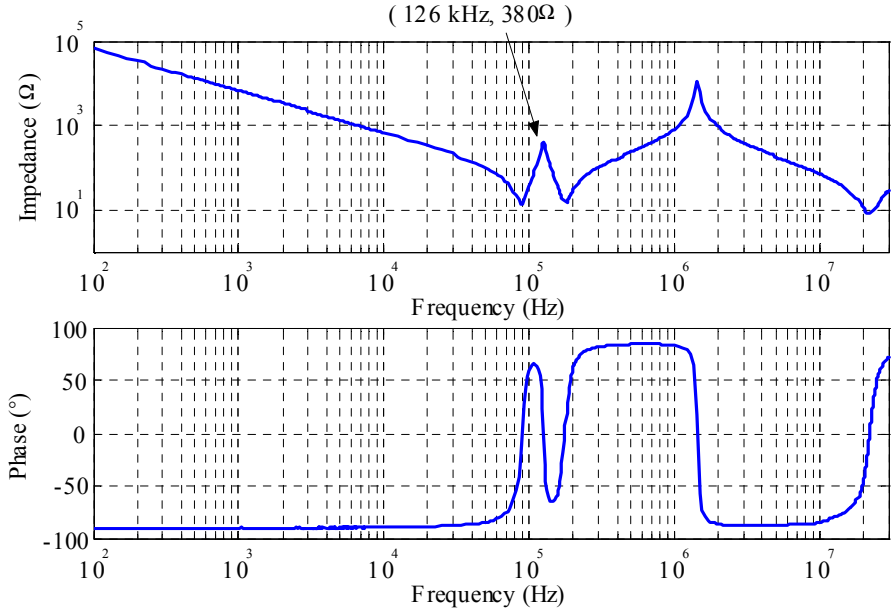

Figure 4.5. Measured input impedance of the designed power-line interface in the frequency band 10 kHz - 30 MHz. The input impedance is measured from the mains voltage side and an HP 4194A Impedance/Gain Phase Analyser is used in measurement.

4.3 Data Transfer Tests

In this chapter, power-line data transfer tests are carried out and the results of the tests are analysed. The pilot environment build for the tests is illustrated in figure 4.11. However, during the tests some modifications are made in the pilot environment (figure 4.12). The objectives of the tests are to determine how the constructed test equipment operates in an industrial environment and what are the most significant factors that affect the reliability of power-line data transfer. Finally, the applicability of the constructed test equipment and possible differences between the constructed test environment and real industrial environment are evaluated. The test sequence consists of three parts:

1. Data transfer tests in pilot the environment without supply voltage.
2. Data transfer tests in the pilot environment with supply voltage switched on.
3. Data transfer tests when the inverter is connected to the pilot environment.

The power-line transmitters were installed in the electric motors and the receiver unit was installed in the distribution transformer or the safety switch depending on the test. Signal couplings (L1, PE) and (L1, L2) were tested.

In order to test data transmission, the software for the receiver and the transmitter were developed. The data transmission was set unidirectional, even though the constructed power-line modems were capable of performing half-duplex operation. Depending on the test, the transmitters were programmed to send a data frame once in ten seconds or once in two seconds. The carrier detection property of the transmitter was used. If the power-line channel already was reserved, the transmitter willing to transmit the data waited until the power-line channel became free. The receiver unit collected the data frame sent by the transmitter, calculated a CRC checksum and sent the statistics of the received packet to a PC computer through a RS-485 serial link. The data was stored into files. The bit rate used in the data transfer tests was 1200 bits/s and the length of data frame was ten bytes. Each byte was sent asynchronously and contained eight data bits, a start bit and a stop bit (figure 4.6). The data frame used by both transmitters (figure 4.7) consisted of five fields:

- Preamble
- Header
- Device identification code
- User data
- Cyclic redundancy check

The preamble was required for the activation of the carrier detection signal of the modem and the activation of the power-line interface. The FSK demodulator of the ST7537HS1 modem circuit requires maximally a period of $t_{CD} = 6.5\ \text{ms}$ of carrier signal at voltage level $V_{CD} = 10\ \text{mV}_{RMS}$ in order to detect an incoming transmission (ST, 1995). Correspondingly, the fourth order analog filter used as a power-line coupling interface needs a stimulus in order to stabilise into stationary state. However, the stimulus needed by the power-line interface is only a fraction of the time required for the carrier detection. In communications tests, a single byte FF is set as a preamble.

The header byte was added to the data frame in order to minimise the number of false data packets. In many cases, the FSK demodulator of the receiving modem misinterprets perturbations in the distribution network as a carrier signal. The impulsive noise in the distribution network gives a stimulus to the power-line interface that starts to resonate at the characteristic frequency of the filter. In order to minimise the number of error detections, a specific 8-bit

header was added into each data frame as an identification code. In the tests, the applied header byte was 4Ah.

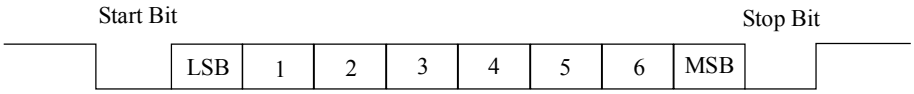

Figure 4.6. Each transmitted byte is synchronised using start and stop bits. The least significant bit is sent first.

The first byte belonging to the data was the device identification code of the transmitting modem. In the tests, the transmitting modems were identified by codes 1 and 2. The user data was located after the identification code. The data consisted of five bytes of counter values of the microcontroller. The two last bytes of the data frame were reserved for a 16-bit cyclic redundancy checksum. The checksum was calculated for header, device id and data bytes. It was used to detect possible errors in received data frames.

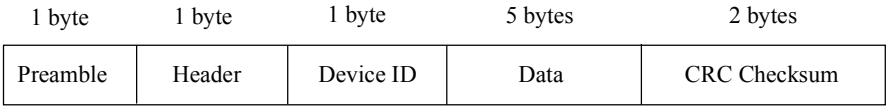

Figure 4.7. Data frame used by both transmitters. The total length of the data frame is ten bytes.

Before the data transfer tests were carried out, the developed power-line interface was tested in the pilot environment. The interface was installed at safety switch and the output voltage of the interface was sampled by Agilent 54622D oscilloscope (figure 4.12). The sampling frequency was 1 MHz and the number of samples was 2000. The oscilloscope was set to trigger to impulses. The noise voltage spectrum passing through the power-line interface in the signal coupling (L1, PE) is illustrated in figure 4.8 and the noise voltage spectrum in the signal coupling (L1, L2) is shown in figure 4.9. In signal coupling (L1, PE), the switching of the output stage of the inverter effectively generates noise. The noise level at the pass band frequency 130 kHz rises about 20-25 dB when the output stage is switched on. In signal coupling (L1, L2), both the operation of the rectifier unit and the output stage of the inverter effectively produce noise (figure 4.9). In figure 4.10, the power-line modem is installed into the pilot environment and a sample is taken during data transmission. The spike of the carrier signal at the frequency near 130 kHz can be clearly seen. The level of the spike is about 10-15 dB higher than the level of noise when the inverter is turned on and about 60 dB higher than the level of noise when the inverter is not active (figure 4.8).

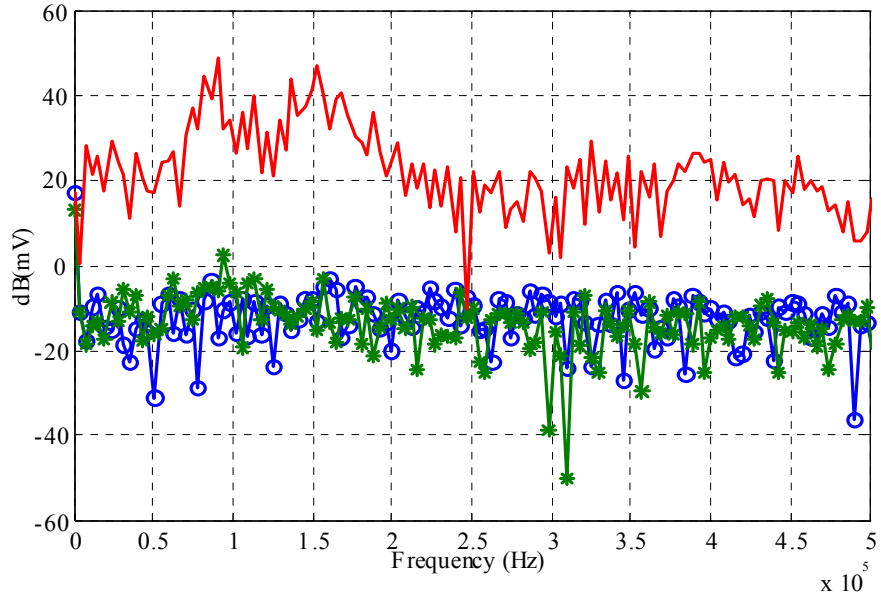

Figure 4.8. Noise spectrum of the pilot environment measured through the coupling interface. The signal coupling is (L1, PE). The markings are: a) curve with circles, noise in distribution network the inverter not being connected to the pilot environment, b) curve with asterisks, noise when the inverter is connected to the pilot environment but not operating, c) curve without markings, noise when the inverter is in operation.

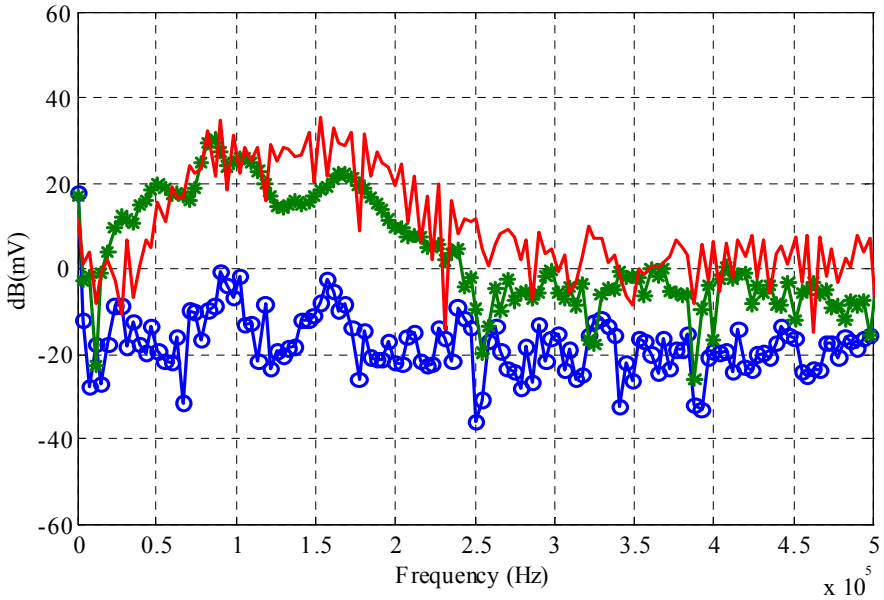

Figure 4.9. Noise voltage spectrum of the pilot environment measured through the coupling interface. The signal coupling is (L1, L2). The markings are: a) curve with circles, noise in distribution network the inverter not being connected to the pilot environment, b) curve with asterisks, noise when the inverter is connected to the pilot environment but not operating, c) curve without markings, noise when the inverter is in operation.

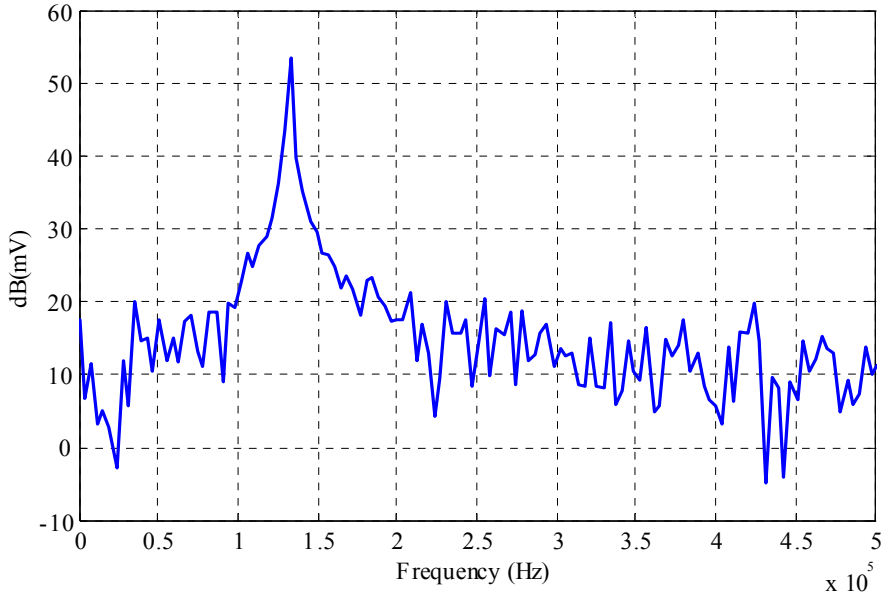

Figure 4.10. Signal coupling (L1, PE), the inverter being switched off. The frequency spike of the carrier signal of the transmitting power-line modem (f~130 kHz) is visible.

Test 1: Data transfer in a pilot environment without supply voltage

The first data transfer test was carried out in order to determine the functionality of the test equipment in a low noise environment. The pilot environment was disconnected from the mains network and the motor feeder cables were connected to the low voltage side of the distribution transformer (France Transfo, 50 kVA). The transmitter was installed in the motor and the receiver in the transformer (figure 4.11). The distance between receiver and transmitter was 100 metres. The results of the test are illustrated in table 4.1. All data frames were received correctly. The missing frames (table 4.1) may be explained by an inaccuracy or drifting of the clock of the transmitter. According to the test, the functionality of the test equipment was proved.

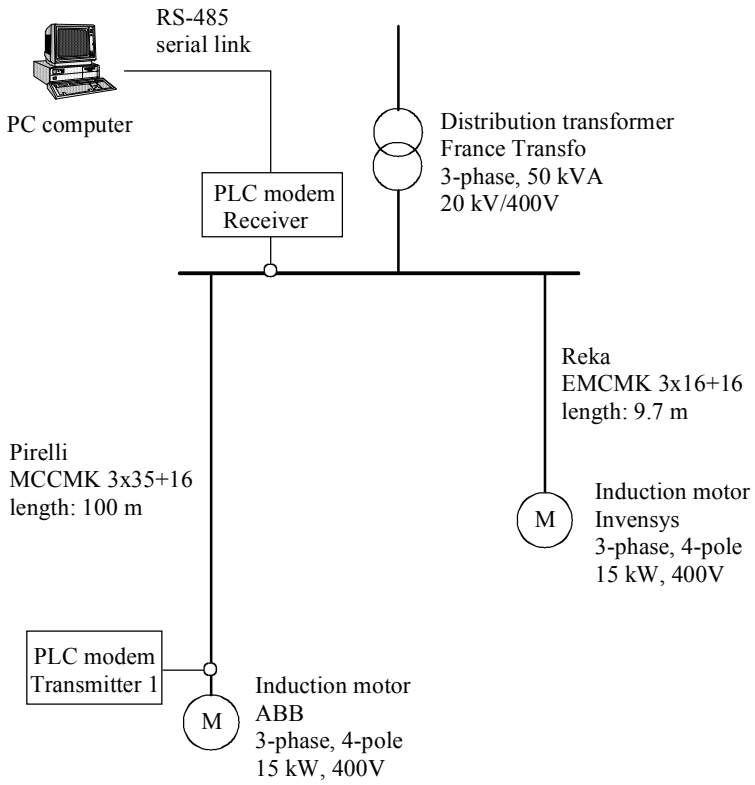

Figure 4.11. Configuration of the pilot environment for the first data transfer test.

Table 4.1. Results of the first data transfer test. The transmitter sent a data frame once in ten seconds to the receiver installed in the distribution transformer.

Coupling: (L1,PE) Transmitter 1		
Transmitted	34806	100 %
OK	34683	99.65 %
Corrupted	0	0.00 %
Missing	123	0.35 %

Test 2: Data transfer in a pilot environment with supply voltage switched on

The pilot environment (figure 4.11) was connected to the supplying grid with safety switch after the distribution transformer was uninstalled. Both transmitters were installed in the 15 kW induction motors and the receiver was in safety switch. After these actions, the supply voltage was switched on. Data transfer tests were carried out for the signal couplings (L1, PE) and (L1, L2). The results of the test are illustrated in table 4.2. Some conclusions can be made:

- Almost all packets sent were correctly received.
- There was no significant difference in data transfer reliability between signal couplings (L1, PE) and (L1, L2).
- Compared to the test without supply voltage the percentage of missing packets increased.

The increase in percentage of missing packets was caused by the carrier sense property of the transmitter. A random impulsive noise in the distribution network can be misinterpreted to the carrier signal and the transmitter will postpone the beginning of transmission until the channel becomes free. The clocks of the transmitters drift also as a function of time. Both transmitters have unique characteristics due to the manufacturing tolerances. At a certain rate, the transmitting times of both transmitters will become overlapped. Due to this overlapping, transmission has to be postponed by another transmitter, which again increases the number of missing packets.

Table 4.2. Test carried out when the supply voltage was switched on. Both transmitters send a data frame once in two seconds. The signal couplings (L1, PE) and (L1, L2) are tested. The percentual values are illustrated in the table below.

		Coupling: (L1,PE)		Coupling: (L1,L2)	
	Total	Transmitter 1	Transmitter 2	Transmitter 1	Transmitter 2
Transmitted	149502	42829	42832	31920	31921
OK	146352	41688	41806	31430	31428
Corrupted	23	10	13	0	0
Missing	3127	1131	1013	490	493

		Coupling: (L1,PE)		Coupling: (L1,L2)	
	Total	Transmitter 1	Transmitter 2	Transmitter 1	Transmitter 2
Transmitted	100 %	100 %	100 %	100 %	100 %
OK	97.89 %	97.34 %	97.60 %	98.46 %	98.46 %
Corrupted	0.02 %	0.02 %	0.03 %	0.00 %	0.00 %
Missing	2.09 %	2.64 %	2.37 %	1.54 %	1.54 %

Test 3: Data transfer in a modified pilot environment with supply voltage switched on

The pilot environment was again modified for the third test. An ABB ACS 200 inverter was installed to the pilot environment. The ACS200 was connected to feed the Invensys 15 kW motor (figure 4.12). There was no EMI filtering on the distribution network side of the inverter. Due to this, the noise generated by the inverter effectively spreads out into the pilot distribution network. The transmitters were installed in the ABB 15 kW motor and in the ACS 200 inverter. The receiver was installed in the safety switch. The purpose of the test was to demonstrate the effect of the inverter on data transmission. Test results are presented in table 4.3. Some conclusions from the test results can be made:

- The signal coupling (L1, L2) had poor performance. The data frames sent by transmitter 1 were lost or corrupted almost completely. Correspondingly, almost half of the data frames sent by transmitter 2 were lost or corrupted.
- Data transmission using signal coupling (L1, PE) was more reliable compared to data transmission using signal coupling (L1, L2). The percentage of corrupted packets remained low and there was no difference in the percentage of corrupted data frames between the transmitters.
- Compared to test 2 in both signal couplings, the percentage of the missing packets increased significantly.

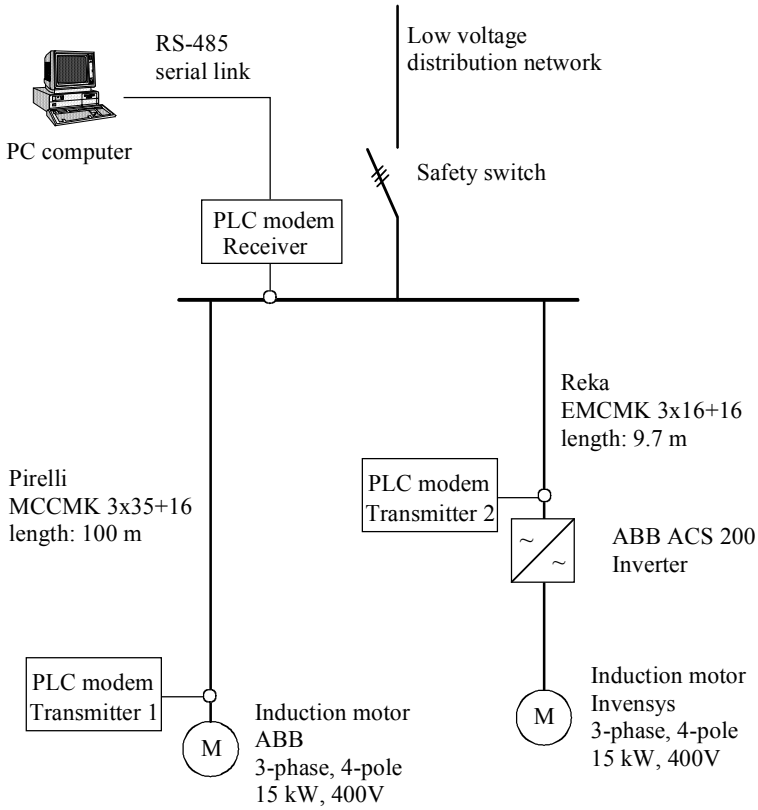

Figure 4.12. Configuration of pilot environment for the third data transfer test.

Table 4.3. Test carried out with the supply voltage switched on and with the ACS 200 inverter connected to the pilot environment. Both transmitters send a data frame once in two seconds. Signal couplings (L1, PE) and (L1, L2) are tested. The percentual values are illustrated in the table below.

		Coupling: (L1,PE)		Coupling: (L1,L2)	
	Total	Transmitter 1	Transmitter 2	Transmitter 1	Transmitter 2
Transmitted	119881	35003	35001	24925	24952
OK	70809	27965	28181	250	14413
Corrupted	7929	8	9	3085	4827
Missing	41143	7030	6811	21590	5712

		Coupling: (L1,PE)		Coupling: (L1,L2)	
	Total	Transmitter 1	Transmitter 2	Transmitter 1	Transmitter 2
Transmitted	100 %	100 %	100 %	100 %	100 %
OK	59.07 %	79.89 %	80.51 %	1.00 %	57.76 %
Corrupted	6.61 %	0.02 %	0.03 %	12.38 %	19.35 %
Missing	34.32 %	20.08 %	19.46 %	86.62 %	22.89 %

According to the tests, the signal coupling (L1, L2) showed serious weaknesses when the inverter was connected to the distribution network close to the receiver. The problem is caused by two factors. The worst problem appears to be the time variant and nonlinear input impedance of the inverter. The charging of the DC-link capacitor suddenly drops the impedance of the distribution network between two phases close to zero. Due to this, the data frames become missing

and corrupted. This happens although the output stage of the inverter is switched off. Impulsive noise is the other factor causing missing and corrupted data frames. When the inverter is located close to the receiver, this also increases the number of missing data frames in the signal coupling (L1, PE). However, in the signal coupling (L1, PE), the percentage of corrupted data frames remains low. This indicates that the missing of data frames in the signal coupling (L1, PE) mainly results from the impulsive noise generated by the inverter. This prevents the transmitter from starting transmission because of the misdetection of the carrier signal. When the signal coupling (L1, PE) is used, the input impedance of the inverter is not highly time variant due to fact that the DC-link of the inverter was isolated from the earth potential. Therefore, the signal coupling (L1, PE) performs better than the signal coupling (L1, L2). However, if the inverter is equipped with the serial inductors for the mains filtering, the signal coupling (L1, L2) will probably perform better than the signal coupling (L1, PE). The noise voltage level in the signal coupling (L1, L2) is lower than in the signal coupling (L1, PE) at the carrier frequency (figures 4.8 and 4.9). This is based on the assumption that the network impedances in both signal couplings are equivalent.

4.4 Applicability of the Developed Power-Line Communications System

The developed power-line communications system complies with GENELEC standard (EN, 1991). According to the data transfer tests carried out in the previous chapter, the system performed relatively well in the pilot environment. However, there are some limitations. For example, signal coupling between two phases should be avoided if three-phase rectifiers without network side EMI filtering are connected to the distribution network. With respect to the predictive condition monitoring of electric motors following aspects are considered:

- Required data transfer rate
- Reliability of data transfer
- Connectivity to industrial field bus
- Cost of system
- Reliability of system

The required data transfer rate depends on many aspects. The intelligent low-cost condition monitoring sensor of an electric motor may contain a low-cost microcontroller consisting of an on-chip A/D converter and on-chip serial communications interface and external data memory. The sensor does not have significant processing capabilities. The intelligent sensor is capable of measuring acceleration, humidity, temperature, currents and voltages of the electric motor. In order to perform the bearing condition analysis, the intelligent sensor samples the acceleration measurement and stores it to the external data memory. According to (Lindh, 2001), the bearing fault of the electric motor can be detected using the sampling frequency $F_S = 20\,\mathrm{kHz}$, sample length 33000 and 12-bit A/D conversion. The total memory space required by these samples is about 0.4 Mb. The data transfer rate of the developed power-line communications system is 1200 b/s and the amount of user data in a data frame is about half of the total frame size. Thus, the data transfer of a single acceleration measurement will take approximately ten minutes. However, this data transfer is required only once a day or once a week. The bearings of the electric motor do not break up suddenly. Therefore, it is unnecessary to transfer an excessive number of measurements. On the other hand, the microprocessor of the intelligent condition monitoring sensor may pre-process the measurement data by forming an envelope spectrum for the acceleration measurement. After this operation, the amount of transferred data is only a fraction of the original measurement data and the same applies to the time spend for the data transfer. Correspondingly, temperature and humidity measurements do not require high data transfer rates. The time constants of both phenomena are long. According to these considera-

tions, data transfer of on-line condition monitoring of electrical motors does not require a wide data transfer bandwidth and the data transfer rate of the developed system is sufficient. The data transfer rate provided by the developed system corresponds to the estimates given in table 1.1.

The reliability of data transfer is important in controlling loops and in systems where an occasional communications failure could cause accidents or large economical losses. Due to the nature of on-line condition monitoring, these conditions are no fulfilled. Primarily, the faults of electric motors develop slowly and it is the task of the on-line condition monitoring system to detect these faults before they interrupt the process. Therefore, the reliability of the data transfer is not a key design criterion. The occurring data transfer errors may be detected using error detection methods, like cyclic redundancy checksum. Instead, the reliability of the condition monitoring sensor and analysis software is crucial. A healthy motor that is misclassified as faulty increases the maintenance costs of the industrial plant.

The on-line condition monitoring system of electric motors can be connected to the other information systems of the industrial plant. The receiver unit of the power-line communications system is located at the mains switching board. It can be connected e.g. to the existing industrial field bus. In the switching board, there already exist devices that are remotely controlled or read and belong to the automation system of the industrial plant. For example, a simple Modbus protocol was embedded into the developed receiver unit and the receiver was connected as a slave device to the Modbus field bus. In any case, in order to guarantee the operation of the on-line condition monitoring system of electric motors as part of the larger information system, a standard field bus interface is required. This assures e.g. outsourced and mainly remotely performed condition monitoring service.

The cost of the system is also an important parameter. Many things affect the cost of the on-line condition monitoring system of electric motors. The cost of the power-line communications equipment is only a fraction of the total costs. However, the power-line communications alternative may effectively reduce the total cost when comparing it to the traditional solution where conventional data transfer cables are used. Power-line data transfer does not require the installing of new cables. Additionally, the cost of the developed communications system is low, because standard integrated circuits and other standard components are used, which all are in the mass production.

An important issue is the reliability of the on-line condition monitoring system using power-line communications as a data transfer method. It must be prevented that a failure of the condition monitoring system leads to a fault in the industrial process. Furthermore, it must be prevented that an operation or failure of the power-line modems causes tripping of the relays protecting the industrial low voltage distribution network. The power-line interface of the modem, the power supply required by the modem and the condition monitoring sensor can be protected using fuses and varistors. These prevent the occurrence of process faults in case a failure occurs in the condition monitoring system. Additionally, coupling of power-line modems between phase and protective earth should be avoided if the risk exits that this may cause problems to the operation of the protection relays supervising the state of the distribution network.

According to these arguments, the developed system fills the requirements set to the sensor level data transfer of the on-line condition monitoring of electric motors in chapter 1.3.

4.5 Use of Power-Line Data Transfer in an Industrial Environment

This evaluation concerns narrowband data transfer and sensor level data transfer needs. The broadband data transfer is interesting mainly from the point of view of providing Internet data access for customers. Systems providing broadband data transfer are automatically more expensive and more complex than narrowband systems. The difference results from DSP (digital signal processor) based implementation as compared to single chip analog implementation of low-cost narrowband power-line modems. However, this may be a situation that will change rapidly if DSP based systems are taken into mass production and implemented e.g. in home automation products.

In the GENELEC frequency band (3–148.5 kHz), the success of power-line data transfer mainly depends on the number and type of loads, the number of branch cables and the number and type of active devices producing interference into the distribution network. According to the practical tests in chapter 4.3, almost all sent packets reached the receiver when the inverter was not connected to the distribution network. Connecting the inverter to the distribution network degraded the performance of the system significantly. Signal coupling should be considered carefully.

In the frequency band 148.5 kHz – 30 MHz, the topology of the distribution network, signal frequency and the attenuation of the cabling begin to affect the characteristics of the power-line channels. Generally, the attenuation of the cabling increases and the noise power in the distribution network decreases as a function of frequency. Characteristically, frequently repeating peaks and notches occur in the amplitude response of the power-line channel. In the European countries, signalling in the low voltage distribution network is currently standardised only in the GENELEC frequency band. However, there are not technical obstacles for the implementing e.g. narrowband modems that operate at megahertz class frequencies. On the contrary, the implementation of the power-line coupling interface would become simpler and the reliability of data transfer could increase due to the decrease of the noise power level.

4.6 Suggestions for Future Work

Many topics in the field of narrowband power-line communications in the industrial environment are still open for research. The applicability of more sophisticated modem ASIC:s applying digital signal processing techniques should be researched. In addition, extensive field trials should be performed in different types of industrial environments in order to get a better insight into the limitations and possibilities of power-line data transfer.

Another very interesting topic is the possibility to transfer data in the motor cable between inverter and motor. The topology of the data transfer channel is simple but the environment is extremely hostile for data transfer and coupling electronics. However, low-cost data transfer between motor and inverter may be a real demand in condition monitoring as well as motor controlling.

The main problems concerning power-line data transfer in the feeder cable between inverter and electric motor are surge waves and noise generated by the inverter and input impedance of the inverter. In addition, there is no communications equipment available that could be directly applied. The switching of the inverter output stage generates high frequency and high energy pulses (~100 kHz – 1 MHz) into the feeder cable. The maximum voltage amplitude of the pulse between two phases may be even more than 1000 V at the interface of the motor and feeder cable. In order to withstand these pulses the power-line coupling interface requires an appropri-

ate design. Additionally, the input impedance of the inverter between two phases is close to zero, when the phases are coupled by means of IGBT:s together or coupled to the DC-link capacitor. Thus, the signal coupling between phase and protective earth conductor should be used. However, the situation may change if the inverter is equipped with an output filter. Additionally, the carrier frequency used in communications should be increased significantly above the GENELEC frequency band in order to the avoid noise generated by the inverter.

5. Summary and Conclusions

5.1 Introduction to Chapter 5

In this chapter, the main results of this work are summarised. There were two main objectives in this research. Firstly, it was aimed at the measuring, analysing and modelling of the high frequency characteristics of an individual network components and industrial low voltage distribution network up to frequency 30 MHz. The second objective was to develop and test a narrowband power-line data transfer system that operates in the GENELEC frequency band and that may be used for sensor level data transfer of the on-line condition monitoring system of electric motors.

5.2 Key Results of the Work

There are two main scientific contributions in this research. The first contribution is comprised of measurements, analysis and modelling of MCMK low voltage power cables in the frequency band 100 kHz – 30 MHz. The second contribution is the producing of a measurement based termination impedance model for low voltage electric motor with slotted stator for the frequency band 10 kHz – 30 MHz.

Main Contribution 1: High Frequency Characteristics of MCMK Power Cables

The characteristics of three MCMK type low voltage power cables were measured and modelled in the frequency band 100 kHz – 30 MHz. According to the measurements, the transmission line parameters of the cables were determined and a general attenuation formula for the cables was formed.

Due to the thin insulation layer in relation with the cross-sectional conductor dimensions, the characteristic impedances of the cables are low as compared to conventional data transfer cables. This is a result from the fact that low voltage power cables are designed to carry heavy currents at low voltage levels. In general, the characteristic impedances vary from 5 to 50 ohms depending on the signal coupling and cable structure. The characteristic impedance of the cable is lowest when all phases are coupled as a signal conductor and the protective screen (PEN) is used as a return conductor. Correspondingly, the characteristic impedance is highest when the signal is coupled between the phases.

The signal voltage attenuation in the cable increases as a function of frequency. In the frequency band 100 kHz – 30 MHz, the main loss mechanism of the low voltage power cable is the dielectric loss of the used PVC insulation material. According to the measurements, the signal voltage attenuation in the cable is approximately 0.15 dB/m at the signal frequency 30 MHz. Generally, the signal attenuation in the researched low voltage power cables in the frequency band 100 kHz – 30 MHz corresponds to the attenuation of generally used low-cost data transfer cables.

Main Contribution 2: High Frequency Input Impedance Model for the Electric Motor with a Slotted Stator

The electric motor acts as a termination impedance for a power-line communications system operating in an industrial low voltage distribution network. Thus, the input impedance of the electric motor as a function of frequency is an important parameter. In order to form a simple

input impedance model, a group of induction motors ranging from 15 kW to 250 kW was measured. The group consisted of five induction motors and one SR motor. The input impedances of all measured motors behave similarly in the frequency band 10 kHz – 30 MHz. When the signal is coupled between phases, strong parallel resonance occurs in the frequency band 10–100 kHz and strong serial resonance occurs in the frequency band 1–20 MHz. When the signal is coupled between phase/phases and motor frame, strong serial resonance occurs only in the frequency band 1-20 MHz. At the parallel resonance frequency, the input impedance of the motor is in the order of kilo-ohms. Correspondingly, at the serial resonance frequency the input impedance is in the order of ohms. The high frequency characteristics are caused by the parasitic components of the slotted stator winding. The rotor and end plates do not significantly affect the behaviour of the input impedance.

According to the measurements and analysis, a simple input impedance model for electric motors was formed. The model describes the main characteristics of input impedance as a function of frequency in the frequency band 10kHz – 30 MHz. Regarding power-line communications, the interface between motor and power cable is practically always mismatched. Although the absolute value of the input impedance of the motor may be close to the characteristic impedance of cable, the input impedance of the motor is either capacitive or inductive.

Main Contribution 3: Characteristics of the DC-Voltage Link Inverter with Respect to Power-Line Communications

An inverter that is connected to a distribution network can be considered to be both an effective noise source and nonlinear and time-variant load impedance. As power-line communication is concerned, all these characteristics are harmful. According to the noise current measurements performed for the frequency band 9 kHz – 30 MHz, the disturbances generated by the inverter spread out to the whole frequency band. The disturbances are mainly caused by the three-phase rectifier unit and the inverter stage. The time-variant input impedance is problematic when the power-line data transfer equipment is coupled between the phase conductors. The conducting phases of the rectifier unit effectively short-circuit and distort the carrier signal injected into the distribution network. The situation may be different, if the electric appliances with three-phase rectifiers are equipped with inductors that perform the input filtering at the mains side.

Main Contribution 4: Characteristics of the Pilot Environment with Respect to Power-Line Communications

The signal voltage attenuation in communication channels was measured in the pilot environment. The simulation models for the channels were formed by applying developed high frequency models for cables and motors. The standard transmission matrix theory and two-port models were applied as a modelling tool. At least in the pilot environment, the simulated and measured frequency responses are corresponding for frequencies up to 15 MHz. However, at higher signal frequencies, there may occur differences between the two-port model and the measurement. The signal voltage attenuation in the industrial power-line channel is dependent on the characteristics and length of cabling, the topology of distribution network and electric appliances connected to the distribution network.

In the GENELEC frequency band 3-148.5 kHz, the losses of the cable with industrial cable lengths are low. Notches in the frequency responses of power-line channels may occur. These are caused by the serial resonances of the electric appliances connected to the network, which are e.g. distribution transformers. Due to the fact that the length of cabling is limited and the carrier frequencies are relatively low, the notches and peaks in the frequency response caused

by the standing waves are rare. The phase response in the GENELEC band can be considered to be relatively linear due to the missing standing waves. The noise content of the distribution network depends mainly on the loads connected to the network. Especially inverters and other appliances equipped with rectifiers effectively inject noise into the distribution network. According to the channel capacity analysis performed for the pilot environment, theoretical data rates about 1 Mb/s may be theoretically achieved by using 10 mW transmit power and the whole frequency band 3-148.5 kHz for data transfer.

In the frequency band 148.5 kHz – 30 MHz, the voltage attenuation of power-line channels increases due to the increasing losses of cabling. The length of the distribution network does not limit the formation of standing waves. Additionally, electric appliances, such as motors, inverters and transformers connected to the distribution network, are mismatched loads in the whole frequency band. Hence, standing waves are formed which can be noticed in the frequency responses of the power-line channels as frequently repeating notches and peaks. Correspondingly, the phase response at the frequencies of notches and peaks is nonlinear and may cause problems for data transfer. The noise in the frequency band 148.5 kHz – 30 MHz is mainly caused by the rectifier and the output stage of inverter. The output stage generates noise in the whole frequency band. According to the channel capacity estimations for the pilot environment, theoretical channel capacities of 50-250 Mb/s for the frequency band 3 kHz – 30 MHz can be achieved by using transmit power of 10 mW.

Main Contribution 5: Development and Tests of the Power-Line Modem for Sensor Level Data Transfer of the On-line Condition Monitoring System of Electric Motors.

In the second part of the work, a power-line communications system was developed for the GENELEC frequency band for the purposes of on-line condition monitoring of electric motors. The system was build using standard low-cost integrated circuits and a modem circuit designed for home automation. Thus, the cost of the communications equipment remained low. The system was designed with the aim of connecting it to the standard industrial field bus and it was tested in the pilot environment. Signal coupling between the phase conductors appears to be problematic when appliances equipped with six-pulse rectifiers are connected to the distribution network close to the transmitting or receiving power-line modems. On the other hand, the signal coupling between phase and protective earth may be also problematic. The low frequency signal injected between phase and protective earth do not necessarily use only the screen of the power cable as a return path. The data transfer rate of the developed modem is appropriate for data transfer that is required by the on-line condition monitoring of electric motors.

5.3 Usability of the Results

The results of this research may be applied both in research and development. The proposed high frequency model for the electric motor together with the measured cable parameters and the cable attenuation model can be applied in the simulation of power-line communications, inverter feeder cable oscillations and the spreading out of high frequency electromagnetic interference in the distribution network. Correspondingly, the introduced data transfer schema that uses power-line communications in sensor level data transfer is applicable for industrial diagnostics purposes.

5.4 Conclusions

The applying of power-line communications in industrial sensor level data transfer is feasible and even reasonable. The GELELEC frequency band currently standardised for power-line

communications in Europe offers enough capacity for most of the sensor level data transfer tasks. However, higher carrier frequencies could be used if this would be allowed by regulations. The use of the higher carrier frequencies would also be feasible in order to avoid noise generated by active appliances as e.g. inverters. Generally, the power-line channel corresponds to the radio channel. The characteristics of both channels are time variant and multipath signal propagation occurs in both channels. Due to the nature of power-line channel, it is not suitable for tasks that need deterministic and robust data transfer, such as controlling. However, it is applicable and cost-effective way of data transfer for monitoring purposes. In order to develop better modems for industrial sensor level data transfer in the GENELEC frequency band, ASIC:s and coupling interfaces could be adopted e.g. from automatic meter reading applications.

The role of end users in the industry is very significant. To enable the selling of devices that are using power-line data transfer, the idea of exploiting the low voltage distribution network as a communication channel has to be accepted first. This will not be an easy task, because the conception of power-line communications is generally perceived as negative, which is the result of the campaign of people and instances that are using low, medium and high frequency radios.

References

(Ahola, 2000) Jero Ahola, Tuomo Lindh, Jarmo Partanen, Pertti Järventausta and Markku Kauppinen, Data ”Management System for DMS in Industrial Environment”, Distributech DA/DSM Europe 2000, Austria, 10-12 October 2000.

(Ahola, 2001) Ahola Jero, Pienjännitevoimakaapelien ominaisuudet sähköverkkotiedonsiirron kannalta, LTKK, 2001. (In Finnish)

(Ahola, 2002) Jero Ahola, Tuomo Lindh, Jarmo Partanen, ”Determination of Properties of Low Voltage Power Cables at Frequency Band 100 kHz – 30 MHz”, ICEM 2002, Bruges, Belgium, August 26-28, 2002.

(Ahola, 2003) Jero Ahola, Tuomo Lindh, Jarmo Partanen, ”Simulation Model for Input Impedance of Low Voltage Electric Motor at Frequency Band 10 kHz – 30 MHz”, IEEE IEMDC’03, Madison, Wisconsin, USA, 1-4 June 2003.

(Alatalo, 1975) Pentti Alatalo, Voimakaapelit ja asennusjohdot, Oy Nokia Ab Kaapelitehdas, Espoo, Finland, 1975, ISBN 951-99072-7-0. (In Finnish)

(Albrecht, 1986) Albrecht P.F., McCoy R.M., Owen E.L., “Assesment of the reliability of motors in utility applications”, IEEE Transactions on Energy Conversion, Vol. EC-1, No. 1, March 1986.

(Anastasiadou, 2002) Despina Anastasiadou, Theodore Antonakopoulos, “An Experimental Setup for Characterizing the Residental Power Grid Variable Behaviour”, ISPLC 2002, Athens, Greece, March 27-29, 2002.

(Banwell, 2001) T.C. Banwell, S. Galli, “A New Approach to the Modelling of the Transfer Function of The Power Line Channel”, ISPLC 2001, Lund University, Malmö, Sweden, April 4-6, 2001, pp. 319-324.

(Bartolucci, 2001) Bartolucci Ettore J., Finke Bob H., “Cable Design for PWM Variable-Speed AC Drives, IEEE Transactions on Industry Applications, Vol. 37, No 2, March/April, 2001.

(Bostoen, 2000) Tom Bostoen, Olivier Van de Wiel, “Modelling the Low Voltage Power Distribution Network in the Frequency Band from 0.5 MHz to 30 MHz for Broadband Power-line Communications”, IEEE Proceedings of Broadband Communications, Zurich, Switzerland pp. 171-178, 2000.

(Brown, 1999) P. A. Brown, “Power Line Communications – Past Present and Future”, 3rd International Symposium on Power-Line Communications and It’s Applications, Lancaster UK 30.5-1.4.1999, pp. 1-7.

(Dostert, 1998) Klaus Dostert, “RF Models of the Electrical Power Distribution Grid”, ISPLC 1998, Soka University, Tokyo, Japan, pp. 105-114, 1998.

(Dostert, 2001) Klaus Dostert, Powerline Communications, Prentice-Hall, Upper Saddle River, USA, 2001, ISBN 0-13-029342-3.

(EN, 1991) EN 50 065-1, Signalling on low voltage electrical installations in the frequency range 3 kHz to 148.5 kHz, GENELEC, Brussels, 1991.

(Erdman, 1996) Jay Erdman, Russel Kerkman, David Schlegel, Gary Skiblinski, ”Effect of PWM Inverters on AC Motor Bearing Currents and Shaft Voltages”, IEEE Transactions on Industry Applications, vol. 32, pp. 250-259, March/April 1996.

(Esmailian, 2002) T. Esmailian, F.R. Kschischang, P.G. Gulak, “An In-building Power Line Channel Simulator, ISPLC 2002, Athens, Greece, March 27-29, 2002.

(Fahie, 1883) J.J. Fahie, ”Edward Davy”, The Electrician, pp. 181-227, 7th July, 1883.

(Farnell, 2002) Farnell cataloque, 2002.

(Gallager, 1968) R. G. Gallager, Information Theory and Reliable Communication, Wiley, New York, 1968.

(Haataja, 2003) J. Haataja, A comparative performance study of four-pole induction motors and synchronous reluctance motors in variable speed drives, Dissertation, Lappeenranta University of Technology, 2003.

(Harper, 1975) Charles Harper, Handbook of Plastics and Elastomers, McGraw-Hill, New York, 1975. ISBN 0-07-026681-6.

(Hensen, 1999) C. Hensen, W. Schultz, S. Schwartze, “Characterisation, Measurement and Modelling of Medium Voltage Power-Line Cables for High Data Rate”, 3rd International Symposium on Power-Line Communications and It’s Applications, Lancaster, UK, 30.5-1.4.1999, pp. 37-44.

(Hooijen, 1998) Hooijen Han Vinck, ”On the Channel Capacity of a European-style Residental Power Circuit”, ISPLC 1998, Soka University, Tokyo, Japan, pp. 31-44, 1998.

(Huloux) J. Huloux, L. Hanus, ST7537 Power Line Modem Application, ST Microelectronics.

(Im, 1997) Gi-Hong Im, J. J. Werner, “Effect of Bridged Taps at VDSL Frequencies”, ANSI T1E1.4/97-324, Minneapolis, USA, September 22-26, 1997.

(Kingery, 1999) P. Kingery, “Digital X-10”, http://gardentoys.com/htinews/feb99/articles/kingery/kingery13.htm, Leviton TelCom, USA, 1999. 17.12.2002.

(Kovacs, 1984) Kovacs P.K., Transient Phenomena in Electrical Machines, Budapest, Hungary, 1984, ISBN 0-444-99663-X.

(Lakervi, 1989) Erkki. Lakervi, E. J. Holmes, Electricity distribution network design, Peter Peregrinus Ltd, London, United Kingdom, 1989, ISBN 0 86341 151 7.

(Lempiäinen, 1995) Tommi Lempiäinen, Yhteenveto Kaukopään kunnossapidollisista häiriöistä ja kunnossapidon toteutuksesta, Insinöörityö, 1995. (In Finnish)

(Lin, 1991) Clara Lin, Joseph Curilla, ”Temperature-Related Changes in Dielectric Constant and Dissipation Factor of Increase Attenuation in Data Cables Used in Building Plenums”, IEEE 16th Conference on Local

Computer Networks, Minneapolis, USA, 14-17 October 1991, pp. 74-79.

(Lindh, 1999) Tuomo Lindh, Jarmo Partanen, Sähkökäyttöjen mittaavan kunnonvalvonnan menetelmiä, LTKK, Finland, 1999. (In Finnish)

(Lindh, 2001) Tuomo Lindh, Jero Ahola, Jarmo Partanen, Oikosulkumoottorin laakerivien tunnistaminen mikrotyöstetyn kiihtyvyysanturin avulla, LTKK, Finland, 2001. (In Finnish)

(Lindh2, 2001) Tuomo Lindh, Jero Ahola, Jarmo Partanen, Sauli Antila, Pertti Järventausta, Kimmo Kivikko, Pekka Verho, Pekka Ruupunen, "Web-based monitoring functions utilising data management system", DistribuTECH Europe 2001, Berlin, Germany, 6-8 November 2001.

(Lindh, 2002) Tuomo Lindh, Jero Ahola, Jarmo Partanen, Heikki Pirttiniemi, "Communication Possibilities for Remote Control and Condition Monitoring of Small-Scale Hydro Power Plant", NORDAC 2002, Copenhagen, Denmark, 7-8 November, 2002.

(Liu, 1992) Yilu Liu, Stephen. A. Sebo, Ross Caldecott, Donald G. Kasten, Selwyn e. Wright, "Power Transformer Resonance – Measurements and Prediction", IEEE Transactions on Power Delivery, Vol. 7 No. 1, January 1992.

(Microchip, 1999) PIC16F87X Datasheet, Microchip, 1999, USA.

(Mäkinen, 1998) Antti Mäkinen, Markku Kauppinen, Kuormitusmallit, Mittausraportti, TTKK, Finland, 1998. (In Finnish)

(Nannapareni, 2000) Nannapareni Narayana Rao, Elements of Engineering Electromagnetics, 5th edition, Prentice-Hall Inc., Upper Saddle River, New Jersey, USA, 2000, ISBN 0-13-013201-2.

(Paul, 1994) Paul C. R., Analysis of Multiconductor Transmission Lines, John Wiley & Sons, New York, USA, 1994, ISBN 0-471-02080-X.

(Persson, 1991) E. Persson, "Transient Effects in Application of PWM Inverter to Induction Motor", Record of the Annual Pulp and Paper Industry Technical Conference, Montreal, Canada, 3-7 June, 1991, pp 228-233.

(Pitkänen, 1991) I. Pitkänen, Keskijänniteverkko MELKO –järjestelmän tiedonsiirtotienä, M. Sc. Thesis, Tampere, 1991. (In Finnish)

(Philips, 1999) TDA5051A Home Automation Modem Specification, Philips Semiconductors, Eindhoven, Netherlands, 1999.

(Phillips, 1998) Holger Phillips, "Performance Measurements of Power-line Channels at High Frequencies", ISPLC 1998, Soka University, Tokyo, Japan, pp. 229-237, 1998.

(Phillips, 1999) Holger Phillips, "Modelling of Power-line Communication Channels", 3rd International Symposium on Power-Line Communications and It's Applications, Lancaster UK 30.5-1.4.1999, pp. 14-21.

(Phillips, 2000) Holger Phillips, "Development of a Statistical Model for Power-line Communication Channels", ISPLC 2000, Limerick, UK, 5th – 7th April 2000.

(Polytrax, 2000) Polytrax Information Technology AG, “Tehcnical Description Polytrax Method”, January, 2000.

(Popov, 2001) M. Popov. L. van der Sluis, G. C. Paap, “Investigation of the Circuit Breaker Reignition Overvoltages Caused by No-load Transformer Switching Surges”, ETEP Vol. 11, No. 6, November/December 2001.

(Proakis, 1989) John Proakis, Digital Communications, 2nd Edition, Mc Graw-Hill, 1989, ISBN 0-07-100269-3.

(Proakis, 1996) John Proakis, Dimitris Manokolakis, Digital Signal Processing, Prentice-Hall, New Jersey, USA, 1996.

(Routin, 1897) J. Routin, C. E. L. Brown, ”Power line signalling electricity meters”, UK Patent Office, British Patent No. 24833, 1897.

(Räisänen, 1993) Antti Räisänen, Arto Lehto, Radiotekniikka, Otatieto Oy, Helsinki, 1993, ISBN 951-672-224-5. (In Finnish)

(Sartenaer, 2001) Th. Sartenaer, P. Delogne, “Powerline cables modelling for broadband communications”, ISPLC 2001, Lund University, Malmö, Sweden, April 4-6, 2001, pp. 331-337.

(Saunders, 1996) Lawrence Saunders, Gary Skiblinski, Steve Evon, David Kempkes, ”Riding the Reflected Wave –IGBT Drive Technology Demands New Motor and Cable Considerations”, IEEE Petroleum and Chemical Industry Conference, Philadelphia, PA, September 23-26, 1996, pp. 75-84.

(Schlegel, 1999) Schlegel D., Wrate G., Kerkman R., Skibinski G., ”Resonant Tank Motor Model For Voltage Reflection Simulations With PWM Drives”, Proceedings of the IEEE International Electrical Machines and Drives Conference, Seattle, USA, 9-12 May 1999, pp- 463-465.

(Skiblinski, 1994) Skiblinski G., Kerkman R., Leggate D., Pankau J., Schlegel D., “Reflected Wave Modeling Techniques for PWM AC Motor Drives”, Proceedings of 13th Annual Applied Power Electronics Conference and Exposition, vol. 2, Anaheim, USA, 23-27 Feb. 1998, pp. 1021-1029.

(Spare, 2001) John Spare, “Building the Business Case for Condition-Based Maintenance”, Transmission and Distribution Conference and Exposition, 2001 IEEE/PES, Vol. 2, 2001.

(ST, 1995) ST7537HS1 Home Automation Modem, ST Microelectronics, USA, 1995.

(Strong, 2001) Peter Strong, “Regulatory & Consumer Acceptance of Power-line Products”, ISPLC 2001, Lund University, Malmö, Sweden, April 4-6, 2001, pp. 253-258.

(Silventoinen, 2001) Pertti Silventoinen, Electromagnetic Compatibility and EMC measurements in DC-Voltage Link Converters, Dissertation, Lappeenranta University of Technology, 2001, ISBN 951-764-588-0.

(Takahashi, 1995) Toshio Takahashi, Mike Tetmeyer, Hong Tsai, Tom Lowery, ”Motor Lead Length Issues for IGBT PWM Drives”, IEEE Pulp and Paper Conference, 1995, pp. 21-27.

(Tarkiainen, 2002) Antti Tarkiainen, Jero Ahola, Juha Pyrhönen, ”Modelling the Cable Oscillations in Long Motor Feeder Cables”, PCIM Europe 2002, Nuremberg, Germany, May 14-16, 2002.

(Thoradson, 1905) C. Thoradson, “Meters”, US Patent Office, US Patent Nos. 784712 and 784713, USA, 1905.

(Tomasini, 2001) Wayne Tomasini, Electronic Communications Systems: Fundamentals Through Advanced, 4th edition, Prentice-Hall Inc., Upper Saddle River, New Jersey, USA, 2001.

(Zimmermann, 1999) Manfred Zimmermann, Klaus Dostert, “A Multi-Path Signal Propagation Model for the Power Line Channel in the High Frequency Range”, 3rd International Symposium on Power-Line Communications and It’s Applications, Lancaster UK 30.5-1.4.1999, pp. 45-51.

(Zimmermann, 2000) Manfred Zimmermann, Klaus Dostert, “An Analysis of the Broadband Noise Scenario in Power-line Networks”, ISPLC 2000, Limerick, UK, 5th – 7th April 2000, pp. 131-138.

(Zhong, 1995) Zhong Erkuan, Lipo Thomas, “Improvements in EMC Performance of Inverter-Fed Motor Drives”, IEEE Transactions on Industry Applications, Vol. 21, No. 6, November/December 1995.

Appendix I

Impedance Measurements for the Electric Motors of the Test Group

The impedance measurements performed with the HP 4194A impedance analyser for electric motors are presented in this appendix. All measured motors were connected in delta.

Manufacturer	Type	IN(A)	VN(V)	PN(kW)	r/min
ABB	M2BA200MLA4B3	56	400	33	1473

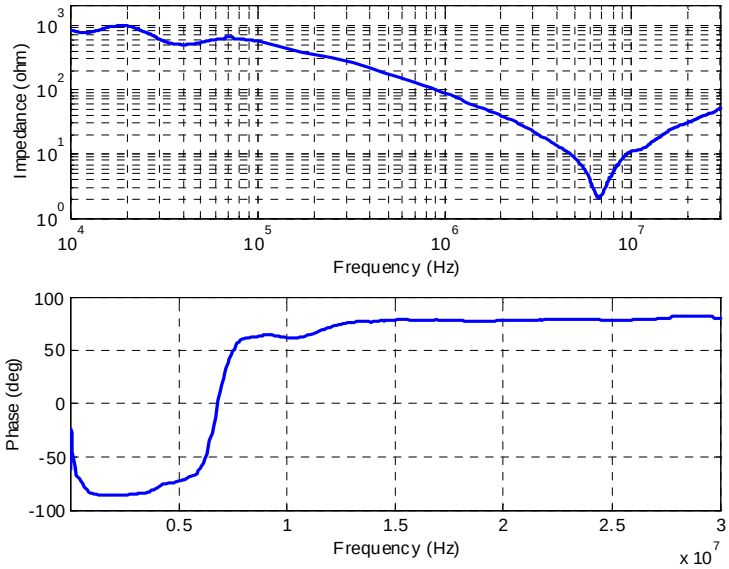

Figure I.1. Measured input impedance and phase of input impedance as a function of frequency in the frequency band 10 kHz – 30 MHz. The signal coupling is (L1, PE).

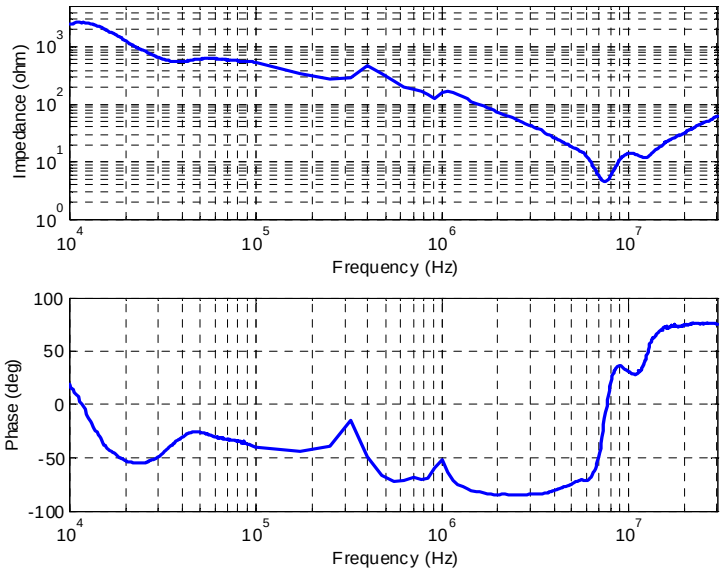

Figure I.2. Measured input impedance and phase of input impedance as a function of frequency in the frequency band 10 kHz – 30 MHz. The signal coupling is (L1, L2).

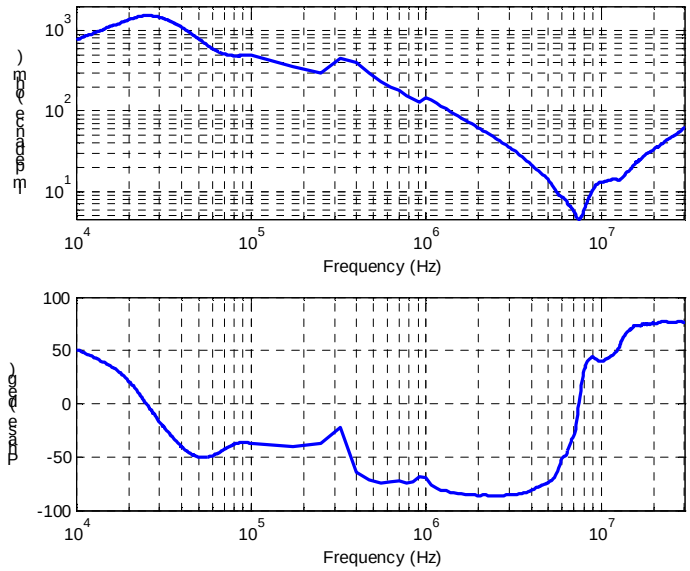

Figure I.3. Measured input impedance and phase of input impedance as a function of frequency in the frequency band 10 kHz – 30 MHz. The signal coupling is (L1, L2+L3).

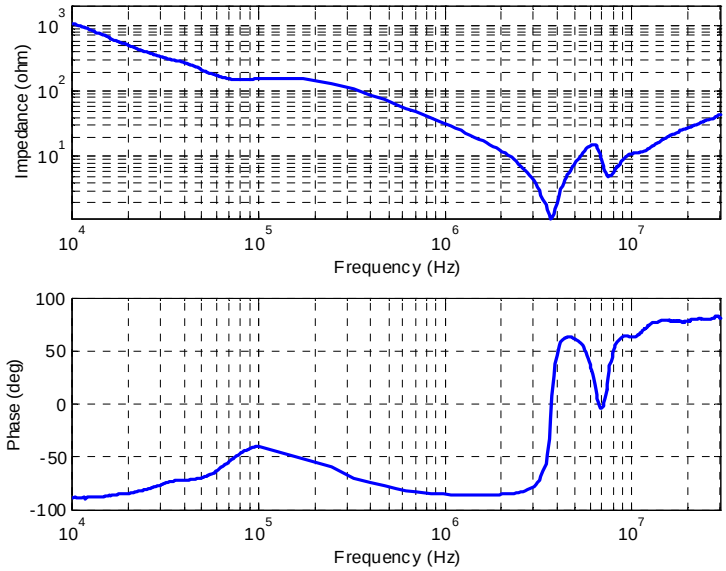

Figure I.4. Measured input impedance and phase of input impedance as a function of frequency in the frequency band 10 kHz – 30 MHz. The signal coupling is (L1+L2+L3, PE).

Manufacturer	Type	IN(A)	VN(V)	PN(kW)	r/min
Invensys	T-01F160L4/01	28.5	400	15	1460

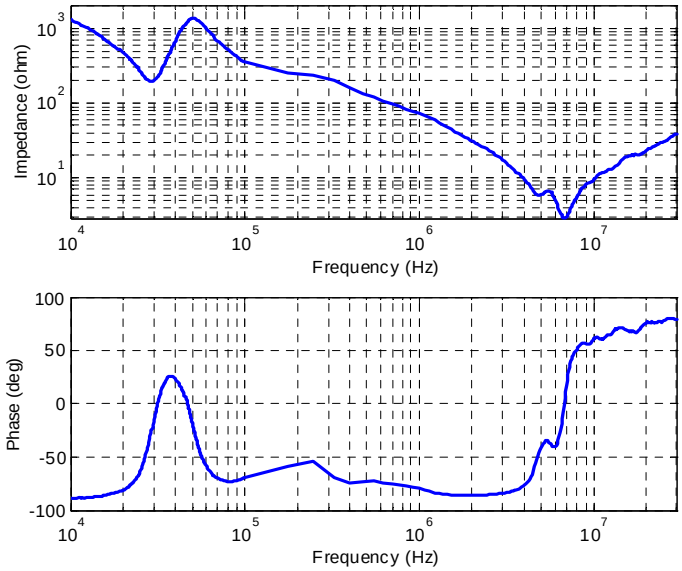

Figure I.5. Measured input impedance and phase of input impedance as a function of frequency in the frequency band 10 kHz – 30 MHz. The signal coupling is (L1, PE).

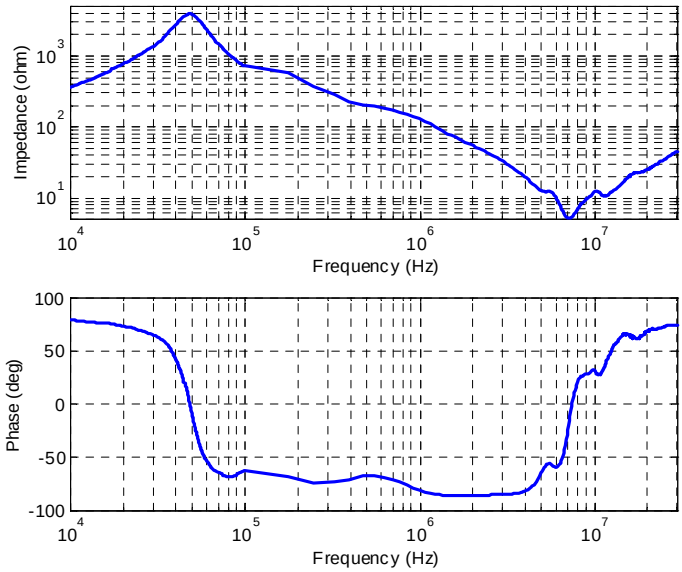

Figure I.6. Measured input impedance and phase of input impedance as a function of frequency in the frequency band 10 kHz – 30 MHz. The signal coupling is (L1, L2).

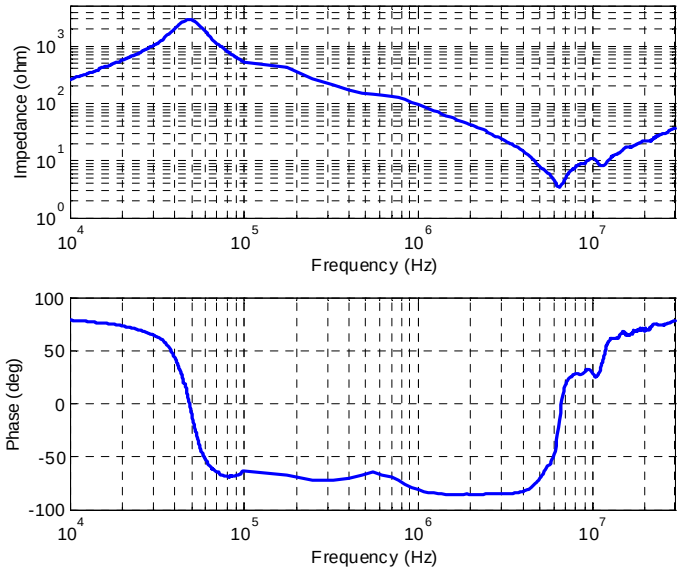

Figure I.7. Measured input impedance and phase of input impedance as a function of frequency in the frequency band 10 kHz – 30 MHz. The signal coupling is (L1, L2+L3).

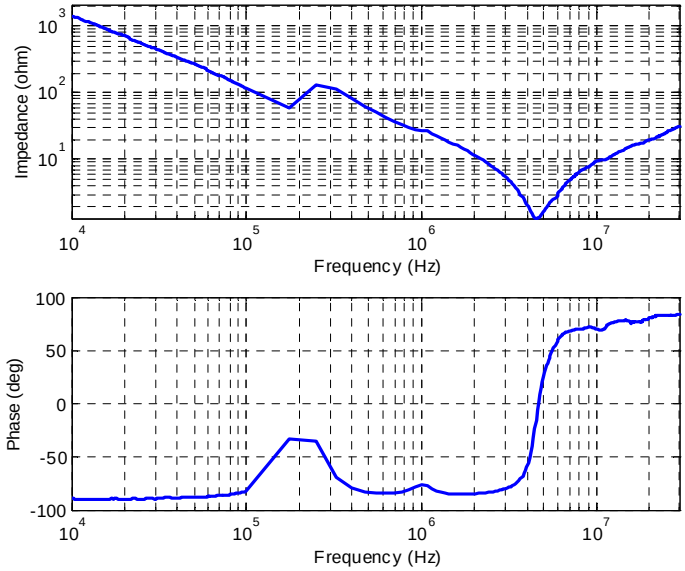

Figure I.8. Measured input impedance and phase of input impedance as a function of frequency in the frequency band 10 kHz – 30 MHz. The signal coupling is (L1+L2+L3, PE).

Manufacturer	Type	IN(A)	VN(V)	PN(kW)	r/min
Strömberg	HXUR505G2(1)B3	100	400	55	1475

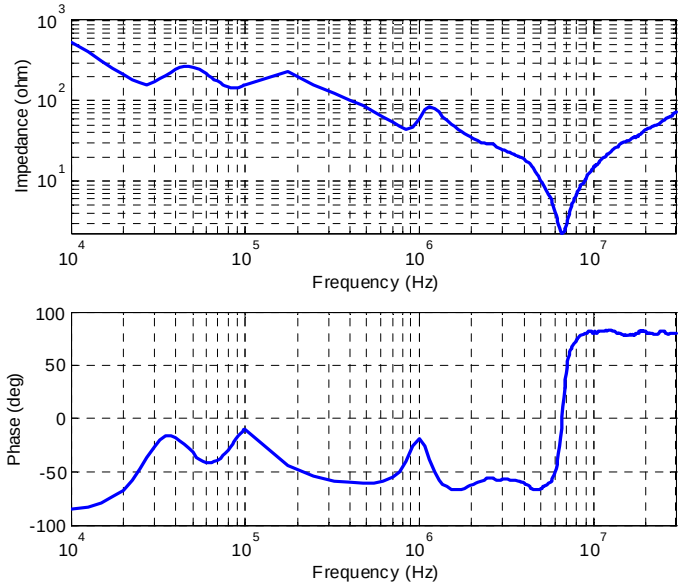

Figure I.9. Measured input impedance and phase of input impedance as a function of frequency in the frequency band 10 kHz – 30 MHz. The signal coupling is (L1, PE).

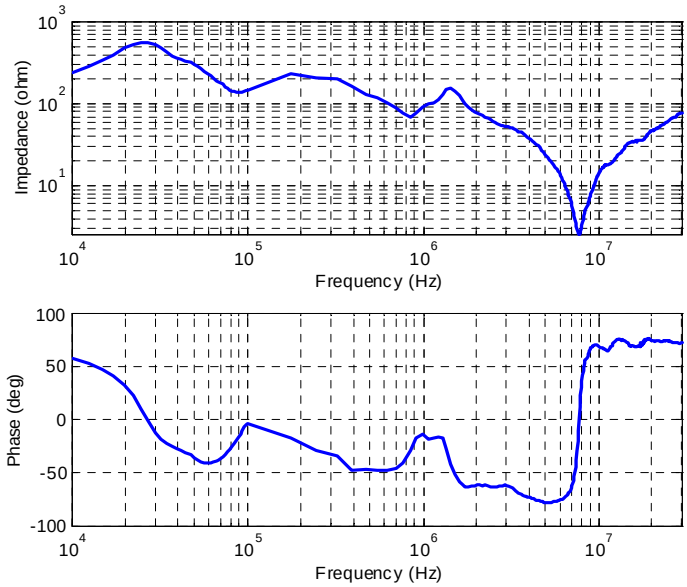

Figure I.10. Measured input impedance and phase of input impedance as a function of frequency in the frequency band 10 kHz – 30 MHz. The signal coupling is (L1, L2).

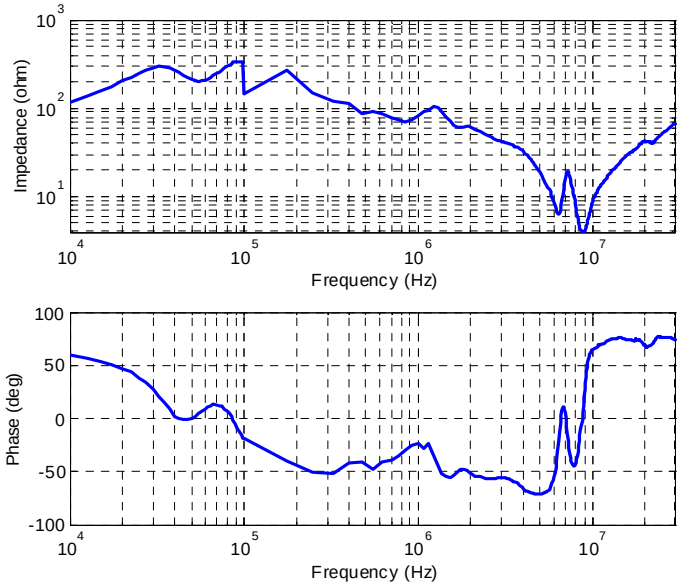

Figure I.11. Measured input impedance and phase of input impedance as a function of frequency in the frequency band 10 kHz – 30 MHz. The signal coupling is (L1, L2+L3).

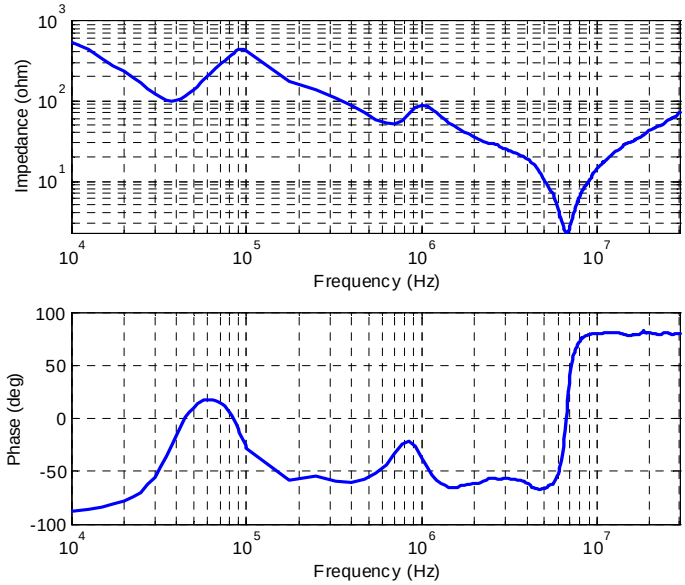

Figure I.12. Measured input impedance and phase of input impedance as a function of frequency in the frequency band 10 kHz – 30 MHz. The signal coupling is (L1+L2+L3, PE).

Manufacturer	Type	IN(A)	VN(V)	PN(kW)	r/min
Strömberg	HXUR368G2B3	43	400	22	1460

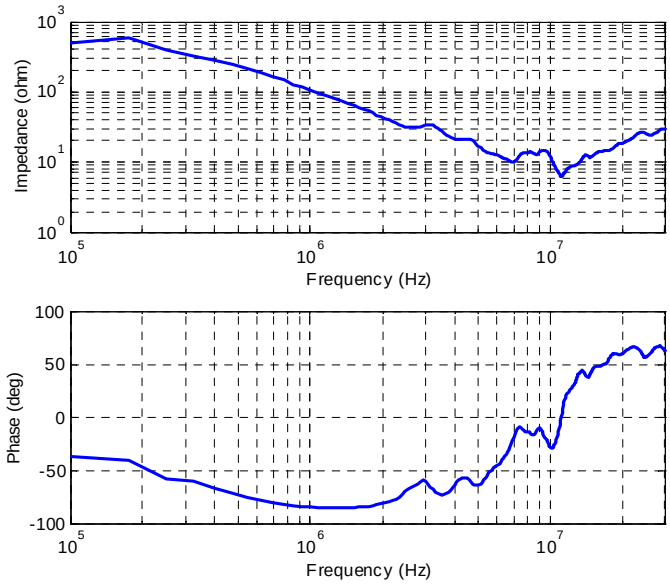

Figure I.13. Measured input impedance and phase of input impedance as a function of frequency in the frequency band 100 kHz – 30 MHz. The signal coupling is (L1, PE).

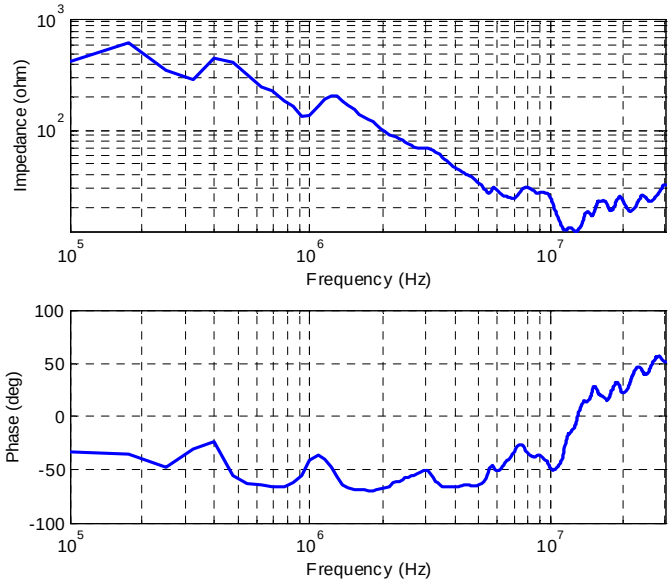

Figure I.14. Measured input impedance and phase of input impedance as a function of frequency in the frequency band 100 kHz – 30 MHz. The signal coupling is (L1, L2).

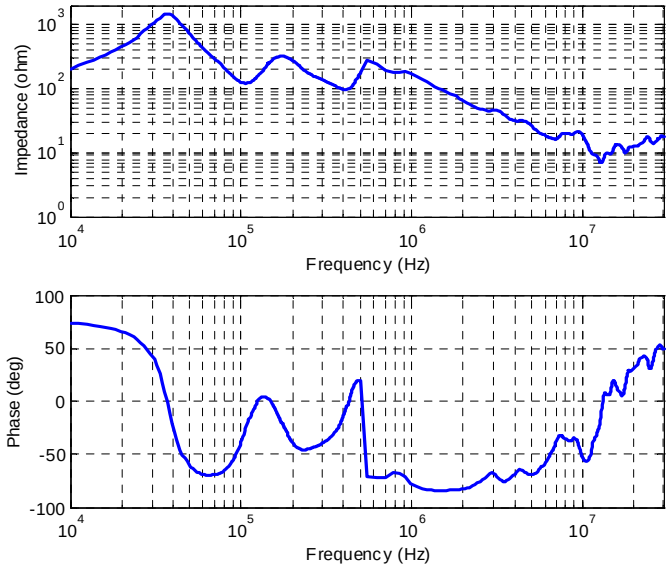

Figure I.15. Measured input impedance and phase of input impedance as a function of frequency in the frequency band 10 kHz – 30 MHz. The signal coupling is (L1, L2+L3).

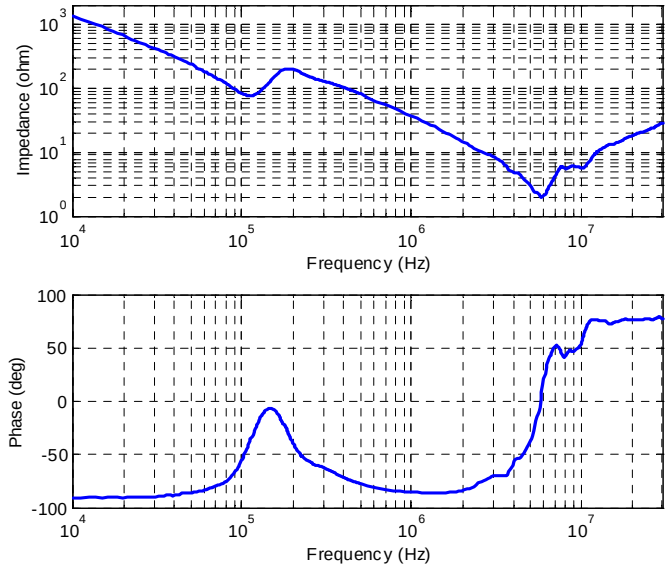

Figure I.16. Measured input impedance and phase of input impedance as a function of frequency in the frequency band 10 kHz – 30 MHz. The signal coupling is (L1+L2+L3, PE).

Manufacturer	Type	IN(A)	VN(V)	PN(kW)	r/min
ABB	M2BA35532B3	410	400	250	2980

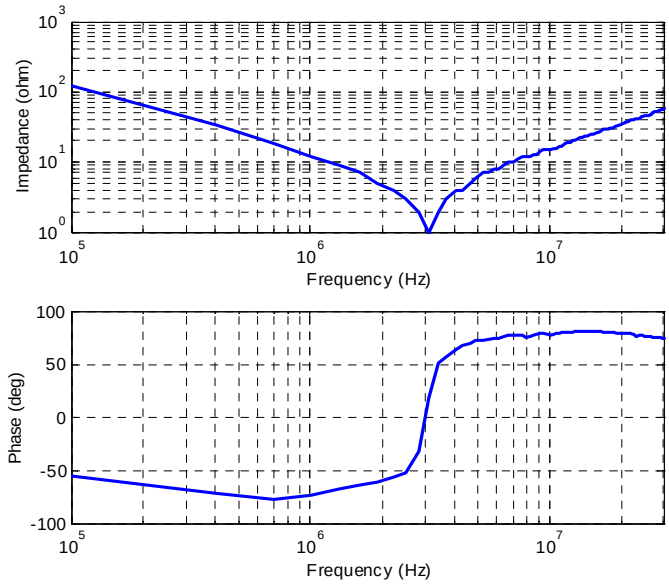

Figure I.17. Measured input impedance and phase of input impedance as a function of frequency in the frequency band 100 kHz – 30 MHz. The signal coupling is (L1, PE).

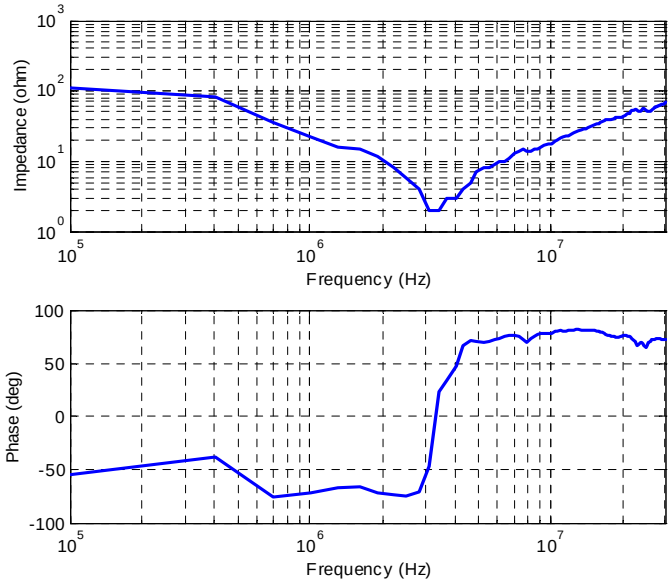

Figure I.18. Measured input impedance and phase of input impedance as a function of frequency in the frequency band 100 kHz – 30 MHz. The signal coupling is (L1, L2).

Manufacturer	Type	IN(A)	VN(V)	PN(kW)	r/min
ABB	M2AA160L4	30	400	15	1455

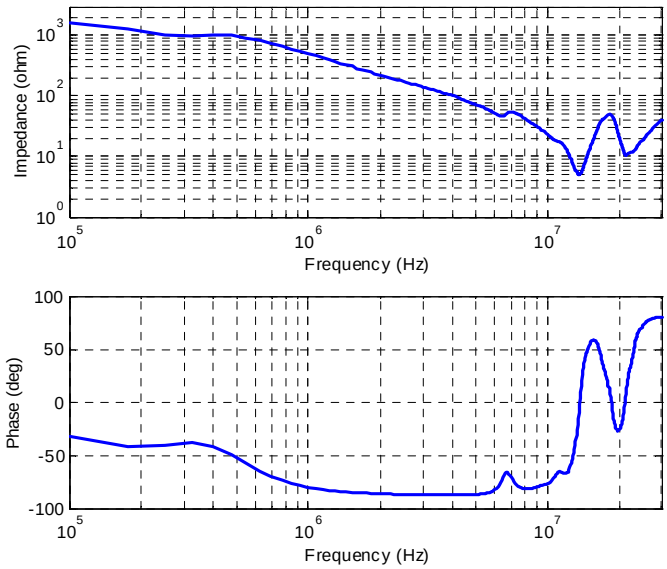

Figure I.19. Measured input impedance and phase of input impedance as a function of frequency in the frequency band 100 kHz – 30 MHz. The signal coupling is (L1, PE).

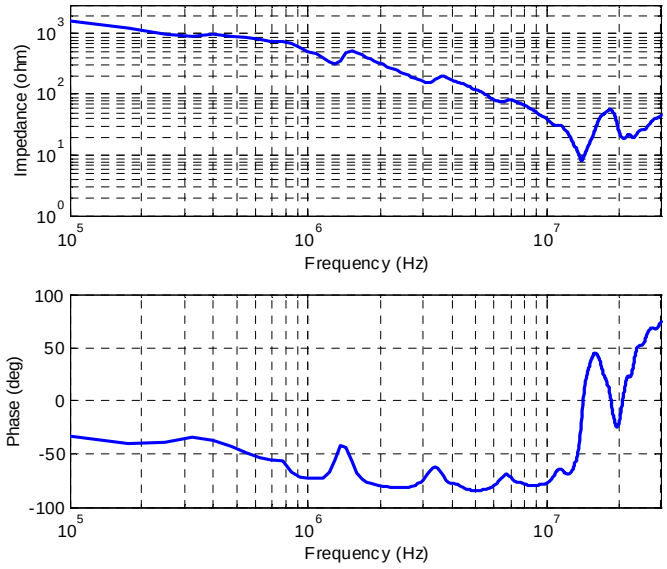

Figure I.20. Measured input impedance and phase of input impedance as a function of frequency in the frequency band 100 kHz – 30 MHz. The signal coupling is (L1, L2).

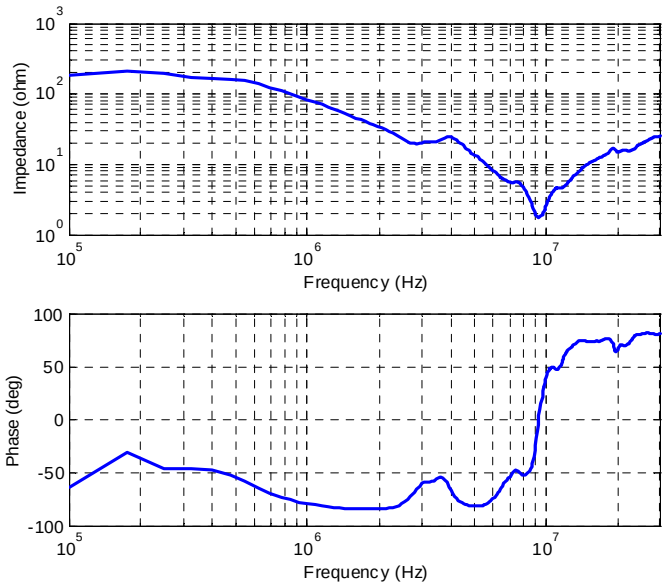

Figure I.21. Measured input impedance and phase of input impedance as a function of frequency in the frequency band 100 kHz – 30 MHz. The signal coupling is (L1+L2+L3, PE).

Appendix II

Example of Forming a Simulation Model for a Power-Line Channel

In this appendix, the frequency response for the voltage attenuation of a power-line channel is formed. The distribution network and the modelled channel are presented in figure II.1. The measured cable parameters, transmission line model and motor input impedance model developed in this thesis are applied to the modelling of the power-line channel. Since the transformer high frequency model is missing, it is replaced with the input impedance measurements performed for the transformer. The signal coupling is (L1, PE) and two-port transmission matrices are applied as a modelling method.

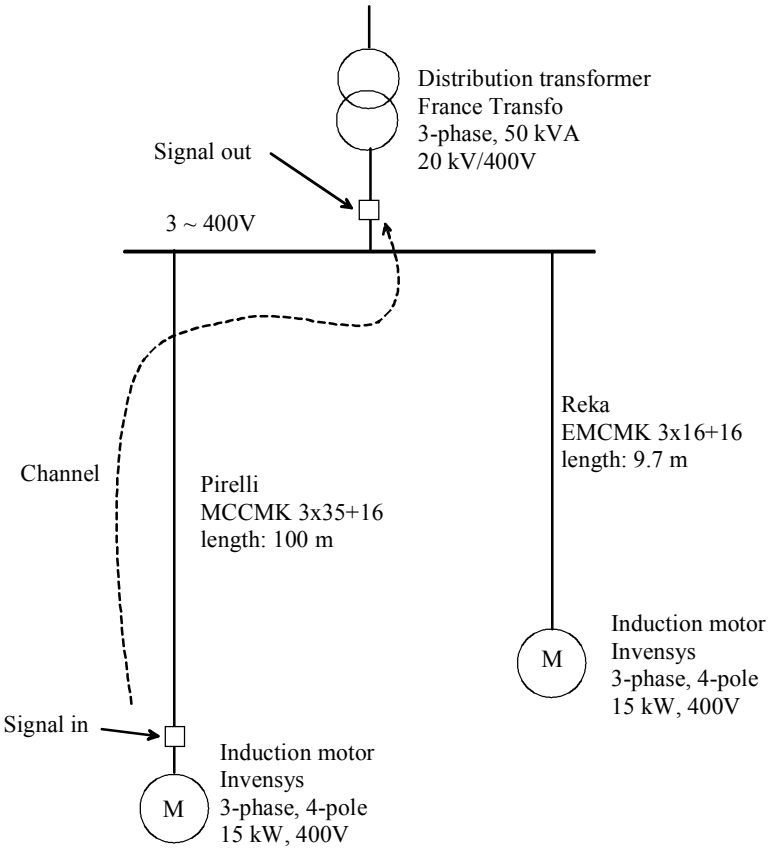

Figure II.1. Pilot distribution network and modelled channel. The signal is injected into the distribution network at the motor and received at the transformer. The distance between transmitter and receiver is 100 metres.

First, a two-port representation for the modelled power-line channel is formed (figure II.2). It consists of two transmission matrices and the load impedance. The first transmission matrix represents the electric motor connected in parallel with the signal source. Respectively, the second transmission matrix represents the low voltage power cable between signal source and load. The load impedance (figure II.2) consists of impedance the formed by serial connection of

the low voltage power cable and the induction motor and impedance of distribution transformer (figure II.3). These impedances are conncted in parallel.

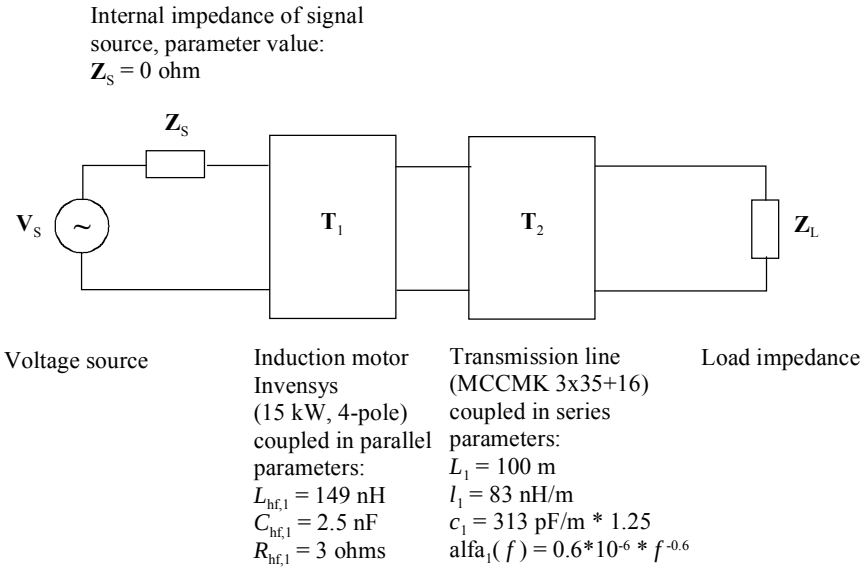

Figure II.2. Two-port representation for the modelled power-line channel. It consists of two transmission matrices and the load impedance. The first transmission matrix represents the induction motor connected in parallel with the signal source. The second transmission matrix represents the low voltage power cable in series with the signal source. The voltage of the received signal is measured over the load impedance.

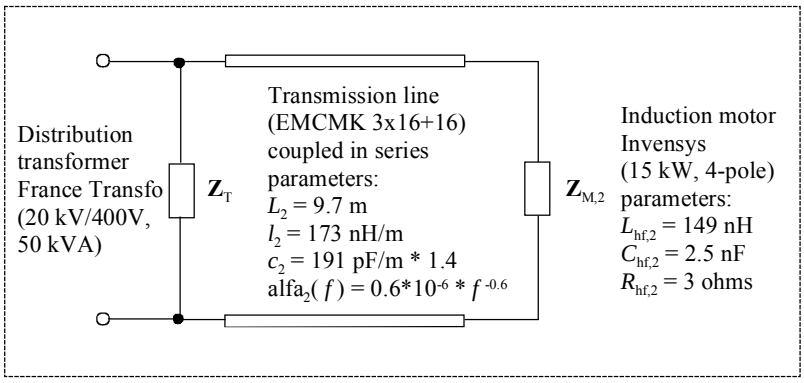

Figure II.3. The load impedance consists of a transformer, a low voltage power cable and an electric motor. The voltage of the received signal is measured over the load impedance.

The value $\mathbf{Z}_s = 0\Omega$ is selected for the serial impedance of the signal source, since in the measurements performed for the modelled communications channel the voltages at both input port and output port were directly measured. The first transmission matrix in the power-line channel (figure II.2) is the electric motor (Invensys, 15 kW). It is connected in parallel with the signal source. Transmission matrix $\mathbf{T}_1(f)$ is formed for the electric motor (figure II.2):

$$\mathbf{T}_1(f)=\begin{bmatrix} 1 & 0 \\ \dfrac{1}{\mathbf{Z}_{\mathrm{M},1}(f)} & 1 \end{bmatrix}, \tag{II.1}$$

where $\mathbf{Z}_{\mathrm{M},1}(f)$ represents the input impedance of the electric motor, which is calculated with the input impedance model presented in chapter 2.4.2.

$$\mathbf{Z}_{\mathrm{M},1}(f)=R_{\mathrm{hf},1}+j2\pi f L_{\mathrm{hf},1}+\frac{1}{j2\pi f C_{\mathrm{hf},1}} \tag{II.2}$$

The parameters for the electric motor (Invensys, 15 kW) and signal coupling (L1, PE) are (table 2.3):

$$\begin{aligned} L_{\mathrm{hf},1} &= 149\,\mathrm{nH} \\ C_{\mathrm{hf},1} &= 2.5\,\mathrm{nF} \\ R_{\mathrm{hf},1} &= 3\,\Omega \end{aligned}$$

The next transmission matrix $\mathbf{T}_2$ is formed for motor cable (MCCMK 3x35+16), which is connected in series with the signal source:

$$\mathbf{T}_2(f)=\begin{bmatrix} \cosh[\boldsymbol{\gamma}_1(f)L_1] & \mathbf{Z}_{0,1}\sinh[\boldsymbol{\gamma}_1(f)L_1] \\ \dfrac{1}{\mathbf{Z}_{0,1}}\sinh[\boldsymbol{\gamma}_1(f)L_1] & \cosh[\boldsymbol{\gamma}_1(f)L_1] \end{bmatrix}, \tag{II.3}$$

where the propagation constant for the cable is:

$$\boldsymbol{\gamma}_1=\alpha_1(f)+j\beta_1=\alpha_1(f)+j2\pi f\sqrt{l_1 c_1} \tag{II.4}$$

and the characteristic impedance of the cable is:

$$\mathbf{Z}_{0,1}=\sqrt{\frac{l_1}{c_1}}\,. \tag{II.5}$$

The parameters for cable (MCCMK 3x35+16) are (table 2.1):

$$\begin{aligned} L_1 &= 100\,\mathrm{m} \\ l_1 &= 83\,\mathrm{nH/m} \\ c_1 &= 313\,\mathrm{pF/m} * 1.25 \\ \alpha_1(f) &= 0.5\cdot 10^{-6}\cdot f^{0.6} \end{aligned}$$

The distributed capacitance of the cable is increased 25% in order to match the simulation with the measurement. Both transmission matrices are combined using chain rule:

$$\mathbf{T}(f)=\mathbf{T}_1(f)\mathbf{T}_2(f)=\begin{bmatrix}1 & 0\\ \frac{1}{\mathbf{Z}_{\mathrm{M},1}(f)} & 1\end{bmatrix}\begin{bmatrix}\cosh[\boldsymbol{\gamma}_1(f)L_1] & \mathbf{Z}_{0,1}\sinh[\boldsymbol{\gamma}_1(f)L_1]\\ \frac{1}{\mathbf{Z}_{0,1}}\sinh[\boldsymbol{\gamma}_1(f)L_1] & \cosh[\boldsymbol{\gamma}_1(f)L_1]\end{bmatrix} \quad \text{(II.6)}$$
$$=\begin{bmatrix}\cosh[\boldsymbol{\gamma}_1(f)L_1] & \mathbf{Z}_{0,1}\sinh[\boldsymbol{\gamma}_1(f)L_1]\\ \frac{\cosh[\boldsymbol{\gamma}_1(f)L_1]}{\mathbf{Z}_{\mathrm{M},1}(f)}+\frac{1}{\mathbf{Z}_{0,1}}\sinh[\boldsymbol{\gamma}_1(f)L_1] & \frac{\mathbf{Z}_{0,1}\sinh[\boldsymbol{\gamma}_1(f)L_1]}{\mathbf{Z}_{\mathrm{M},1}(f)}+\cosh[\boldsymbol{\gamma}_1(f)L_1]\end{bmatrix}$$

The received voltage is measured over the load impedance $\mathbf{Z}_{\mathrm{L}}$ (figure II.3), which consists of two load impedances connected in parallel. The first one is the serial connection of the motor cable (EMCMK 3x16+16, length 9.7 m) and the electric motor (Invensys, 15 kW). The second one is the input impedance of the distribution transformer (France Transfo, 50 kVA). The impedance formed by the cable and motor is:

$$\mathbf{Z}_{\mathrm{eq}}(f)=\mathbf{Z}_{0,2}\frac{\mathbf{Z}_{\mathrm{M},2}(f)+\mathbf{Z}_{0,2}\tanh[\boldsymbol{\gamma}_2(f)L_2]}{\mathbf{Z}_{0,2}+\mathbf{Z}_{\mathrm{M},2}(f)\tanh[\boldsymbol{\gamma}_2(f)L_2]}. \quad \text{(II.7)}$$

The propagation constant for the cable is calculated using equation:

$$\boldsymbol{\gamma}_2=\alpha_2(f)+j\beta_2=\alpha_2(f)+j2\pi f\sqrt{l_2c_2}\,. \quad \text{(II.8)}$$

The characteristic impedance of the cable is calculated using equation:

$$\mathbf{Z}_{0,2}=\sqrt{\frac{l_2}{c_2}}\,. \quad \text{(II.9)}$$

The parameters for the input impedance model of the electric motor and for the power cable are (table 2.3, 2.1):

$L_{\mathrm{hf},2}=149\,\mathrm{nH}$
$C_{\mathrm{hf},2}=2.5\,\mathrm{nF}$
$R_{\mathrm{hf},2}=3\,\Omega$

$L_2=9.7\,\mathrm{m}$
$l_2=173\,\mathrm{nH/m}$
$c_2=191\,\mathrm{pF/m}*1.4$
$\alpha_2(f)=0.5\cdot10^{-6}\cdot f^{0.6}$

The distributed capacitance of the cable is increased 40% in order to match the simulation with the measurement. The input impedance measured for the distribution transformer (France Transfo, 50 kVA) in signal coupling (L1, PE) is illustrated in figure II.4.

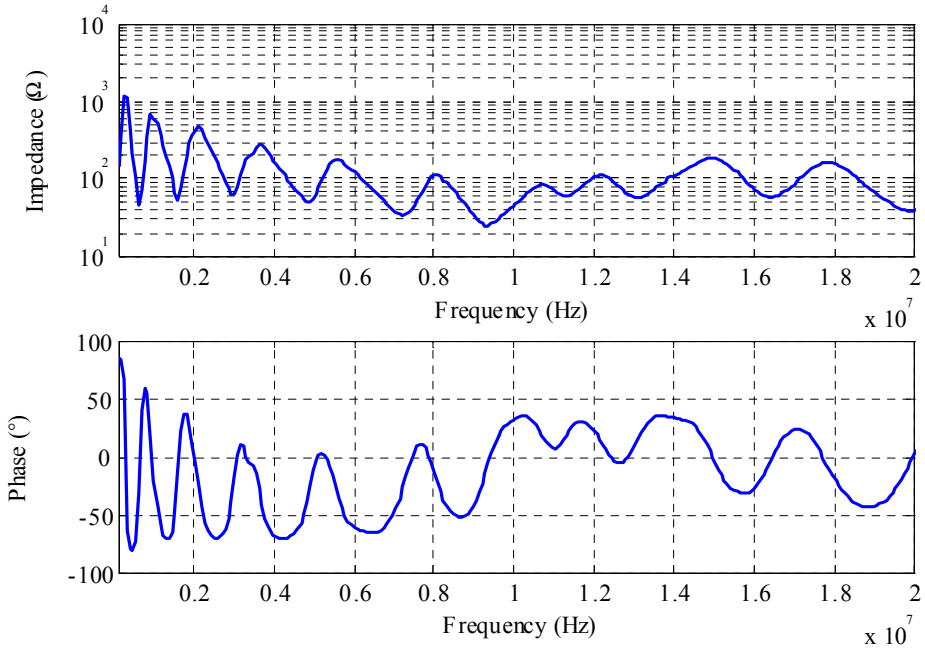

Figure II-4. Measured input impedance of the distribution transformer (France Transfo, 50 kVA) in signal coupling (L1, PE) and at frequency band 100 kHz – 20 MHz.

The total load impedance is given by equation:

$$\mathbf{Z}_{\mathrm{L}}(f)=\frac{\mathbf{Z}_{\mathrm{T}}(f)\mathbf{Z}_{\mathrm{eq}}(f)}{\mathbf{Z}_{\mathrm{T}}(f)+\mathbf{Z}_{\mathrm{eq}}(f)}=\frac{\mathbf{Z}_{\mathrm{T}}(f)\mathbf{Z}_{0,2}\dfrac{\mathbf{Z}_{\mathrm{M},2}(f)+\mathbf{Z}_{0,2}\tanh[\gamma_2(f)L_2]}{\mathbf{Z}_{0,2}+\mathbf{Z}_{\mathrm{M},2}(f)\tanh[\gamma_2(f)L_2]}}{\mathbf{Z}_{\mathrm{T}}(f)+\mathbf{Z}_{0,2}\dfrac{\mathbf{Z}_{\mathrm{M},2}(f)+\mathbf{Z}_{0,2}\tanh[\gamma_2(f)L_2]}{\mathbf{Z}_{0,2}+\mathbf{Z}_{\mathrm{M},2}(f)\tanh[\gamma_2(f)L_2]}}. \quad \text{(II.10)}$$

The transfer function for the voltage attenuation of the communications channel is given by equation:

$$\mathbf{H}(f)=\frac{\mathbf{V}_2(f)}{\mathbf{V}_{\mathrm{S}}(f)}=\frac{\mathbf{Z}_{\mathrm{L}}(f)}{\mathbf{A}(f)\mathbf{Z}_{\mathrm{L}}(f)+\mathbf{B}(f)+\mathbf{C}(f)\mathbf{Z}_{\mathrm{L}}(f)\mathbf{Z}_{\mathrm{S}}+\mathbf{D}(f)\mathbf{Z}_{\mathrm{S}}}=\frac{\mathbf{Z}_{\mathrm{L}}(f)}{\cosh[\gamma_1(f)L_1]\mathbf{Z}_{\mathrm{L}}(f)+\mathbf{Z}_{0,1}\sinh[\gamma_1(f)L_1]}. \quad \text{(II.11)}$$

The simulated and measured amplitude responses for power-line channel and for the frequency band 100 kHz – 20 MHz are illustrated in figure (II.5). Notches and peaks in the amplitude responses are at the same frequencies after modification of the cable capacitance. In addition, the gains of the simulated and measured channel behave similarly.

Phase response and group delay for the simulated power-line channel are illustrated in figure (II.6). The group delay is calculated from phase response applying equation:

$$\tau_g(f) = -\frac{1}{2\pi}\frac{d\theta(f)}{df}. \qquad \text{(II.12)}$$

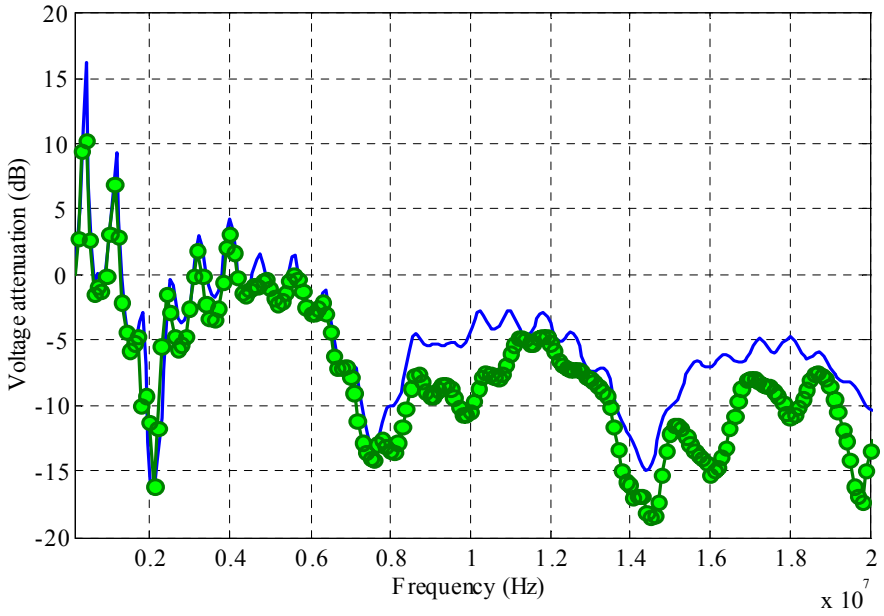

Figure II.5. Modelled and measured frequency responses for the power-line channel in the frequency band 100 kHz – 20 MHz.

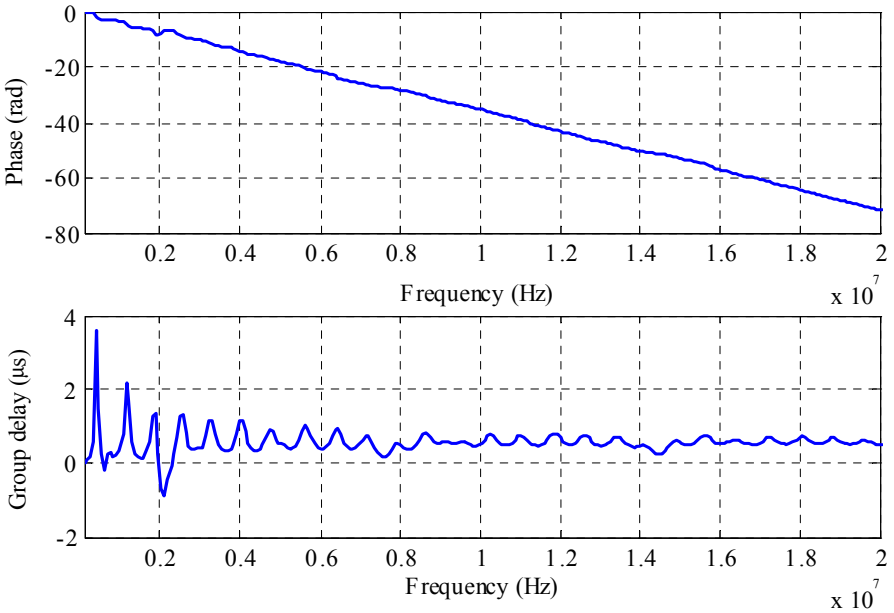

Figure II.6. Simulated phase response and group delay for the communications channel in the frequency band 100 kHz – 30 MHz.